

Relevance of surface freshwater flux for global
ocean circulation and Atlantic freshwater
content variability

Dissertation

zur Erlangung des Doktorgrades
an der Fakultät für Mathematik, Informatik und Naturwissenschaften
im Fachbereich Geowissenschaften
der Universität Hamburg

vorgelegt von

Xin Liu

Hamburg 2017

Gutachter:

Prof. Dr. Detlef Stammer

Dr. Armin Köhl

Tag der Disputation:

February 1st, 2018

Abstract

Over the next century changes in the ocean will occur as a consequence of an intensified water cycle and the associated surface freshwater flux changes under global warming. One objective of this thesis is concerned with the dynamical ocean response to the associated surface volume flux anomalies. The other objective is to detect the contributions of surface freshwater flux and freshwater transport to the regional freshwater content variations in the Atlantic, specifically at interannual and decadal time scales.

To address the first objective, the model configuration of the German contribution to the Estimating the Circulation and Climate of the Ocean (GECCO2) is used with two salinity boundary conditions (virtual salt flux version and volume flux version). Both versions are forced first by the present-day freshwater flux and then by the additional freshwater flux anomalies, which are estimated over the period 2081–2100 relative to 1986–2005 under the Representative Concentration Pathway (RCP) 8.5 scenario from the Max-Planck-Institute Earth System Model.

The resulting differences between the two salinity boundary conditions show that the adjustment of ocean circulation involves a barotropic response as predicted from the Goldsbrough-Stommel theory. In comparison to the present-day Goldsbrough-Stommel circulation, the corresponding barotropic circulation driven by the RCP8.5 freshwater flux anomalies intensifies by about 20% globally with a stronger intensification about 50% in the Southern Ocean. The barotropic circulation anomaly induced by the intensified volume flux reaches to 0.6 Sv in the Antarctic Circumpolar Current region. The adjustment also involves

changes in the meridional overturning circulation, mirroring the convergence and divergence of the mass transport driven by surface volume flux. The subsequent pathway of fresh water and the spreading of volume flux match with each other in the shallow cells but diverge substantially with depth. Associated with the circulation changes are the changes in the meridional heat and freshwater transports, which appear mostly as transport changes related to the meridional overturning circulation. Changes in the circulation also lead to a redistribution of temperature and salinity, which results in a significant contribution to the regional sea level changes in form of steric change. The sea level changes due to the projected freshwater flux anomalies are in the range of ± 0.5 cm and can be largely attributed to the displacement of the isopycnals.

The second part of the thesis investigates the freshwater budgets of three regions in the Atlantic using the GECCO2 ocean synthesis over the period 1961–2014. The freshwater content changes in the subtropical and subpolar North Atlantic ($23.5^{\circ}\text{N} - 60^{\circ}\text{N}$) can be attributed to the combined impacts of the surface freshwater flux and the net freshwater transport across the boundaries. The strongly increased surface freshwater input over the last two decades is located to the north of 37°N and tends to enhance the southward transport at 37°N through the overturning circulation. The increased southward transport at 37°N turns out to be the dominant contribution to the freshwater content variability in the sub-region to the south of 37°N . Over the tropical region, the surface flux plays a role in changing the freshwater content in the northern box ($0^{\circ} - 23.5^{\circ}\text{N}$), but shows no significant impact in the southern box ($23.5^{\circ}\text{S} - 0^{\circ}$) because of its relatively small interannual variability. Overall, the results indicate the importance of the convergence/divergence of the freshwater transports across the boundaries to the freshwater content changes in every region. In addition, the shallow overturning cells in the tropical Atlantic are found to be important for the interannual variations of the freshwater transport, while the deep overturning circulation shows profound impacts on the decadal variations.

Zusammenfassung

Die globale Erwärmung führt zu einer Intensivierung des globalen Wasserkreislaufes. Die damit einhergehenden Änderungen des Süßwasserflusses an der Meeresoberfläche führen im Laufe des nächsten Jahrhunderts zu Veränderungen in den Weltmeeren. Diese Arbeit befasst sich zum einen mit der dynamischen Reaktion der Ozeane auf die Anomalien des Oberflächenflusses, die mit den Änderungen des Süßwasserflusses einhergehen. Zum anderen werden die Beiträge des Süßwasserflusses an der Meeresoberfläche sowie des Süßwassertransportes zu den regionalen zwischenjährlichen und dekadischen Variabilitäten des Süßwassergehalts im Atlantik erfasst.

Für die Bearbeitung des ersten Ziels wird die Modellkonfiguration des deutschen Beitrages des Projekts Estimating the Circulation and Climate of the Ocean (engl.: German contribution to the Estimating the Circulation and Climate of the Ocean, GECCO2) mit zwei Randbedingungen für den Salzgehalt (virtueller Salzfluss und Volumenfluss) verwendet. Beide Versionen werden zuerst mit dem gegenwärtigen Süßwasserfluss und dann mit den zusätzlichen Süßwasserflussanomalien angetrieben. Letztere basieren auf den Max-Planck-Institut Erdsystemmodellläufen unter dem Representative Concentration Pathway (RCP) 8.5 Szenario und wurden über den Zeitraum 2081–2100 relativ zu dem Zeitraum 1986–2005 berechnet.

Die daraus resultierenden Unterschiede zwischen den beiden Randbedingungen des Salzgehaltes zeigen, dass die Anpassung der Ozeanzirkulation eine barotrope Komponente beinhaltet, wie sie von der Goldsbrough-Stommel-Theorie vorhergesagt wurde. Im Vergleich

zur gegenwärtigen Goldsbrough-Stommel-Zirkulation ist die entsprechende barotrope Zirkulation, die mit dem RCP8.5 Süßwasserflussanomalien angetrieben wird, um etwa 20 % stärker mit einem Maximum von 50 % im Südpolarmeer. Die durch den verstärkten Volumenfluss induzierte barotrope Zirkulationsanomalie erreicht im antarktischen Zirkumpolarstrom 0,6 Sv. Die dynamische Anpassung beinhaltet auch Änderungen in der meridionalen Umwälzzirkulation, die die Konvergenz und Divergenz des Massentransports widerspiegeln, welcher wiederum vom Oberflächenvolumenfluss angetrieben wird. Der darauffolgende Pfad des Süßwassers und die Verteilung des Volumens stimmen in den flachen Zellen überein, divergieren jedoch im Wesentlichen mit der Tiefe. Mit den Zirkulationsänderungen gehen Änderungen im meridionalen Wärme- und Süßwassertransport einher, welche meist als Transportänderungen im Zusammenhang mit der meridionalen Umwälzzirkulation auftreten. Veränderungen der Zirkulation führen zusätzlich zu einer Umverteilung der Temperatur und des Salzgehaltes, was einen signifikanten Beitrag zu regionalen sterischen Meeresspiegeländerungen leistet. Die Änderungen des Meeresspiegels aufgrund der prognostizierten Anomalien des Süßwasserflusses liegen im Bereich von $\pm 0,5$ cm und sind größtenteils auf die Verlagerung von Isopyknen zurückzuführen.

Der zweite Teil der vorliegenden Dissertation untersucht die Süßwasserbudgets in drei Regionen im Atlantik mit Hilfe der GECCO2 Ozean Synthese im Zeitraum 1961–2014. Die Änderungen des Süßwassergehaltes im subtropischen und subpolaren Nordatlantik ($23,5^{\circ}\text{N} - 60^{\circ}\text{N}$) lassen sich auf die kombinierten Auswirkungen des Oberflächensüßwasserflusses und dem Nettosüßwassertransport über die Grenzflächen zurückführen. Der über die letzten zwei Jahrzehnte stark erhöhte Süßwassereintrag an der Oberfläche liegt nördlich von 37°N und steigert den südwärtigen Süßwassertransport mittels der Umwälzzirkulation bei 37°N . Der verstärkte Transport nach Süden trägt maßgeblich zur Variabilität des Süßwassergehaltes in der Subregion südlich von 37°N bei. In den tropischen Regionen ändert der Oberflächenfluss den Süßwassergehalt in der nördlichen Box ($0^{\circ} - 23,5^{\circ}\text{N}$), hat jedoch aufgrund geringer zwischenjähriger Variabilität keine signifikanten Auswirkungen auf den Süßwassergehalt in der südlichen Box ($23,5^{\circ}\text{S} - 0^{\circ}$). Insgesamt zeigen die Ergebnisse wie wichtig die Konvergenz/Divergenz des Süßwassertransportes über die Grenzflächen für die Änderungen des Süßwassergehaltes in allen Regionen ist. Zusätzlich konnte gezeigt werden, dass die

flachen Umwälzzellen im tropischen Atlantik für die zwischenjährigen Variationen des Süßwassertransportes von Bedeutung sind, während die tiefe Umwälzzirkulation großen Einfluss auf dekadische Variationen hat.

Contents

Abstract	i
Zusammenfassung	iii
Contents	vii
1 Introduction	1
1.1 Global water cycle	1
1.2 Goals of the thesis	5
1.3 Outline of the thesis	6
2 Background	9
2.1 Goldsbrough-Stommel circulation	9
2.1.1 Development of the theory	10
2.1.2 Literature review on the GSC	12
2.2 Global water cycle intensification	15
2.2.1 Projected change in global surface temperature	15
2.2.2 Projected change in evaporation and precipitation	16
3 Data and Methodology	19
3.1 Freshwater flux data	19
3.2 GECCO2 set-up	26
3.3 Salinity boundary conditions	27
3.3.1 Virtual salt flux formulation	27
3.3.2 Volume flux formulation	28
3.4 Experiments	29
3.4.1 NCEP response experiments	29

3.4.2	Perturbation experiments.....	30
3.4.3	Relaxation tests.....	30
4	Dynamical ocean response to projected changes of the global water cycle	33
4.1	Introduction	33
4.2	Dynamical adjustment processes.....	34
4.2.1	Changes of the gyre circulation.....	34
4.2.2	Impact on meridional overturning circulation.....	38
4.2.3	Sea level changes associated with surface volume flux	43
4.2.4	Synthesis.....	46
4.3	Projected changes in the future	49
4.3.1	Future dynamical response	49
4.3.2	Transport changes.....	53
4.4	Concluding remarks	60
5	Freshwater budget in the Atlantic	63
5.1	Introduction	63
5.2	Data and study area	65
5.3	Freshwater transport variability.....	68
5.4	Freshwater content variability.....	70
5.4.1	Subtropical and subpolar North Atlantic.....	71
5.4.2	Tropical North Atlantic	75
5.4.3	Tropical South Atlantic	77
5.4.4	Importance of the shallow overturning cells	79
5.5	Discussion and summary.....	81
6	Conclusions and outlook.....	85
6.1	Thesis overview.....	85
6.1.1	The impacts of surface volume flux on ocean circulation.....	85
6.1.2	The roles of surface freshwater flux and freshwater transport in the Atlantic freshwater content variations.....	87
6.2	Future work	88
	References	91
	List of figures.....	103

List of symbols	111
Abbreviations.....	113
Acknowledgements	115
Declaration	117

CHAPTER 1

Introduction**1.1 Global water cycle**

One of the most important consequences of future climate change to society might arise from an accelerated global water cycle projected to occur during the current century and beyond in response to a warmer climate. This acceleration has been reported by a number of studies (see also the Intergovernmental Panel on Climate Change the Fifth Assessment Report (IPCC AR5) Chapter 12 [Collins *et al.*, 2013], and references therein). As an example, Durack *et al.* [2012] suggested an intensification of the global water cycle at a rate of $8 \pm 5\%$ per degree of surface warming based on observed surface salinity changes. Given the projected multi-model mean warming of $1.0\text{ }^{\circ}\text{C}$ for the Representative Concentration Pathway (RCP) 2.6 scenario and $3.7\text{ }^{\circ}\text{C}$ for the RCP8.5 scenario by the end of the 21st century [Collins *et al.*, 2013], this should result in an accelerated water cycle of up to 30% for the RCP8.5 scenario. Over land, this could lead to an intensification of droughts, floods and storms [Trenberth, 2011; Chou *et al.*, 2013; Liu and Allan, 2013; Allan *et al.*, 2014]. Because 86% of the global evaporation and 78% of the precipitation occur over the ocean as shown schematically in Fig. 1.1 [Schmitt, 1995; Rodell *et al.*, 2015; Durack *et al.*, 2016], any change in the water cycle will inevitably affect the net surface freshwater flux over the ocean and thereby change the ocean circulation.

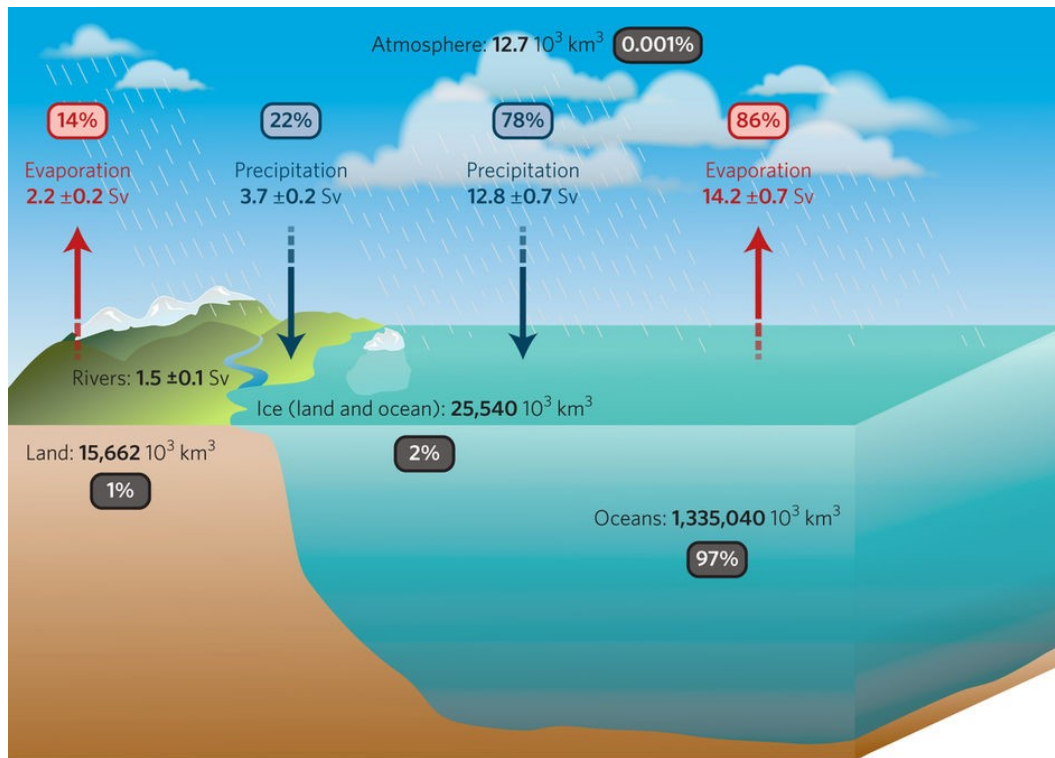


Figure 1.1 The global water cycle — the oceanic perspective. Reservoirs are represented by grey boxes with units 10^3 km^3 . Fluxes are represented by arrows and the red and blue boxes with units of Sv (Sverdrups; $10^6 \text{ m}^3 \text{ s}^{-1}$). [Figure 1 from Durack *et al.*, 2016]

Despite the discrepancies in distribution and magnitude across climate models and forcing scenarios, there are common features of the changes in surface freshwater flux over the ocean, which can be referred to as the “rich get richer” mechanism [Chou and Neelin, 2004]. Projections of future climate generally indicate that parts of the dry regions tend to become drier while wet regions get wetter, shown schematically in Fig. 1.2 [Collins *et al.*, 2013]. Durack and Wijffels [2010] hypothesized that associated with changes in the oceanic surface freshwater flux will be regional changes in salinity. Using model simulations with enhanced freshwater flux forcing, they verified that the observed salinity changes over the last decades are consistent with this mechanism, while Lago *et al.* [2016] suggested that surface temperature changes are important as well. Since salinity is an active tracer, impacting the

density of the ocean, any regional-scale salinity change should modify the circulation as well as transport properties, change regional sea level, and impact the thermohaline circulation. However, beyond a purely kinematic analysis mentioned above, the dynamical consequences of future changes in surface freshwater flux are among the least understood elements of the changing climate system [Schmitt, 2008; Lagerloef *et al.*, 2010].

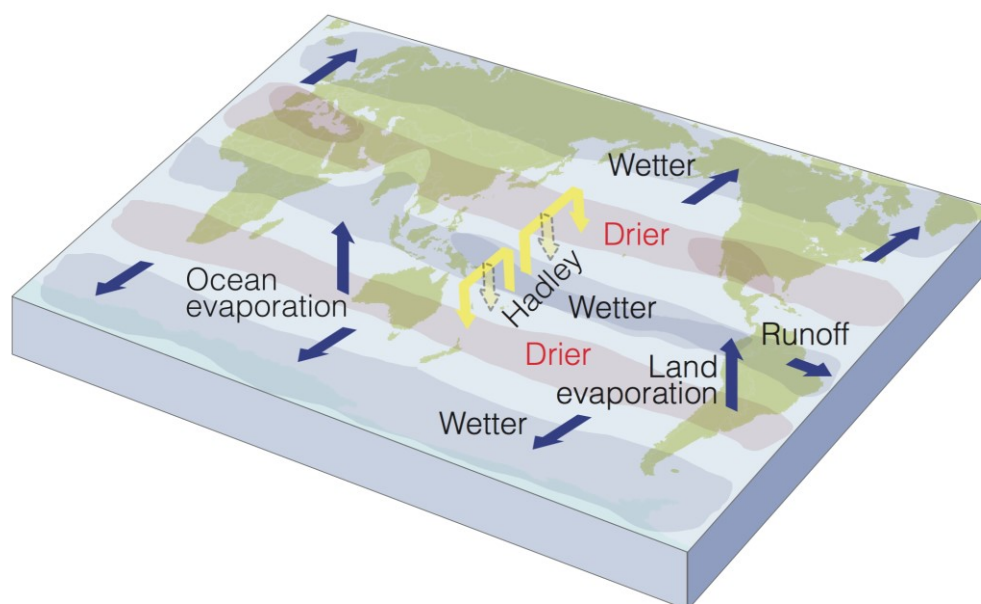


Figure 1.2 Schematic diagram of projected changes in major components of the water cycle. The blue arrows indicate major types of water movement changes through the Earth's climate system: poleward water transport by extratropical winds, evaporation from the surface and runoff from the land to the oceans. The shaded regions denote areas more likely to become drier or wetter. Yellow arrows indicate an important atmospheric circulation change by the Hadley Circulation, whose upward motion promotes tropical rainfall, while suppressing subtropical rainfall. Model projections indicate that the Hadley Circulation will shift its downward branch poleward in both the Northern and Southern Hemispheres, with associated drying. Wetter conditions are projected at high latitudes, because a warmer atmosphere will allow greater precipitation, with greater movement of water into these regions. [FAQ 12.2, Figure 1 from Collins *et al.*, 2013]

While investigating changes of the ocean circulation in response to future surface freshwater forcing anomalies, one can start from the guiding principles that on the rotating Earth, any loss or gain of fresh water through the ocean surface (volume flux) can be expected to result in a barotropic gyre-type circulation described by the theory of the Goldsbrough-Stommel circulation (GSC) [Goldsbrough, 1933; Stommel, 1957; 1984]. This holds for the time-mean situation discussed by *Huang and Schmitt* [1993], for which the amplitude of the GSC is of a modest order of 1 Sv ($1 \text{ Sv} = 10^6 \text{ m}^3 \text{ s}^{-1}$) and opposes the wind-driven currents. Because of its seemingly small contribution to the large-scale circulation, the GSC did not attract much attention in the studies of ocean circulation.

Another fact is that the numerical models that use virtual salt flux as salinity boundary condition are unable to simulate the GSC and its impact on a changing ocean circulation as part of the climate system. *Huang* [1993] proposed to implement natural boundary conditions by using real freshwater flux across the air-sea interface as vertical velocity to allow a dynamical impact of surface volume flux in model simulations. *Yin et al.* [2010] compared the virtual salt flux formulation with the real freshwater flux formulation with and without the external forcings (0.1 and 1 Sv water hosing imposed in the high-latitude North Atlantic) and found that the differences between these two formulations are generally small except for the large water hosing experiments.

Although it is understood that the changes induced by surface volume flux on the general circulation are assumed to be small [*Tartinville et al.*, 2001; *Yin et al.*, 2010], it remains unclear how the dynamical adjustments respond to the surface volume flux forcing in terms of ocean circulation, sea level and transport properties. Moreover, much less is known about how fresh water spreads in the interior ocean and how it is related to the pathways of the surface volume flux forcing.

It can be expected that the same mechanism acting in response to the present-day surface volume flux should be involved in the adjustment of ocean circulation in response to a changing global water cycle. In particular, one can expect that any change in volume flux will lead to an anomalous GSC type barotropic circulation with respective dynamical

consequences resulting from it. Therefore, the dynamical impact of future changes in surface volume flux on ocean circulation as simulated by numerical models still needs to be understood in detail.

Associated with changes in the global water cycle, the freshwater content variability in the Atlantic Ocean is of great importance since it plays a role in changing the large-scale thermohaline circulation [Dickson *et al.*, 2002] and the regional sea level in the Atlantic [Antonov *et al.*, 2002; Levitus *et al.*, 2005; Durack *et al.*, 2014]. The freshwater flux across the air-sea interface and the freshwater transport by the ocean circulations are two vital processes responsible for the changes in freshwater content. One of the focuses of the previous research is to illustrate the impacts of the surface freshwater flux and the upper ocean dynamics on the surface salinity variability [Qu *et al.*, 2011; Yu, 2011; Vinogradova and Ponte, 2013], while another focus is the dynamics associated with the high-latitude Atlantic freshwater content changes [Dickson *et al.*, 2002; Curry *et al.*, 2003; Curry and Mauritzen, 2005; Boyer *et al.*, 2007; Holliday *et al.*, 2008; Deshayes *et al.*, 2014]. However, much less is known about the Atlantic freshwater content variations and the related processes at mid and low latitudes over the past 50 years, which are of interest and need to be addressed.

1.2 Goals of the thesis

One of the objectives is to investigate the dynamical aspects of the global ocean circulation in response to the surface volume flux for the present-day and more importantly for the future. To that end, in a first step, the mechanisms that potentially can be involved in such a dynamical adjustment will be reviewed using the present-day volume flux forcing. This will be done through model runs in which changes in salinity boundary conditions are imposed. In a subsequent step, similar runs will be performed, but specifically with prescribed RCP8.5 surface freshwater flux anomalies. These runs are designed to identify which of the previously identified mechanisms might be relevant for the future dynamical ocean circulation adjustment to the accelerated global water cycle.

The other target is to detect the contributions from the meridional freshwater transport and surface freshwater flux to the regional freshwater content changes in the Atlantic Ocean. For this purpose, the evolutions of these two contributors are diagnosed with a focus on the processes that are potentially responsible for their variations.

The two key questions to be addressed in this thesis are listed below. The answers to these questions will provide a more comprehensive understanding of these aspects as well as new insight into the ocean dynamics research.

Key questions to be addressed in this thesis include:

- What is the dynamical GSC response to the acceleration of the global water cycle in a future warmer world?
- What roles do surface freshwater flux and freshwater transport play in changing the regional freshwater content in the Atlantic?

1.3 Outline of the thesis

The remaining thesis is organized as follows:

Chapter 2 provides an overview of the Goldsbrough-Stommel theory and a detailed introduction about its related previous studies. With respect to the climate change, especially the acceleration of the global water cycle, the projected changes in the future surface temperature and freshwater flux are illustrated in this chapter, and so is the “rich get richer” mechanism.

Chapter 3 includes the introduction of the evaporation and precipitation data sets as well as the comparison among them. The model set-up used in the study will be described and followed by the explanations of the two salinity boundary conditions and the experiments. The mathematical definitions of the virtual salt flux formulation and the volume flux

formulation are specified in this chapter, along with the definition of the “volume flux” components.

Chapter 4 contains the detailed analysis of the ocean’s dynamical response to the present-day surface volume flux forcing and later on to the projected freshwater flux anomaly perturbation. The barotropic circulation induced by surface volume flux in the model simulation and the GSC are revisited and compared first. Then, the surface volume flux related sea level changes, the MOC changes and the pathways of volume flux and fresh water in the interior ocean are illustrated. Especially, the circulation changes through the projected freshwater flux anomaly perturbation in a future warmer world will then be discussed and followed with the analysis of the heat and freshwater transport changes.

Chapter 5 explores the freshwater budget of three regions in the Atlantic Ocean, regarding the temporal evolutions of the freshwater content changes, the surface freshwater flux, and the freshwater transport across the northern and southern boundaries of each region. To detect the related mechanisms that affect the freshwater transport variations, the freshwater transport over the study period will be decomposed into the overturning and gyre components. In the end, there is a discussion about the freshwater transport carried by the shallow overturning cells.

Finally, **Chapter 6** presents an overview and main conclusions of the thesis, as well as recommendations for future work.

Results in Chapter 4 have been published in *Journal of Geophysical Research: Oceans*.

Liu, X., A. Köhl, and D. Stammer (2017), Dynamical ocean response to projected changes of the global water cycle, *J. Geophys. Res. Oceans*, 122(8), 6512–6532, doi: 10.1002/2017JC013061.

CHAPTER 2

Background**2.1 Goldsbrough-Stommel circulation**

It is well known that ocean circulation is mainly driven by wind stress, heat flux, freshwater flux and tidal force. Numerous studies have discussed the wind-driven circulation, and the heat and freshwater fluxes related thermohaline circulation. Surface freshwater flux not only is a key ingredient controlling the oceanic salinity distribution, but also changes the volume of the seawater and has a similar dynamic effect as the wind stress does. Surface volume flux can be expected to drive a barotropic circulation on a rotating earth, which is called the Goldsbrough-Stommel circulation (GSC) [*Goldsbrough*, 1933; *Stommel*, 1957; 1984]. This section will recall the GSC theory and its related previous research in detail.

Before starting, it is necessary to clarify the term “volume flux”. Many terms (i.e. “freshwater flux”, “volume flux”, “evaporation and precipitation”, or “vertical velocity”) have been applied in relevant studies referring to the volume flux aspect of surface freshwater flux. Since freshwater flux has two aspects, changing salinity and volume of the seawater at the same time, some of these terms may lead to a confusing interpretation. As mentioned above, what drives the barotropic GSC in the ocean is actually the volume flux associated with

freshwater flux. The direct impact of freshwater flux on the salinity variations does not contribute. To be distinguishable and more accurate, in this thesis we use the term “volume flux associated with surface freshwater flux”, or “volume flux” as a shorthand. Since this section means to introduce previous studies, we follow the term that was used in each article respectively.

2.1.1 Development of the theory

It has long been noted that the surface freshwater flux is able to drive large-scale ocean circulation. This has been first addressed by *Hough* [1897] at the end of his theoretical study on tides. In *Hough*'s solution [1897], he considered evaporation (E) and precipitation (P) as functions of latitude and found that the effects of E and P would cause a steady flow in the ocean for the initial stage. In the absence of friction and meridional boundaries in the ocean, the currents he found would tend to uniformly accelerate without limit in consequence of the rotation. So the solution was no longer valid as time goes on.

Different from *Hough*'s solution, *Goldsbrough* [1933] presented a case of the ocean with meridional boundaries from pole to pole and more importantly with the specific distribution of E and P. In this way, he successfully constructed a steady freshwater-driven current field without involving friction terms and derived the vorticity constraint in the ocean interior, which is called the *Goldsbrough* relation,

$$\beta M_y = f(E - P). \quad (2.1)$$

Here, M_y represents the northward mass transport, f is the Coriolis parameter, and β its meridional gradient. According to the equation, in the northern hemisphere, P induces equatorward flow and E drives poleward flow in the ocean interior. In order to close the circulation by the freshwater flux alone, *Goldsbrough* assumed a special pattern of E and P, with P in the eastern basin driving water equatorward and E in the western basin to bring water back poleward (Fig. 2.1a).

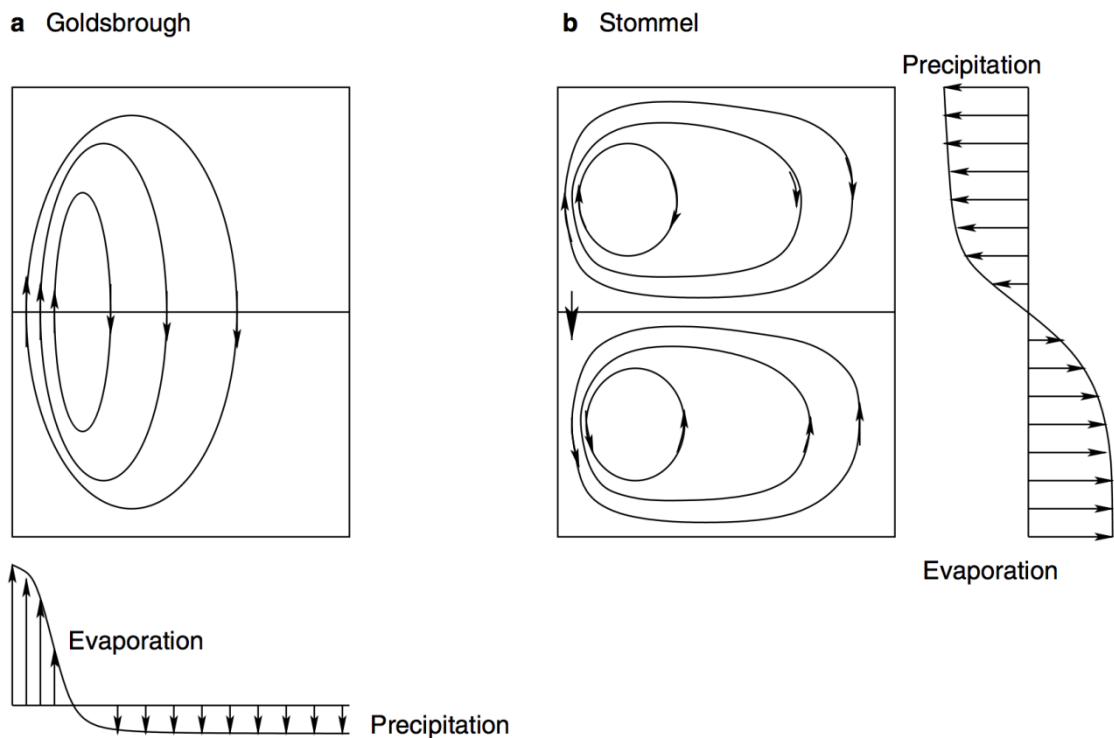


Figure 2.1 (a) The Goldsbrough gyre driven by evaporation and precipitation, and presented by him in 1933 as a model of the North Atlantic. (b) *Stommel's* [1957; 1984] idea of using the western boundary currents to close a circulation forced by a more realistic distribution of evaporation and precipitation. [Figure 5.102 from *Huang, 2010*]

As shown above, the spatial pattern of E and P in Goldsbrough's solution is quite unrealistic because in the northern hemisphere, the pattern of the net freshwater flux is with P at high latitudes and E at low latitudes. *Stommel* [1957, 1984] solved the problem by using the western boundary currents to close the freshwater flux driven circulation in the interior ocean so that a more realistic distribution of E and P is possible (Fig. 2.1b). Therefore, the freshwater flux driven circulation is called the Goldsbrough-Stommel circulation.

The GSC is imposed on the well-known wind-driven circulation. Considering the wind stress and freshwater flux on the ocean surface, the vorticity balance in the ocean interior is presented by the Goldsbrough-Sverdrup relation,

$$\beta M_y = \text{curl}_z \tau + f(E - P). \quad (2.2)$$

Here, τ is the wind stress and $\text{curl}_z \tau$ is the vertical component of the wind stress curl. P (E) provides downward (upward) vertical velocity at the air-sea interface, thus playing a similar role as a convergence (divergence) at the Ekman layer caused by negative (positive) wind stress curl. Take the subtropical gyre in the Northern Hemisphere as an example, where the negative wind stress curl and evaporation dominate. The negative wind stress curl induces southward Sverdrup transport in the interior ocean, which is closed by the northward western boundary current. Meanwhile, E drives northward transport in the interior ocean closed by the southward western boundary flow. Apparently, the effects of wind stress and freshwater flux on the ocean general circulation oppose each other. As for the magnitude, *Huang et al.* [1993] pointed out that the vertical velocity associated with the freshwater flux is about 30 times smaller than the Ekman pumping velocity. The magnitudes of evaporation/precipitation rate and wind stress curl suggest that the freshwater-driven barotropic circulation is only a few percent of the wind-driven circulation and is not detectable from observations. Hence, the freshwater-driven part of the ocean circulation has been overlooked for a long time, until studies estimated it using freshwater data sets [*Huang and Schmitt*, 1993] and model simulations [*Wadley et al.*, 1996; *Roulet et al.*, 2000; *Tartinville et al.*, 2001; *Yin et al.*, 2010]. Still, limited literature can be found on the GSC, which will be introduced below.

2.1.2 Literature review on the GSC

Huang and Schmitt [1993] were the first to present the GSC of the world oceans with zonal averages of $E-P$ in the Indian, Pacific and Atlantic oceans, separately (Fig. 2.2). They found that the southward western boundary current in the North Atlantic, which is required to close the freshwater-driven interior flow and to satisfy the inter-basin transport by the Bering Strait, reaches 2 Sv at 35° N. Since the GSC generally opposes the wind-driven currents, it is

suggested to affect the separation latitude of the western boundary currents. They also suggested that one should use the real freshwater flux formulation as the salinity boundary condition instead of the virtual salt flux formulation, in which all the dynamical effects associated with surface freshwater flux are excluded. Details about these two salinity boundary formulations will be specified in Section 3.3.

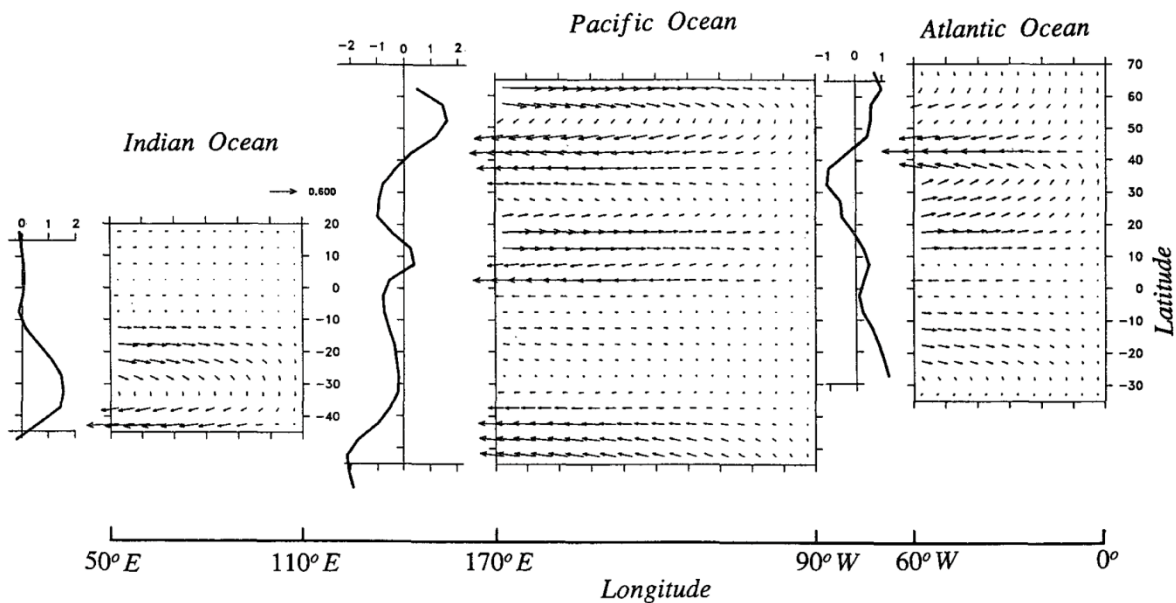


Figure 2.2 The Goldsbrough-Stommel circulation of the world oceans, neglecting the inter-basin transports. Each arrow indicates the horizontal mass flux integrated over a $5^\circ \times 5^\circ$ box, in Sv; along the western boundary of each basin, there is a curve indicating the northward mass flux within the western boundary, which is required to close the circulation. [Figure 2 from *Huang and Schmitt, 1993*]

Starting from the end of last century, the natural boundary condition has been implemented into various ocean models, coupled ocean-sea ice models as well as coupled ocean-atmosphere climate models, and results were compared with those obtained by a virtual salt flux formulation [*Wadley et al., 1996; Roulet and Madec, 2000; Tartinville et al., 2001; Yin et al., 2010*]. *Wadley et al.* [1996] tested the response of the North Atlantic to the surface

forcing in an ocean general circulation model (OGCM). They did not highlight the Goldsbrough-Stommel gyres in their results but found improvements in circulation using real freshwater flux forcing in contrast to the other two experiments with relaxation and virtual salt flux boundary conditions. *Roulet and Madec* [2000] provided the oceanic barotropic response in an OGCM to the surface freshwater flux as the GSC in global perspective. The Goldsbrough-Stommel gyres shown in their study [*Figure 4a* from *Roulet and Madec*, 2000] are less than 1 Sv and opposites the wind-driven barotropic circulation, as noted by *Huang and Schmitt* [1993]. Using a coupled sea ice-ocean general circulation model, *Tartinville et al.* [2001] analyzed the GSC in the Pacific Ocean, which has the intensity of less than 1 Sv and is in accordance with the theoretical considerations. More importantly, with a longer simulation, they investigated the reaction of the thermohaline circulation and revealed the net freshwater inflow/outflow at the ocean surface as well as the global meridional pathway of it in the interior ocean. *Yin et al.* [2010] also presented the GSC of their simulation [*Figure 4d* from *Yin et al.*, 2010] in a coupled atmosphere-ocean general circulation model, but only the subtropical gyre in North Atlantic is clearly detectable. Besides, they tested these two boundary conditions with large external freshwater forcing in the high latitude of the North Atlantic and reported a great enhancement of the El Niño-Southern Oscillation (ENSO) variability in the freshwater flux formulation. *Griffies et al.* [2014] discussed the significance of using natural boundary conditions for simulating sea level changes using ocean circulation models.

In general, much of the literature on the difference between natural boundary condition and virtual salt flux formulation pays particular attention to the salinity redistribution but not to the dynamical impact of surface volume flux. Therefore, there is a need for a better understanding of the dynamical adjustment processes in response to surface volume flux, especially the volume flux associated with the amplified freshwater flux under a warmer climate. The implications from this would allow a fresh view on the dynamical importance of surface freshwater flux.

2.2 Global water cycle intensification

2.2.1 Projected change in global surface temperature

As reported by IPCC AR5, it is clear that there are observed changes in the climate system caused by natural and anthropogenic radiative forcing. The observed warming for the period 1986–2005 relative to the period 1850–1900 is approximately $0.61\text{ }^{\circ}\text{C}$ ($0.55\text{--}0.67\text{ }^{\circ}\text{C}$, likely range). The last three decades of the period 1850–2012 are detected to be warmer than any previous decade since 1850, which is likely due to the increasing human-induced greenhouse gas emissions [IPCC, 2014].

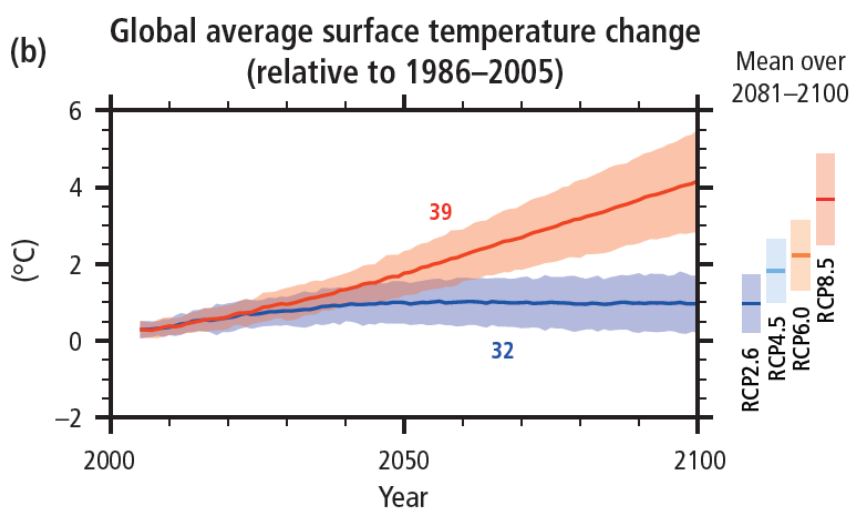


Figure 2.3 Time series of global annual change in mean surface temperature for the 2006–2100 period (relative to 1986–2005) from CMIP5 concentration-driven experiments. Projections are shown for the multi-model mean (solid lines) and the 5 to 95% range across the distribution of individual models (shading). The number of CMIP5 models used to calculate the multi-model mean is indicated above each line. [Figure 2.1b from the IPCC, 2014]

As for future climate changes, the global mean surface temperature is projected to rise over the 21st century under the four RCP scenarios. Relative to the period 1986–2005, the

projected change in global mean surface temperature (likely range is given in brackets) for the period 2081–2100 is 1.0 °C (0.3–1.7 °C) for RCP2.6, 1.8 °C (1.1–2.6 °C) for RCP4.5, 2.2 °C (1.4–3.1 °C) for RCP6.0, and 3.7 °C (2.6–4.8 °C) for RCP8.5, based on the Coupled Model Intercomparison Project Phase 5 (CMIP5) multi-model mean (Fig. 2.3). The warming of the Earth's surface and lower atmosphere has worldwide impacts on natural and human systems, not only the changes in the extreme events (e.g. droughts and floods) and the rising of global mean sea level but also changes in the global water cycle.

2.2.2 Projected change in evaporation and precipitation

It is worth noting that changes in evaporation and precipitation are not uniformly distributed, either on the continents or over the oceans [Liu and Allan, 2013]. The relatively wet regions in the tropics and high latitudes are observed and projected to have more net input of water from the surface, while the dry regions in the subtropics and mid-latitudes experience a decline in the net input of water. These regional changes of the water cycle are referred to as the “rich get richer” mechanism [Chou and Neelin, 2004], which is largely driven by the increased water vapour and enhanced moisture transports in response to the warming [Held and Soden, 2006]. Based on the Clausius-Clapeyron (CC) relation, approximately 7% increase in the saturation vapor pressure is suggested for each degree of warming in the lower troposphere. Santer *et al.* [2007] have demonstrated the increase of the atmospheric moisture content over oceans and the effects from the human activities using satellite-based observation over 1988–2006 and the 20th century simulations from 22 climate models.

The magnitudes of the water cycle amplification to the surface warming vary with observations and methods, as well as with climate models and forcing scenarios. The estimates range from a rate of 4.7 – 8% °C⁻¹ from surface observations [Wentz *et al.*, 2007; Durack *et al.*, 2012; Skliris *et al.*, 2014] to a slower rate of 2 – 4.5% °C⁻¹ from model simulations [Allen and Ingram, 2002; Held and Soden, 2006; Durack *et al.* 2012; Skliris *et al.* 2016].

Sea surface salinity (SSS) has long been suggested as an indicator of the water cycle changes, because of the tight correlation between the distributions of the climatological mean SSS and E–P [Talley, 2002; Schmitt, 2008; Lagerloef *et al.*, 2010; Yu, 2011]. Studies based on salinity observations provide more evidence for the acceleration of the global water cycle, presenting enhanced salinity in E dominated regions and reduced salinity in P dominated regions [Hosoda *et al.*, 2009; Durack and Wijffels, 2010; Helm *et al.*, 2010]. Using 50 years surface salinity observations, Durack *et al.* [2012] found an intensification of the global water cycle at a rate of $8 \pm 5\%$ per degree of surface warming over 1950–2000. Uncertainty, however, does exist in estimating the rate of the global water cycle changes. Based on full-depth salinity observations, Skliris *et al.* [2016] inferred a water cycle amplification rate of $3.0 \pm 1.6\% \text{ } ^\circ\text{C}^{-1}$ over 1950–2010, which is about half the CC rate ($\sim 7\% \text{ } ^\circ\text{C}^{-1}$). Such a rate is also suggested by climate models, which is about $2 - 4.5\% \text{ } ^\circ\text{C}^{-1}$ [Allen and Ingram, 2002; Held and Soden, 2006; Durack *et al.* 2012; Skliris *et al.*, 2016].

Despite the uncertainty of the magnitudes, studies have demonstrated the robustness of a strengthening in the global water cycle. As the global mean surface temperature increases, this robust global water cycle change indicates the enhanced intensity and frequency of the floods and droughts in relatively wet and dry regions, with great potential impacts on local ecosystems and societies [Trenberth, 2011; Chou *et al.*, 2013; Liu and Allan, 2013; Allan *et al.*, 2014]. With respect to the dynamical ocean response, little is known about the impact of the global water cycle intensification on the ocean general circulation, which is one of the objectives of this study and will be addressed in Chapter 4.

CHAPTER 3

Data and Methodology

In this chapter, the freshwater flux data sets will be described and compared in the beginning. The following sections will introduce the model set-up, the salinity boundary conditions, and the experiments. The focus will be on the principle and advantage/disadvantage of each salinity boundary condition. Importantly, the components of the “volume flux” will be dictated.

3.1 Freshwater flux data

In this section, the river runoff data, along with the evaporation and precipitation data sets from the NCEP/NCAR Reanalysis, the Hamburg Ocean Atmosphere Parameters and Fluxes from Satellite Data (HOAPS), and the Max-Planck-Institute Earth System Model (MPI-ESM) are summarized.

River runoff

As one of the basic components of the hydrological cycle, river runoff (R) contributes about 10% to the total freshwater input into the global ocean [*Schmitt, 1995; Oki and Kanae, 2006;*

Schanze et al., 2010]. The contribution from river discharge is also considered in this study. The monthly climatology runoff data on a $1^\circ \times 1^\circ$ grid obtained from *Fekete et al.* [1999] (Fig. 3.1) is incorporated into the forcing as time-constant for each month to adjust the E–P surface flux from NCEP and HOAPS data sets, which will be shown below in Figs. 3.2 and 3.3.

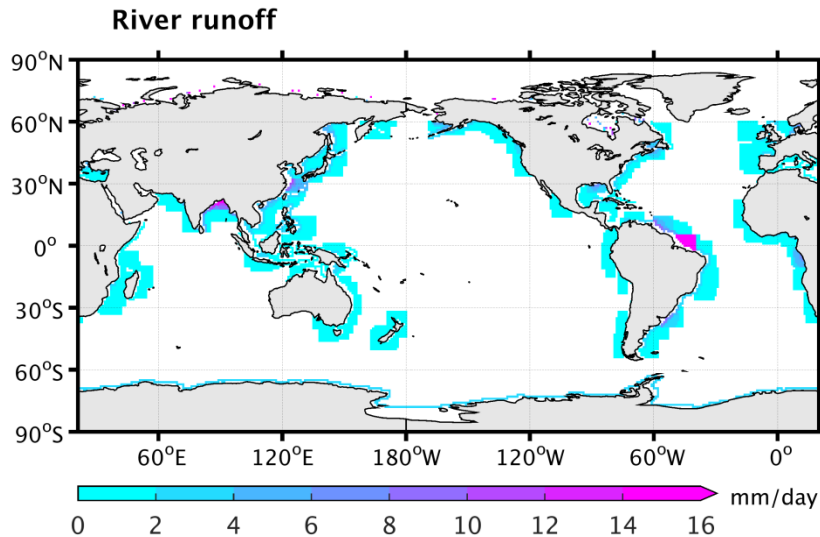


Figure 3.1 Global annual river discharge into the oceans from *Fekete et al.* [1999], which is imposed onto the E–P surface flux from NCEP and HOAPS data sets.

NCEP

The evaporation and precipitation for the volume flux forcing are derived from the NCEP/NCAR Reanalysis 1 surface flux data, covering the period 1948 to present. To compare with the HOAPS data, the climatological E–P–R field and the zonal averages are constructed over the overlapping years with the HOAPS data from 1988 to 2011, expressed in mm/day (Fig. 3.2). The global spatial mean is removed and the positive value means freshwater flux from the ocean to the atmosphere. Evaporation locates predominantly in the western boundary current areas and the subtropical oceans, while precipitation is observable in the intertropical convergence zone (ITCZ) and in the subpolar oceans. The pattern, in general, agrees with the E–P pattern based on other data sets shown in previous research [e.g. *Schmitt*, 1995; *Schanze et al.*, 2010].

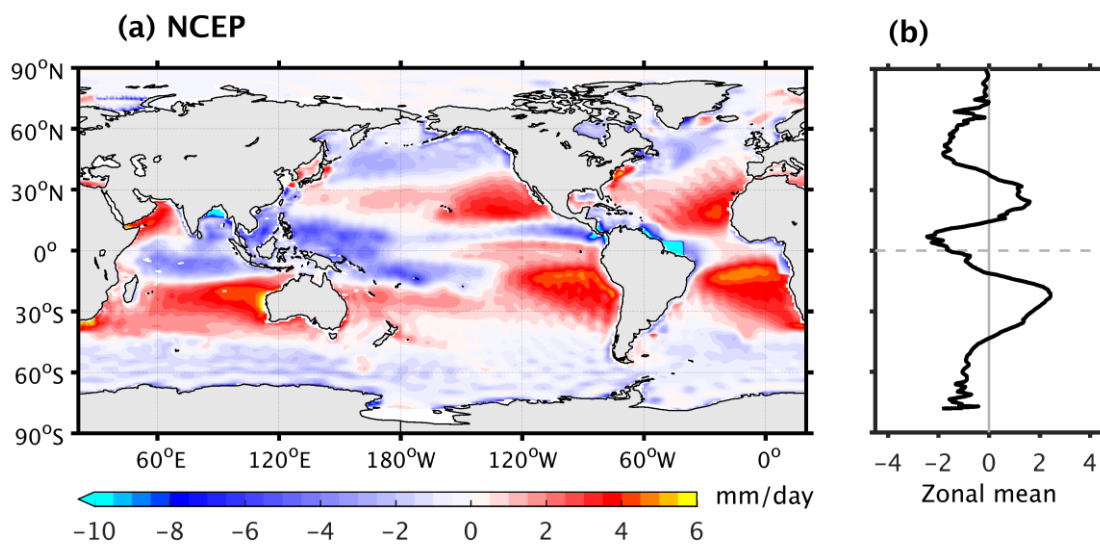


Figure 3.2 (a) Climatological mean field and (b) zonal mean of E–P–R (mm/day) from NCEP for the period 1988–2011.

HOAPS

HOAPS is a completely satellite-based data set providing fields of precipitation, evaporation, turbulent heat fluxes and related atmospheric variables over global ice-free oceans. The monthly averages of the evaporation and precipitation with a spatial resolution of $0.5^\circ \times 0.5^\circ$ from the HOAPS 3.3 [Andersson *et al.*, 2010; Fennig *et al.*, 2012] imposed with the climatological runoff data (hereinafter referred to as HOAPS) are used to compare with the results derived from the NCEP data. The version HOAPS 3.3 is similar to HOAPS 3.2 (the latest public release) with longer temporal coverage from July 1987 to December 2012. It is an unofficially released version produced by the Deutsche Forschungsgemeinschaft funded research group FOR 1740. Figure 3.3 displays the climatological E–P–R field and its zonal mean from HOAPS (global mean removed).

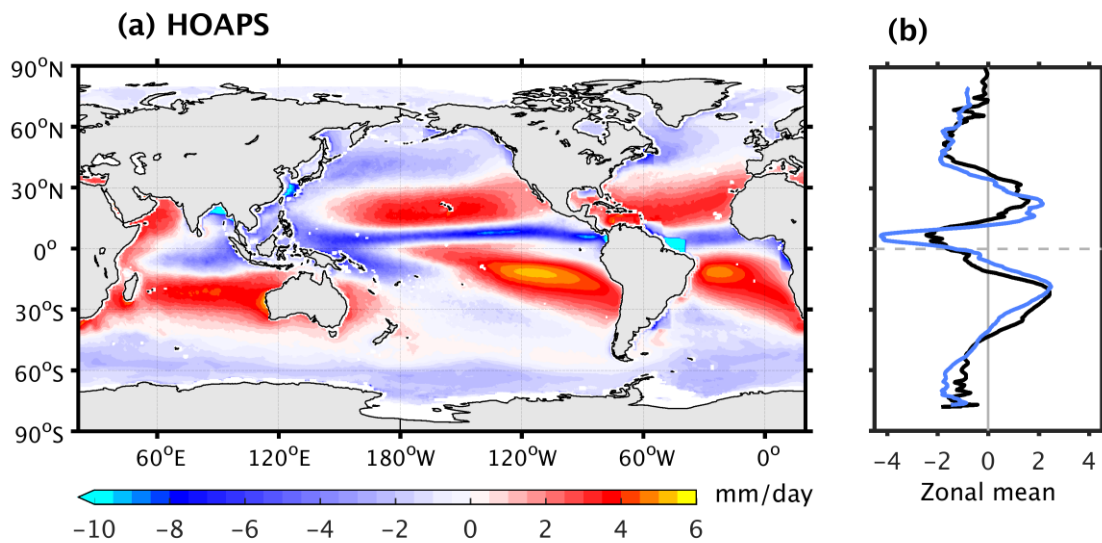


Figure 3.3 (a) Climatological mean field and (b) zonal mean of E–P–R (mm/day) from HOAPS for the period 1988–2011. The superimposed black curve in (b) is the zonal mean from NCEP as a reference for comparison.

Comparing these two data sets, the spatial patterns agree well in general. The large difference locates in the ITCZ regions of the Pacific and Atlantic oceans, where the precipitation in HOAPS is obviously higher than that in NCEP. This is more apparent in the comparison of the zonal averages (Fig. 3.3b), with the minimum of -4.25 mm/day for HOAPS and -2.45 mm/day for NCEP. Another feature is the slight equatorward shift of the evaporation dominated band in the subtropical regions. A more sophisticated intercomparison between these two data sets concerning seasonal and interannual variability can be found in *Romanova et al.* [2010].

MPI-ESM

The MPI-ESM is a coupled atmosphere-ocean general circulation model, including a representation of the carbon cycle. It has been used in a large number of the CMIP5

simulations based on observed forcing or the RCP scenarios [Giorgetta *et al.*, 2013]. The evaporation and precipitation data from three experiments *historical*, *RCP4.5* and *RCP8.5* of the low resolution (LR) version of MPI-ESM (MPI-ESM LR) [Giorgetta *et al.*, 2012a; 2012b; 2012c] are applied in this study to present the projected GSC response to the climate change in the future. The historical experiment starts from 1850 to 2005 with the influence of the natural and anthropogenic forcing derived from observations. The RCP4.5 and RCP8.5 experiments continue from 2006 until 2100 with radiative forcing of 4.5 W/m^2 and 8.5 W/m^2 in 2100, respectively. Three realizations exist for each of these experiments. Therefore, the ensemble-mean of each experiment is used in this analysis.

The regional patterns of the near-surface temperature and precipitation changes from the late 20th century in the historical experiment referred to the 1000 years preindustrial control simulation *piControl* and from the late 21st century in the three RCP scenarios referred to the historical experiment are displayed in *Figure 10* from Giorgetta *et al.* [2013]. As illustrated by Giorgetta *et al.* [2013], the amplitude of the warming strongly depends on the RCP scenarios, while the high similarity among the patterns suggests a robust local amplification factor in MPI-ESM across different scenarios with respect to global warming. The precipitation changes also share similar patterns among all scenarios and the warmest scenario RCP8.5 exhibits the strongest strength of the changes.

The E–P anomalies over the ocean are illustrated in Fig. 3.4a showing the changes for the period 2081–2100 relative to 1986–2005 under the RCP8.5 scenario. The subtropics show enhanced evaporation (water loss from the ocean), while in the tropics and in subpolar regions an enhanced net transport of fresh water into the ocean can be diagnosed. The pattern agrees well except for the lack of signal along the central equatorial Pacific with the ensemble mean shown by Levang and Schmitt [2015]. As expected, the E–P anomalies for RCP4.5 and RCP8.5 share similar intensified spatial patterns, while the amplitude of the anomaly for RCP8.5 is twice as large as the anomaly for RCP4.5 (shown here only by the zonal means in Fig. 3.4b).

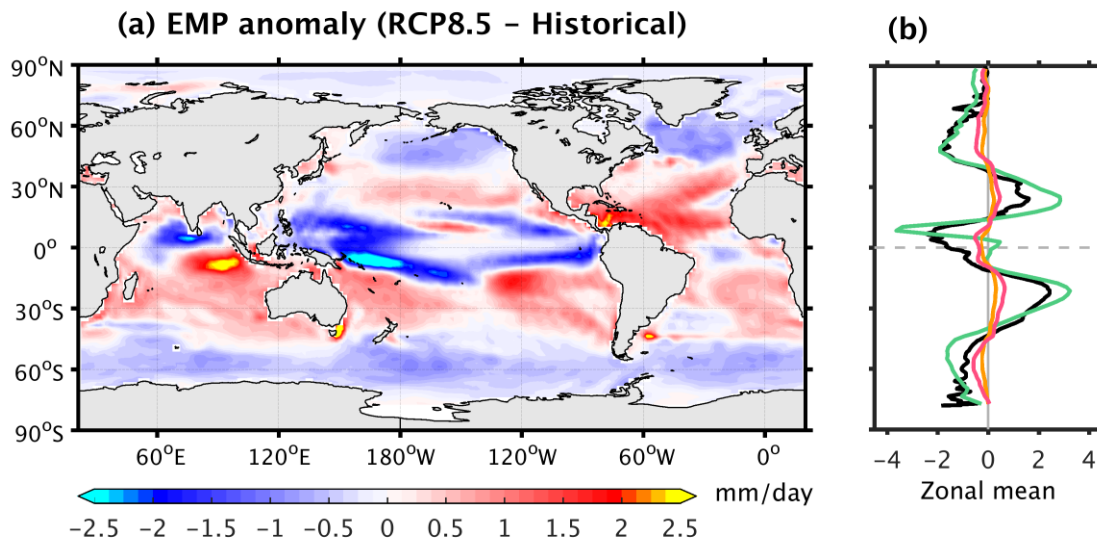


Figure 3.4 (a) E–P anomalies for the RCP8.5 scenario over the period 2081–2100 relative to 1986–2005 from the ensemble-mean of the MPI-ESM LR data set. (b) Zonal means of the E–P anomalies for RCP4.5 (orange) and RCP8.5 scenarios (red); superimposed are the zonal mean E–P over the reference period from the historical experiment (green) and the zonal mean from NCEP (black) as references for comparison.

Figure 3.5 illustrates the projected changes of E–P for historical (green), RCP4.5 (orange), and RCP8.5 scenarios (red) over the E dominating and P dominating regions, separately. The E (P) dominating regions are defined by the positive (negative) grids based on the time-mean E–P from the historical simulation over the reference period 1986–2005. The integral of the time-mean E–P over the E (P) dominating regions for the reference period is 4.77 Sv (–3.75 Sv) and is considered as the reference for the respective region. The time series of the E–P changes are then calculated as the anomalies of the integral of E–P relative to the respective reference value over the same region.

Over the historical period, the warming is relatively weak, which is from 13.5 °C to 14.3 °C for the global mean surface air temperature from climatological 1850 conditions to 2005 [Giorgetta *et al.*, 2013]. For the E dominating regions, the E–P changes have been projected to increase by around 0.29 Sv (6.1%) for RCP4.5 and 0.63 Sv (13.2%) for RCP8.5 over the

period 2081–2100 relative to 1986–2005 (the reference period average is 4.77 Sv), in response to the warming of 1.7 °C for RCP4.5 and 3.6 °C for RCP8.5. Close to the rate from the E dominating regions, the projected E–P changes in P dominating regions are about –0.24 Sv (6.4%) for RCP4.5 and –0.5 Sv (13.3%) for RCP8.5 relative to the reference of –3.75 Sv. Overall, based on this simplified and conservative calculation, the mean changes in E–P over both E dominating and P dominating regions from MPI-ESM-LR RCP8.5 show a 13.2% intensification in response to a 3.6 °C surface warming (3.7% °C⁻¹), which is well within the range of climate model projections.

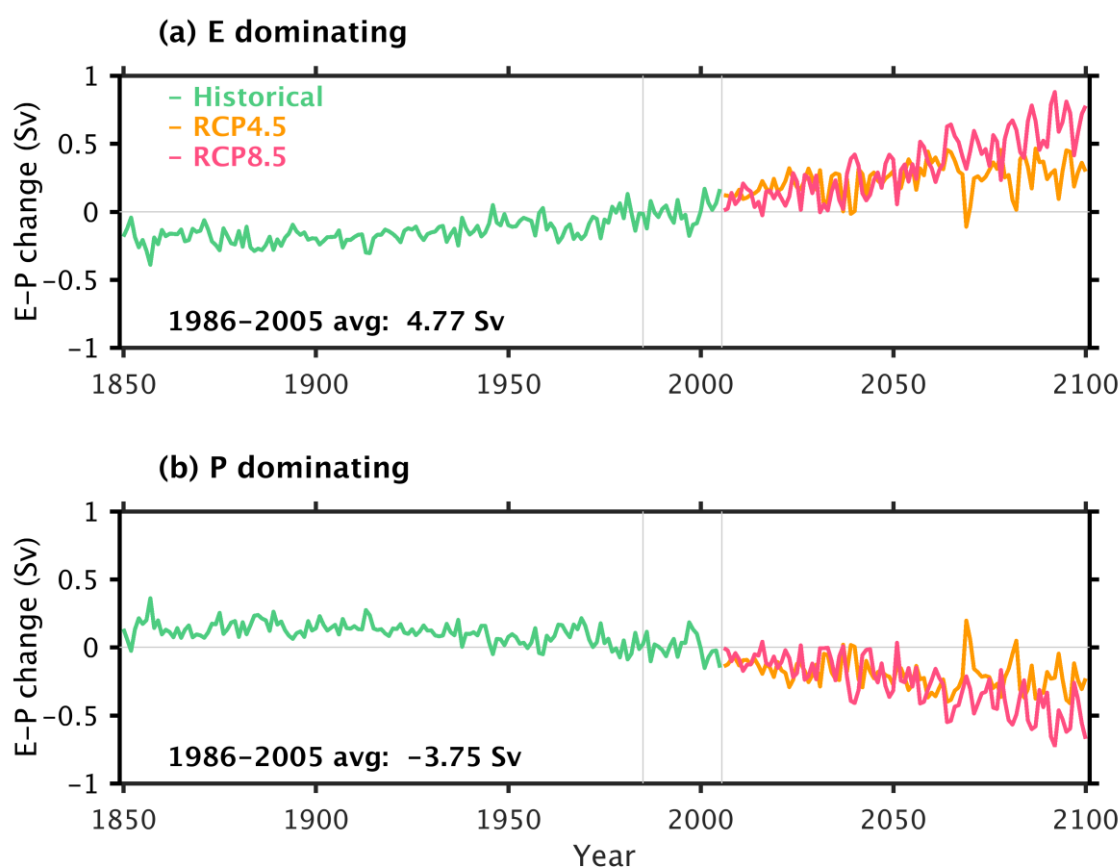


Figure 3.5 Annual time series of the E–P changes (in Sv) over the (a) E dominating and (b) P dominating regions for historical (green, 1850–2005), RCP4.5 (orange, 2006–2100), and RCP8.5 scenarios (red, 2006–2100). The E (P) dominating regions are defined by the positive (negative) grids based on the time-mean E–P from the historical simulation over the reference period 1986–2005, which is marked between the two vertical grey lines.

Because of the similarity in patterns across different scenarios, it is reasonable to analyze one and scale the responses for the others. Therefore, the RCP8.5 E–P anomaly is used as the constant perturbation to the monthly NCEP forcing for the perturbation experiments. The perturbation runs will also use two salinity boundary conditions separately and execute for the same period as the standard runs. In the end, results will be compared with the standard runs, aiming to estimate the GSC response with regard to the hydrological cycle intensification under global warming (Section 4.3).

3.2 GECCO2 set-up

The model configuration used in the study is identical to an ocean synthesis from the German contribution to the Estimating the Circulation and Climate of the Ocean (GECCO2 synthesis) described by Köhl [2015]. It is based on a similar global configuration of the Massachusetts Institute of Technology general circulation model [Marshall *et al.*, 1997], which employs the primitive equations on a staggered C grid [Arakawa and Lamb, 1977]. GECCO2 synthesis is an extension of the 2002–2007 synthesis described in detail by Köhl *et al.* [2012]. The synthesis is configured on z-levels on a spherical coordinate system with a zonal resolution of 1° , meridional resolution of $1/3^\circ$ at the equator, isotropic grids from 25° to 66° in latitude in both hemispheres, and roughly 40 km resolution in the Arctic Ocean. It has 50 vertical levels varying from 10 m in the upper layers to 500 m in the deeper layer expressing full-depth ocean floor topography. The “GM” eddy parameterization [Gent and McWilliams, 1990] is implemented and the vertical mixing is parameterized by the K-Profile Parameterization (KPP) scheme of Large *et al.* [1994]. GECCO2 also includes the dynamic/thermodynamic sea ice model of Zhang and Rothrock [2000]. Further details of the model set-up and the evaluation of the model performance in comparison to the GECCO2 synthesis can be found in Köhl *et al.* [2012] and Köhl [2015]. The model is forced by the National Centers for Environmental Prediction / National Center for Atmospheric Research (NCEP/NCAR; referred to as NCEP) Reanalysis 1 6-hourly atmospheric state [Kalnay *et al.*, 1996], covering the period 1948–2011.

3.3 Salinity boundary conditions

During the course of this study, two different salinity boundary conditions are used. Different processes are involved in these two boundary conditions, which will be introduced in detail below.

3.3.1 Virtual salt flux formulation

A virtual salt flux formulation converts the surface freshwater flux into an equivalent salt flux to represent the concentration/dilution effect resulting from the freshwater flux in the real world. The virtual salt flux at the ocean surface can be presented as:

$$F_{vsf} = (E - P - R + F - M) * S_0, \quad (3.2)$$

where F_{vsf} is the equivalent virtual salt flux into the ocean, $E - P - R$ is the net freshwater flux across the ocean surface (upward positive), F and M represent the freshwater flux associated with sea ice freezing and melting, respectively and $S_0 = 35$ psu is the reference salinity. The contribution from river discharge (R) is derived from the climatological runoff data on a $1^\circ \times 1^\circ$ grid from *Fekete et al.* [1999]. The definition of F_{vsf} ensures that the virtual salt flux has the same effect on the salinity changes as real freshwater flux except for the dilution effect and small differences in case of global volume changes. The virtual salt flux adjusts the salinity of seawater by altering its salt content (zero volume flux), whereas the freshwater flux does this by changing the volume of seawater (zero salt flux).

Discarding the volume input/output due to the real freshwater flux in this formulation, there is no freshwater flux involved vertical velocity (w_{vsf}) or the volume flux at the air-sea interface:

$$w_{vsf} = 0. \quad (3.3)$$

Therefore, ocean's response to a space-time varying volume flux in form of a GSC has been suppressed [*Roullet and Madec, 2000; Lorbacher et al., 2012; Griffies et al., 2014*]. Moreover, the virtual salt flux formulation fails to simulate sea level changes induced in the ocean by

volume flux, and the use of a mean reference salinity to convert volume flux into salt flux cannot accurately represent the local dilution effect, especially over the regions where salinity deviates significantly from the reference salinity [Huang, 1993; Roulet and Madec, 2000; Yin *et al.*, 2010].

3.3.2 Volume flux formulation

The other salinity boundary condition used in the study is represented as natural boundary condition, which was first introduced by Huang [1993]. Instead of equivalent virtual salt flux, this formulation presents the surface freshwater flux more realistically as the vertical velocity at the air-sea interface. It overcomes the above-mentioned downsides of salt flux through the upper surface and involves all dynamical effects of the freshwater flux. For models that do not include sea ice module, the “volume flux” can simply be defined with three components: evaporation, precipitation and runoff (E, P and R). They alter both salinity and volume of the seawater and thus represent a salt flux and a volume flux at the same time.

Because the GECCO2 set-up contains a sea ice model, special attention is required for the sea ice boundary conditions. On one hand, sea ice freezing and melting only influence the salinity of the seawater but not the volume, because the associated volume flux is compensated by the change in pressure loading from the sea ice so that no GSC is initiated. Thus, the salt flux (F_{vf}) associated with this process is presented the same as in equation (3.2):

$$F_{vf} = (F - M) * S_0. \quad (3.4)$$

On the other hand, in addition to the rainfall over the ocean, snowfall on sea ice also affects the volume of the seawater by displacing water via sinking of sea ice but does not directly affect salinity. Since the present configuration does not use pressure loading, the vertical velocity (w_{vf}) or the volume flux at the air-sea interface is defined as follows:

$$w_{vf} = E - P - R - Snow, \quad (3.5)$$

where P is the precipitation, especially the rainfall over the ocean (liquid), and $Snow$ means the snowfall on the sea ice (solid). Different from *Tartinville et al.* [2001], there is no delay until snow melts or is transformed into snow ice. Combining these four components that cause volume changes of the seawater, we present the volume flux formulation. The complementary process of sublimation is, however, not part of the bulk formulae parameterization.

3.4 Experiments

Two pairs of experiments are conducted and contrasted against each other by using different volume flux data sets. For each pair, the reference run uses the virtual salt flux whereas the other run applies the volume flux forcing. From the differences of each pair, mechanisms involved in a dynamical adjustment of ocean circulation to the surface volume flux forcing can be identified and quantified.

3.4.1 NCEP response experiments

Mechanisms involved in the dynamical adjustment of ocean circulation to surface volume flux forcing are analyzed from the differences between the standard runs over the period 1949–2011. Forced with the same present-day monthly freshwater flux data set from NCEP, the standard runs with volume flux formulation and virtual salt flux formulation are hereinafter referred to as VF and VSF, respectively. The difference between VF and VSF will be abbreviated as $\Delta NCEP$ to avoid redundancy when comparing with the difference between the perturbation runs in Chapter 4.

3.4.2 Perturbation experiments

Results and insight obtained from the standard runs will be used to estimate the impact of future changes in the global hydrological cycle as simulated by coupled climate models under climate change scenarios on the ocean circulation. To this end, we conduct another pair of runs with additional RCP8.5 E–P anomaly perturbation (will be shown in Fig. 3.4a) added as constant to the monthly NCEP freshwater flux forcing. In the perturbation runs, again two salinity boundary conditions are used and referred to as VF_{N+RCP} and VSF_{N+RCP} , respectively. The difference between VF_{N+RCP} and VSF_{N+RCP} will be abbreviated as ΔRCP . In Chapter 4, the anomalies from ΔRCP relative to $\Delta NCEP$ (referred to as $\Delta RCP - \Delta NCEP$) will be applied to estimate the changes related to the global hydrological cycle intensification.

3.4.3 Relaxation tests

For all the experiments, a surface salinity relaxation towards the climatological salinity from the World Ocean Atlas 2005 [Antonov *et al.*, 2006] is applied to the top layer (10 m) with a relaxation timescale of 30 days. The relaxation is similar to a virtual salt flux such that it does not influence the volume flux induced differences. To test the possible attenuation effect from the relaxation, shorter runs without relaxation have been carried out.

The results assure that the impact of relaxation on the volume flux induced ocean response is not significant. For the runs without any relaxation, the barotropic circulation induced by surface volume flux is very similar to the results from the configurations we use (Fig. 3.6). Over time scales of several decades, the relaxation component is however required to maintain a reasonable surface salinity distribution and overturning circulation, since flux boundary conditions are known to be unstable to small perturbations [Bryan, 1986].

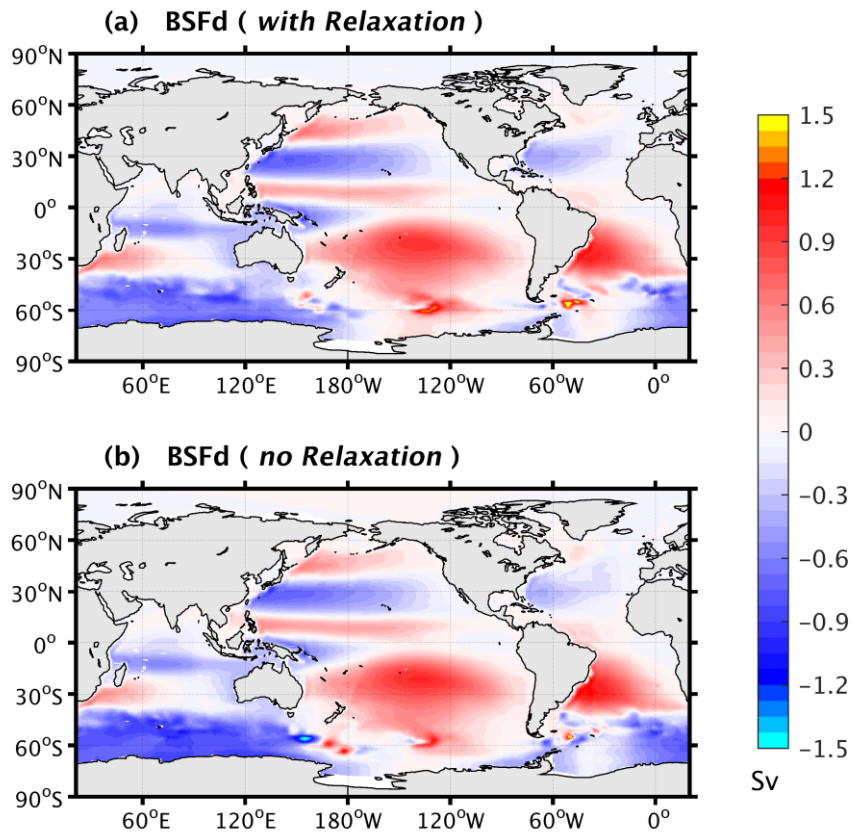


Figure 3.6 Test of the relaxation. The first 10 years time-mean barotropic streamfunction difference (BSFd) between VF and VSF (a) with relaxation and (b) without relaxation.

CHAPTER 4

Dynamical ocean response to projected changes of the global water cycle

4.1 Introduction

This chapter aims to systematically analyze the mechanisms involved in the dynamical adjustment of ocean circulation to the changing surface volume flux, especially to the projected amplification of the global water cycle. Following *Huang* [1993] and *Yin et al.* [2010], this will be done by performing various model runs using the GECCO2 configuration but with differing salinity boundary conditions and forcing data sets. In a first step (Section 4.2), the dynamical ocean response to the NCEP surface volume flux forcing will be studied by comparing the volume flux run (VF) with the virtual salt flux run (VSF) over the period 1949–2011. The resulting difference in the barotropic circulations is ascribed to the GSC from the model simulation and compared with the GSC derived directly from the volume flux data based on the Goldsbrough relation. The rest of the section continues with volume flux forcing associated oceanic changes, such as sea level, heat and freshwater transport properties, MOC and the pathways of the surface volume flux and fresh water in the interior ocean. In a next step (Section 4.3), we will impose the flux anomalies shown in Fig. 3.4a to identify

which of those mechanisms quantitatively act in respect to the intensification of the hydrological cycle in a future warmer world.

Specific questions to be addressed in this chapter include:

- What physical processes are responsible for the sea level changes induced by surface volume flux forcing?
- How does the fresh water spread in the interior ocean?
- Does the changed circulation further influence the oceanic heat and freshwater transport properties? If so, what are the driving mechanisms?

The answers to these questions will lead us to the primary question:

- What is the dynamical GSC response to the acceleration of the global water cycle in a future warmer world?

4.2 Dynamical adjustment processes

The analysis of processes participating in the dynamical adjustment of the ocean to surface volume flux forcing is subdivided into (1) the gyre circulation, (2) the meridional overturning circulation, and (3) the impact on regional sea level changes. The involved processes will be analyzed here. The insight gained will be used in next section to quantify those processes that participate in the adjustment to the RCP8.5 E–P anomaly perturbation.

4.2.1 Changes of the gyre circulation

The barotropic streamfunction (BSF) difference between VF and VSF is depicted in Fig. 4.1 and can be interpreted as the barotropic circulation resulting directly from the presence of surface volume flux. For the present-day volume flux forcing, the associated circulation is on

the order of 1 Sv and shows similar spatial structure but higher magnitude than previous results [Roullet and Madec, 2000; Tartinville et al., 2001].

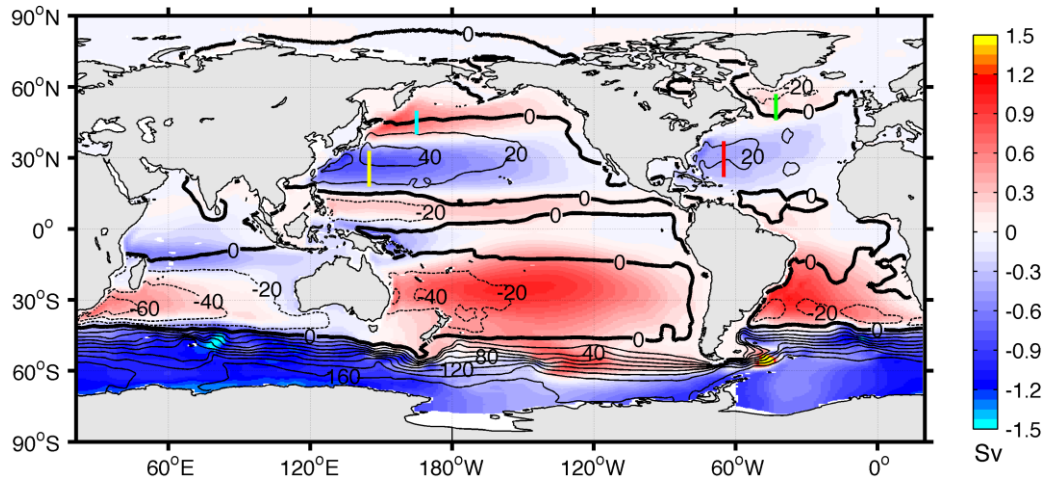


Figure 4.1 Time-mean barotropic streamfunction from VF is shown in contours (in Sv; the contour interval is 20 Sv). Color shading shows the difference between VF and VSF. The solid contours indicate positive values, which in the Northern Hemisphere represent an anticyclonic circulation. The four colored lines in the Northern Hemisphere indicate the locations of the sections from which time series of meridional averages are calculated (Fig. 4.7).

In the subtropical North Atlantic and North Pacific, the differences result in cyclonic gyres with southward western boundary currents amounting up to 0.6 Sv and 1.0 Sv, respectively. The BSF difference in the subpolar North Pacific is anticyclonic and reaches 0.9 Sv at the western boundary. The anticyclonic gyres in the subpolar North Atlantic and in the Pacific Equatorial Current System region are about 0.3 Sv.

For the Southern Hemisphere, the clockwise circulations in subtropical basins are around 1 Sv (~ 1.0 Sv in the Atlantic and Pacific, and ~ 0.6 Sv in the Indian Ocean) and the eastward flow in the Indian South Equatorial Current region is about 0.6 Sv. In the Antarctic Circumpolar Current (ACC) region, the flow is westward with the strength of 1.5 Sv. We note that all these

flows are in the opposite directions to the mean currents in VF and therefore weaken the wind-driven gyres as we would expect from theoretical considerations.

Pattern and amplitude of the BSF difference shown in Fig. 4.1 can be compared with the time-mean dynamical gyre response of the circulation to a surface freshwater forcing as predicted by the Goldsbrough-Stommel theory. Respective results are shown in Fig. 4.2a based on the NCEP surface freshwater flux. A visual comparison of Figs. 4.1 and 4.2a reveals that the GSC and the BSF difference display very similar patterns and amplitudes, suggesting that over large areas the model's dynamical response to the volume flux forcing at the surface can be accurately described by the barotropic GSC formulation. This holds for the subtropical gyres in the Northern Hemisphere, however, due to the lack of meridional boundaries the streamfunction is difficult to define in high latitudes and was not attempted here.

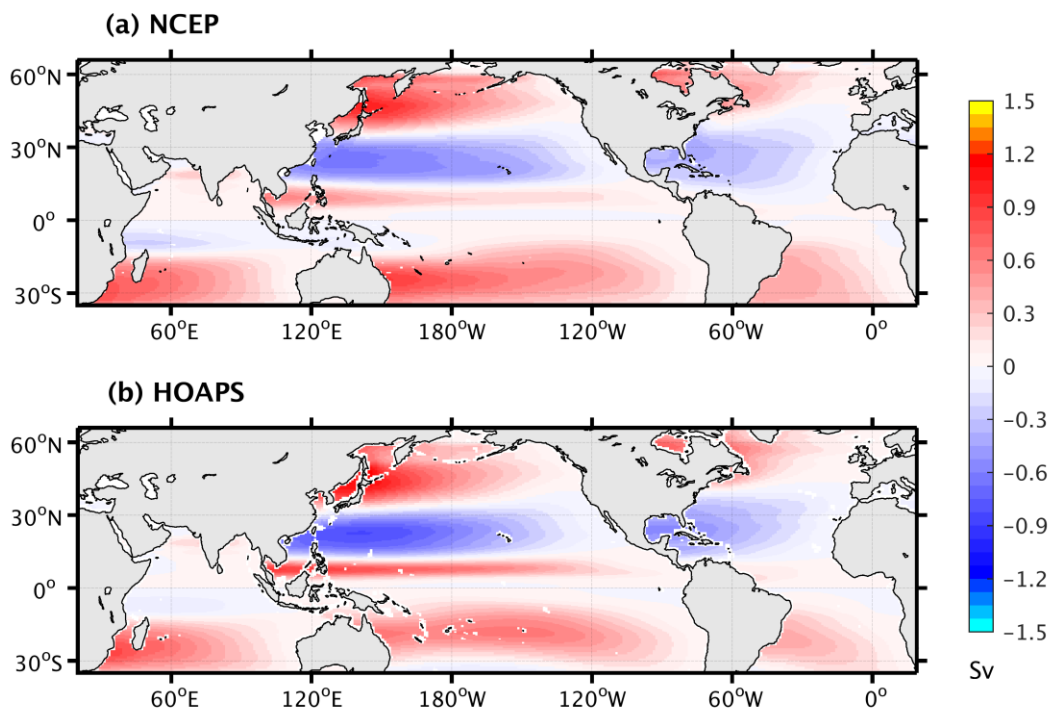


Figure 4.2 Time-mean Goldsbrough-Stommel circulation (in Sv) calculated directly from the surface volume flux from (a) NCEP and (b) HOAPS, averaged over the period 1988–2011.

In the subpolar North Atlantic, the dominating precipitation drives a southward mass transport in the interior ocean, which is closed by northward western boundary current in the Labrador Sea [*Stommel*, 1957]. In contrast, the northward flow forced by excess evaporation in the interior subtropical ocean is balanced by the southward western boundary current thereby opposing the wind-driven western boundary currents there. Relations are of opposite sign in the Southern Hemisphere.

To conduct a further comparison and to provide an uncertainty estimate of the freshwater driven circulation component resulting from uncertainties in the surface freshwater forcing, we use the monthly freshwater flux from HOAPS for a second estimate of the GSC (see the introduction of HOAPS in Section 3.1). The results, shown in Fig. 4.2b basically agree with the previous results from the NCEP volume flux forcing (Fig. 4.2a) in spatial structure; however, they show differences in amplitude, particularly in low latitudes. This results from the fact that the volume flux of HOAPS is stronger in the evaporation-dominated regions and also in the precipitation-dominated ITCZ regions comparing with the NCEP volume flux forcing. Overall, the GSC resulting from the NCEP forcing is slightly weaker in the subtropical basins and stronger in the subpolar basins as compared to the HOAPS solution.

We note that, contrary to intuitions, any river runoff entering the ocean at western boundaries, such as the Amazon River, does not directly induce any distinguishable dynamical GSC gyre feature. In contrast, freshwater sources at eastern boundaries (e.g., the Congo River) integrate up across the basin together with the surface freshwater forcing on the path. Nevertheless, in the global picture of balanced freshwater flux, the Amazon outflow drives a *Stommel-Arons* like circulation [*Stommel and Arons*, 1959] that is accounted for in a GSC driven by the evaporation needed to balance the freshwater input through the Amazon River.

As mentioned above, differences between Figs. 4.1 and 4.2a do exist and are especially clear at high latitudes of both hemispheres. This is similar to the description of the barotropic circulation by the Sverdrup relation. For instance, *Wunsch* [2011] found that at mid and low latitudes the Sverdrup balance provides a useful estimate while it fails at high latitudes due to

the longer adjustment time scales. Moreover, at high latitudes the circulation is more barotropic and interaction with topography becomes more relevant such that the flat bottom assumption breaks down.

4.2.2 Impact on meridional overturning circulation

The meridional overturning circulation (MOC) associated with the surface volume flux forcing is shown in Figs. 4.3b and 4.3d separately for the Atlantic and Pacific-Indian oceans as the difference between VF and VSF. These differences have to be compared with the climatological mean overturning streamfunction resulting from the full forcing (Figs. 4.3a and 4.3c). The MOC is represented by the streamfunction in the latitude-depth plane,

$$\psi(y, z) = \int_{-D}^0 \int_{west}^{east} v(x, y, z) dx dz, \quad (4.1)$$

where $v(x, y, z)$ is the meridional velocity component, and D is the depth of the ocean. The Atlantic MOC in VF (Fig. 4.3a) shows the northward transport of the warm salty water in the upper 1000 m, the formation of the North Atlantic Deep Water (NADW), and the southward return flow of NADW at 1000–3500 m. In the deeper ocean, the anticlockwise meridional cell represents the deep overturning related to the northward transport of the Antarctic Bottom Water. In the Pacific-Indian oceans (Fig. 4.3c), the shallow subtropical cells and the bottom water cell are stronger than in the Atlantic. Overall, our estimates agree with other models [e.g. *Maltrud and McClean*, 2005]; however, in comparison to transport estimates at 26.5°N from the Rapid project [e.g. *Cunningham et al.*, 2007], the overturning transport is about 4–5 Sv weaker.

As for the MOC difference, a visual inspection suggests that the surface volume flux driven overturning circulation mainly occurs in the upper 500 m, weakening the shallow cells (~0.1 Sv in the Atlantic and up to 1 Sv in the southern Pacific-Indian oceans). In addition, the bottom water cells in both Atlantic and Pacific-Indian oceans are enhanced, albeit only slightly (~0.1 Sv).

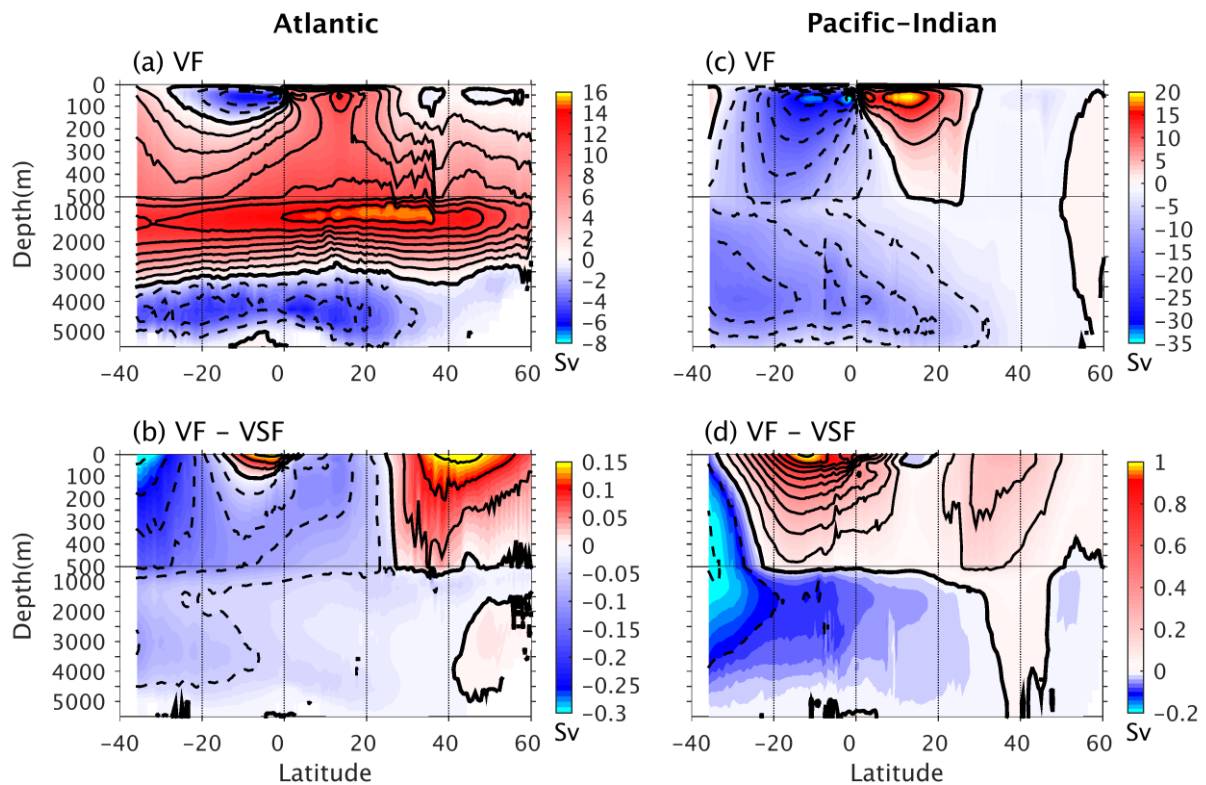


Figure 4.3 Time-mean meridional overturning streamfunction (in Sv), shown for (a and b) the Atlantic and (c and d) the Pacific-Indian oceans. The estimations are displayed as (a and c) VF, and (b and d) the difference between VF and VSF.

Since the overturning circulation describes the meridional and vertical transports of volume, at the surface, the anomalies shown in Figs. 4.3b and 4.3d have to match the volume flux entering the ocean through the surface. Its surface value can therefore independently be calculated from the imposed volume flux forcing. It turns out that the overturning transport and volume transport are in fact identical, suggesting that the MOC changes can be regarded as the pathways of the surface volume flux in the interior ocean.

Combining the results of different basins to compare the volume flux induced overturning transport changes in global perspective (Fig. 4.4a), our estimate in the upper 500 m agrees quite well with previous results both in structure and in amplitude [*Figure 3b* from *Tartinville*

et al., 2001]. However, the bottom cell of the previous result is nearly double in comparison to our simulation and their response to volume flux forcing is more complex below 2000m.

Little is known about how the fresh water entering the ocean through the surface spreads subsequently in the interior ocean and how it is related to the pathways of the surface volume flux forcing. In the volume flux forced run, the fresh water entering the ocean is associated with an equal amount of volume entering the ocean. It is therefore tempting to assume that this tight relation continues into the interior such that the fresh water spreads as the difference between the overturning streamfunctions shown in Figs. 4.3b and 4.3d. This assumption was actually implicitly assumed by *Tartinville et al.* [2001] to arrive at the conclusion that the fresh water entering through the surface spreads mainly in the upper part of the ocean. However, the tight connection is not granted, since the volume flux forcing may drive an additional overturning circulation, which is not associated with the spreading of fresh water. In order to test the assumption, we build on *Boccaletti et al.* [2005], who have introduced a heat function to diagnose the vertical structure of the oceanic heat transport. Analogous to their definition a freshwater function can trivially be introduced by replacing temperature in their calculation with fresh water. Similar to the heat function the freshwater function then illustrates the continuation of the pathways of fresh water in the ocean. Following their guidelines, we define the freshwater function,

$$F = \int \overline{vF_a} - \overline{v\hat{F}_a}(\psi) dz, \quad (4.2)$$

where the overbar represents the zonal integral, and F_a is the freshwater anomaly defined as a negative salinity anomaly normalized by the reference salinity S_0 ,

$$F_a = 1 - \frac{S}{S_0}. \quad (4.3)$$

For the first term on the right-hand side of equation (4.2), the vertical integral of it provides the total northward freshwater transport. As illustrated by *Boccaletti et al.* [2005], there is a redundancy in the calculation, which does not contribute to the total transport. The idea is that the fresh water that contributes to the net meridional freshwater transport is only the portion of the salinity that varies along a closed streamline. Therefore, the transport function related

to a constant salinity along a closed streamline should be eliminated, which is done by subtracting the second term on the right-hand side of equation (4.2). $\widehat{S}_a(\psi)$ is the freshwater anomalies averaged along the appropriate streamlines from ψ in equation (4.1); since closed cells of the streamlines are required this can only be done for the global ocean.

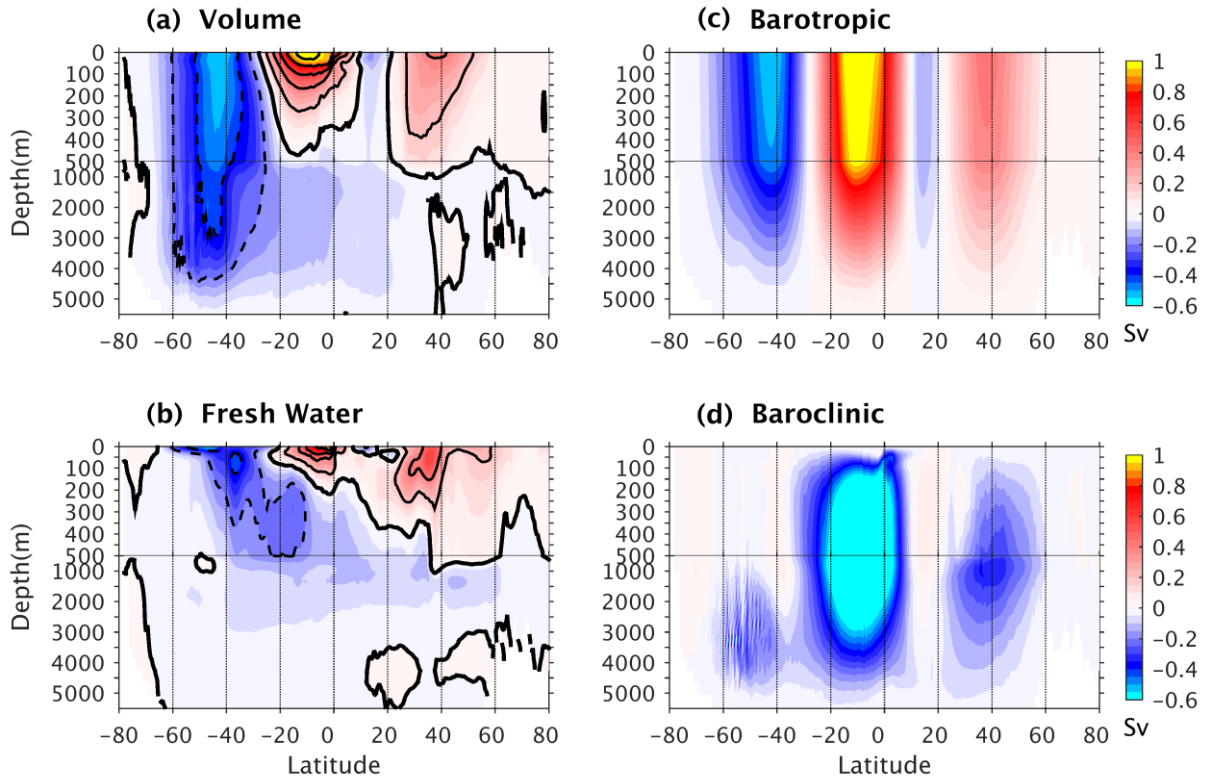


Figure 4.4 Global time-mean meridional overturning streamfunction from (a) the difference between VF and VSF, and (b) the freshwater function (see equation (4.2) and text for details). (c) Barotropic and (d) baroclinic components from the decomposition of the field shown in (a).

The globally integrated streamfunction of fresh water presented in Fig. 4.4b can be compared with the streamlines of the volume flux forcing shown in Fig. 4.4a. By definition, both streamfunctions need to agree at the surface. However, further below in the water column, the structures start to diverge with mostly larger signals for the volume transport. A particularly large difference exists in the Southern Ocean, where the pathway of volume transport reaches to deeper levels. A striking similarity between them remains, however; it reveals that the

transport of fresh water indeed mainly follows the volume flux changes, and similar to the heat function the spreading of fresh water is confined to the upper 500 m of the ocean. The question arises therefore why the spreading of volume and fresh water diverges with depth. The answer to this question will give important hints as to how the circulation is adjusting over its full water column to surface freshwater forcing anomalies.

Treguier et al. [2014] provided a decomposition of the salinity transports in which a barotropic flow is assumed to compensate for the mass flux differences, which implies a certain form of overturning circulation. The respective overturning difference shown in Figs. 4.3b and 4.3d provides a means to evaluate this concept. Our vertical flow distribution shows that the transport is not barotropic but rather surface intensified. The decomposition into the barotropic and baroclinic components of the global overturning difference discloses this in a clearer way by Figs. 4.4c and 4.4d. The global overturning streamfunction difference and its barotropic component look similar but not identical to each other, while the baroclinic component can be as large as -1 Sv. A barotropic flow is only appropriate for the responses on very short time scales of typically less than one month. Beyond this timescale baroclinic compensations will take place, leading to a concentration of the flow changes in the upper layers. The example illustrates why the simple identification of volume with fresh water fails. If the compensation velocity was barotropic and the fresh water would spread as the volume, the freshwater function would be independent of the circulation and determined by the surface flux alone.

However, the calculation of the freshwater function suffers from two main uncertainties that may mask the differences to the volume transport. First, the equilibrium condition that is never perfectly met in a changing ocean and second, there is an arbitrariness associated with the definition of the streamlines of constant freshwater values, which impacts the details of the freshwater streamfunction. Despite these shortcomings, there is a fundamental difference between the spreading of volume and freshwater associated with the additionally diffusive fluxes. Though these are small and they contribute little to the streamfunction itself, in equilibrium the salinity distribution results from a balance between the advective and diffusive fluxes and the latter modify the freshwater spreading pathways.

4.2.3 Sea level changes associated with surface volume flux

As discussed in the previous sections, the presence of a surface volume flux is associated with a change in the ocean circulation. Hence, we expect that integral quantities, such as sea level, are changing as well in response to any change in surface volume flux forcing [see also *Yin et al.*, 2010].

The regional sea level pattern that is associated with the surface volume flux forcing is illustrated in Fig. 4.5a in form of the time-mean sea surface height (SSH) difference between VF and VSF (global mean offsets removed in the figure). In agreement with the general relation between the barotropic streamfunction and the sea level, the figure reveals, except for the sign change across the equator, nearly identical spatial SSH patterns as they have been seen in Fig. 4.1 for the BSF. A visual comparison of both figures suggests that a freshwater volume flux forcing leads to SSH structures that are higher by up to 1 cm in the tropical Pacific, subpolar and ACC regions, and lower by a similar amount in the subtropical basins of the world oceans. Apparently, a freshwater volume flux forcing and its change need to be considered for accurately simulating regional sea level change amplitudes. This will also hold for any coupled climate model used to provide sea level projections under climate change scenarios.

A closer inspection reveals that the sea level change induced by the volume flux also reflects the changes in seawater temperature and salinity, shown by the steric height difference between VF and VSF (Fig. 4.5b). The respective field exhibits almost identical structures and values in most basins as those seen in Fig. 4.5a. However, some differences remain, e.g., the higher steric height anomalies compared with the SSH anomalies in the Arctic, indicative of an additional mass redistribution across the global ocean in response to a surface volume flux forcing.

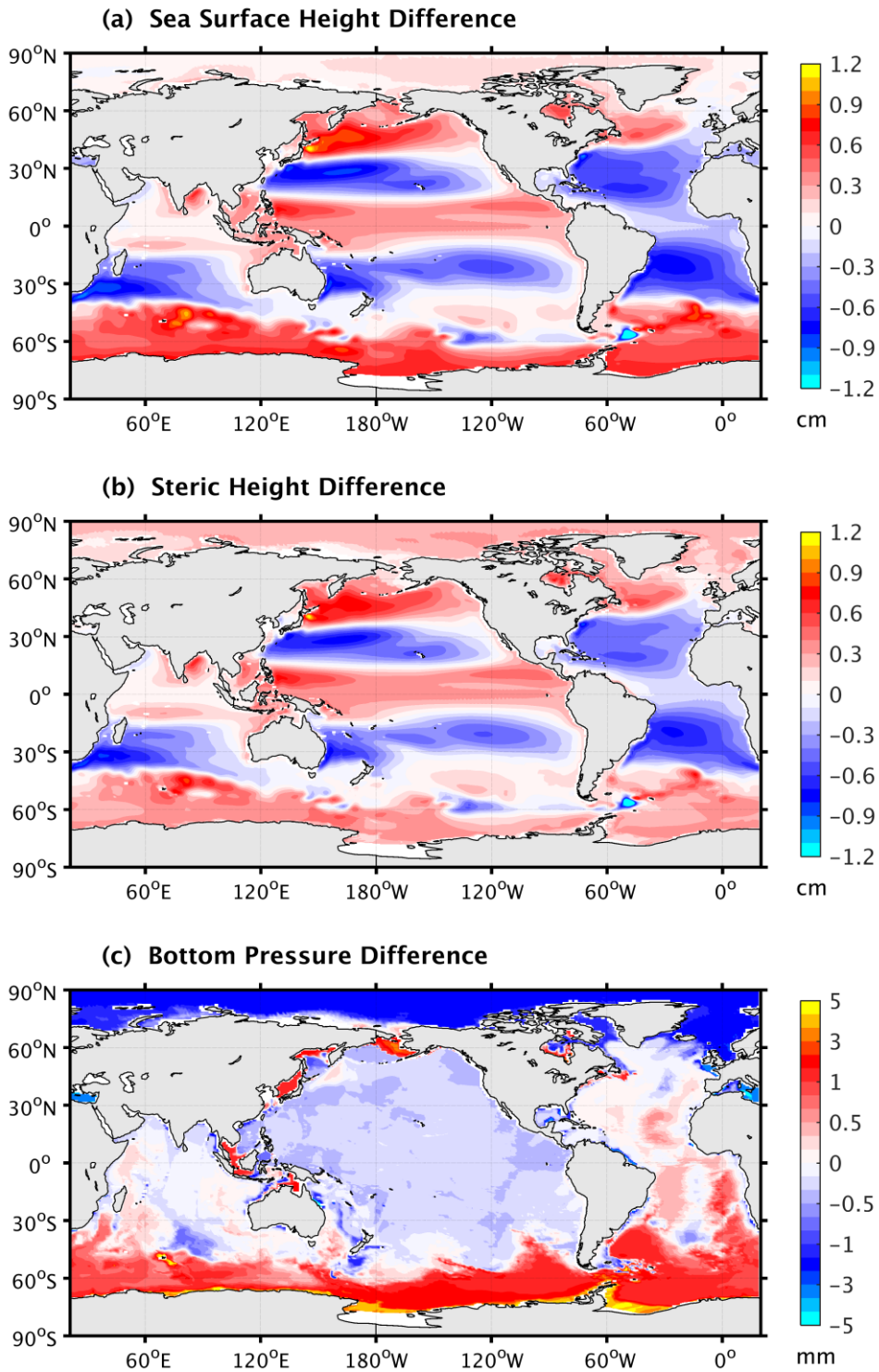


Figure 4.5 Time-mean difference between VF and VSF of (a) sea surface height (in cm), (b) steric height (in cm), and (c) bottom pressure expressed in form of equivalent water height (in mm; note the nonlinear color scale). The global mean offsets have been removed.

This is illustrated in Fig. 4.5c by the bottom pressure difference in form of equivalent water height (in mm) to compare with the other two sea level contributions. A bottom pressure increase reinforces the strong signal in the Southern Ocean while mass is removed from the Arctic reducing the small signal there. This is partly an artifact of the Boussinesq approximation and partly because the dynamics vary between these polar regions. SSH changes in the Southern Ocean are partly barotropic and have a bottom pressure contribution to the signal. This explains the reinforcement in the ACC region. Due to the Boussinesq approximation the positive changes have to be compensated by negative changes elsewhere. These changes concentrate in the Arctic because of the anti-cyclonic anomaly in subpolar North Atlantic, which reduces the freshwater export from the Arctic [Köhl and Serra, 2014] and in turn makes the Arctic water lighter. We confirmed for the VF run that the mass transport out of the Arctic happens mostly through the channels into the North Atlantic. SSH changes in the Arctic are halosteric and relate to changes of the interface between the fresh surface and the deeper more saline layer. In the anti-cyclonic regime, the fresh water is concentrated more at the center of the Arctic, which contributes to the reduction of the export. Since these changes in water mass characteristics are larger than those associated with the dynamic response, a negative bottom pressure signal results.

The steric changes in Fig. 4.5b are caused by a combination of the temperature-driven thermosteric contribution and the salinity-driven halosteric contribution, which are related to the column-integrated temperature and salinity anomalies between VF and VSF (Fig. 4.6). Defined in equation (4.4), they also represent the heat and freshwater content changes caused by the volume flux,

$$\Delta H C = \int_{-D}^0 \Delta T dz \quad \text{and} \quad \Delta F W C = - \int_{-D}^0 \frac{\Delta S}{S_0} dz. \quad (4.4)$$

Here, ΔT and ΔS symbolize the temperature and salinity differences between VF and VSF, respectively. The red (blue) color in Fig. 4.6a reveals a gain (loss) in heat content, while the red (blue) color in Fig. 4.6b indicates a salinity reduction (enhancement). Both heat and freshwater content changes are less than 1% of the reference run.

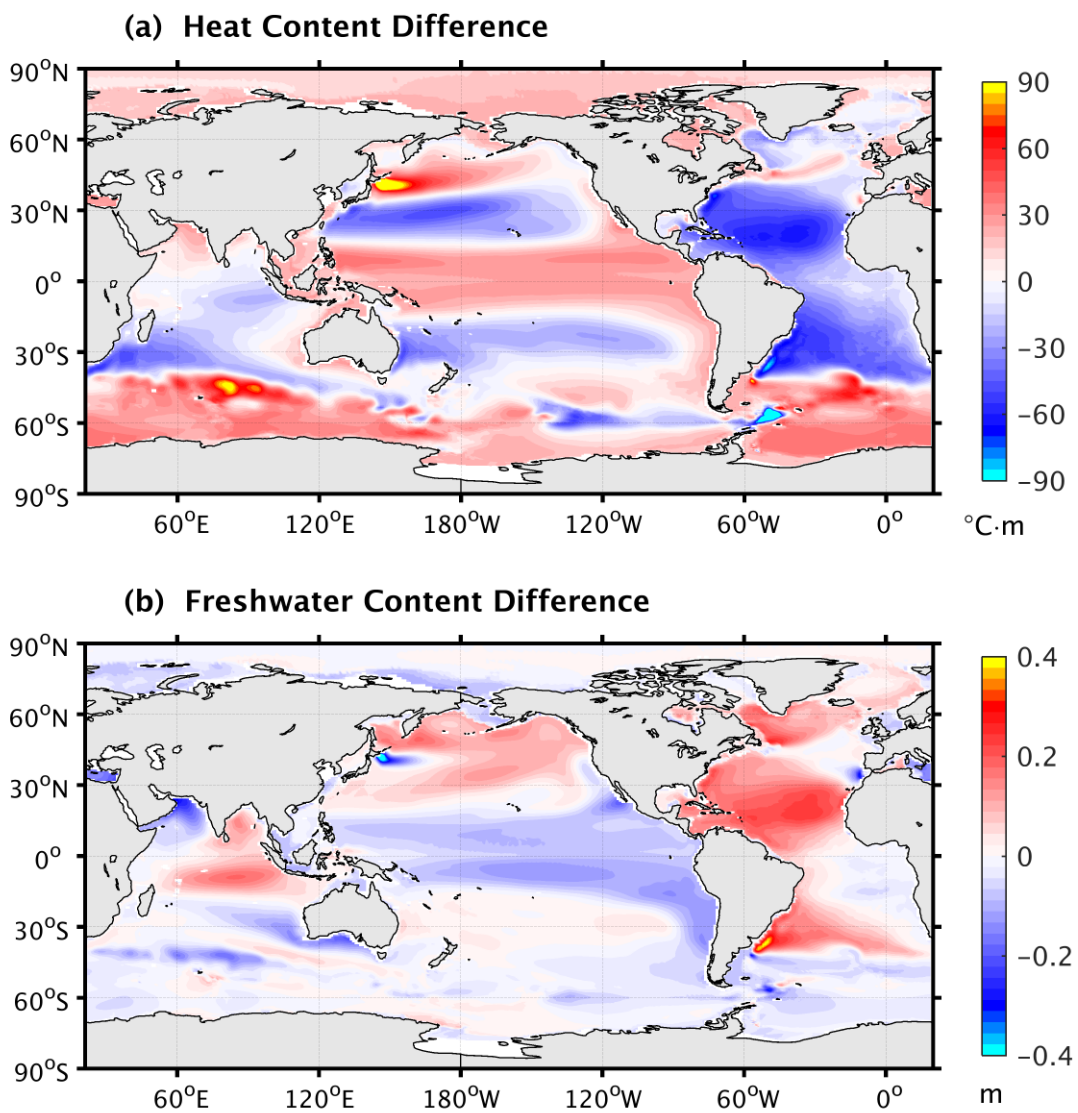


Figure 4.6 Time-mean difference between VF and VSF of (a) heat content (in $^{\circ}\text{C}\cdot\text{m}$) and (b) freshwater content (in m).

4.2.4 Synthesis

To facilitate a more direct comparison between variations of BSF, SSH and the net surface freshwater forcing, thereby allowing to illustrate the various time scales involved in the

impact of a time-varying freshwater forcing on the model results and to study time scales involved in the adjustment, Fig. 4.7 provides time series of the annual-mean BSF difference (red), SSH difference (green), and mean volume flux (blue) in the North Atlantic (Figs. 4.7a and 4.7b) and North Pacific (Figs. 4.7c and 4.7d), illustrating the relation of the temporal variability of all three quantities. The BSF and SSH differences are calculated as the meridional average along the sections marked in Fig. 4.1 with colored lines, written as

$$\overline{\eta} = \frac{\int \eta dy}{\int dy}. \quad (4.5)$$

The overbar represents the average of each variable accordingly. The mean volume flux into the ocean is calculated by averaging the area from the eastern boundary of each basin to the respective meridional section, given by

$$\overline{vf} = \frac{\int vfdA}{\int dA}, \quad (4.6)$$

Where vf denotes the surface volume flux. The meridional sections are located in the subtropical and subpolar gyres in the Northern Hemisphere according to the BSF difference pattern. We recall that according to the Goldsbrough-Stommel relation (equation (2.1)), the mean volume flux is directly proportional to the GSC up to a scaling factor of L^*f/β . Here, L is the length from the eastern boundary of each basin to the respective meridional section.

The figure reveals that over the subtropical areas (Figs. 4.7a and 4.7c) the net freshwater flux out of the ocean (evaporation dominating) is about 1.6 mm/day for 4.7a (1.7 mm/day for 4.7c, time-mean values), which leads to a 0.4 Sv reduction (0.6 Sv for 4.7c) of the barotropic circulation and a 0.6 cm SSH decrease (0.5 cm for 4.7c). For the subpolar regions (Figs. 4.7b and 4.7d), the mean volume flux into the ocean (precipitation dominating) is about 1.0 mm/day (1.9 mm/day for 4.7d), which results in a 0.2 Sv intensification (0.5 Sv for 4.7d) and a 0.4 cm SSH increase (0.8 cm for 4.7d).

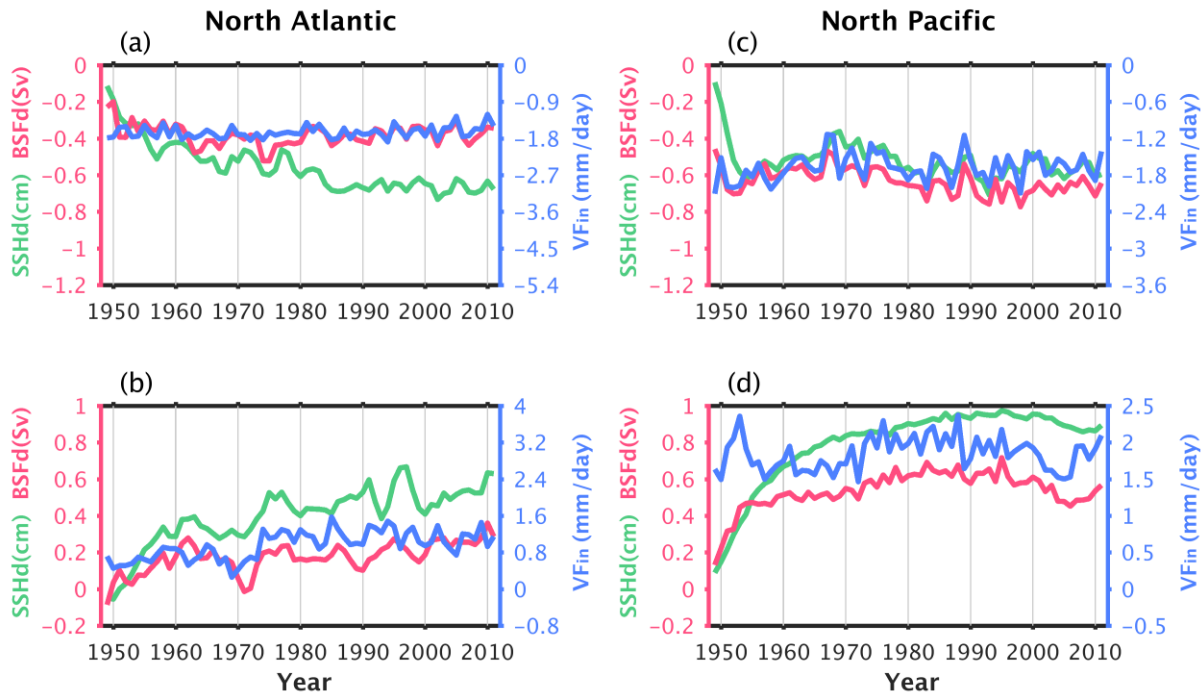


Figure 4.7 Time series of the annual-mean barotropic streamfunction difference (BSFd, in Sv, red), the sea surface height difference (SSHd, in cm, green) along the meridional sections marked in Fig. 4.1 with colored lines, and the mean volume flux into the ocean averaged from the eastern boundary of each basin to the sections considered (VFin, in mm/day, blue), shown for (a and b) the North Atlantic and (c and d) the North Pacific. The results are presented in (a and c) for the subtropical gyres and (b and d) for the subpolar areas. Note the mean volume flux can be interpreted as the GSC using the Goldsbrough relation. Depending on the L^*f/β , the factors are (from a to d) 0.22, 0.25, 0.34 and 0.4 Sv/(mm/day), respectively.

Figure 4.7 illustrates that the theoretical GSC explains much of the simulated BSF variability resulting from a time-varying surface volume flux forcing. This tight relation can be found already on a monthly time scale as the time-dependent Sverdrup balance is established for periods longer than a month [Willebrand *et al.*, 1980]. We also note that the sea level response shows long-term adjustments of several decades (except for the subtropical North Pacific), indicating slower baroclinic adjustment processes in the model in response to the changed surface freshwater volume flux boundary condition. The correlation coefficients of BSF

difference and mean volume flux from Figs. 4.7a–4.7d are 0.58, 0.43, 0.64 and 0.75, respectively; in this computation, the first 5 years were discarded, because they are influenced by the model spin-up. The correlations between the time series of BSF difference and averaged surface volume flux show that the GSC relation explains well the barotropic circulation difference between both model simulations in the subtropical gyres.

4.3 Projected changes in the future

Using the projected RCP8.5 E–P anomaly shown in Fig. 3.4a as the perturbation to the monthly NCEP freshwater flux forcing, ocean circulation changes invoked by the E–P changes can be computed in a way similar to what was obtained in Section 4.2. As described in Section 3.4.2, the difference between the perturbation runs will be compared with the difference between the standard runs. The resulting difference ($\Delta\text{RCP} - \Delta\text{NCEP}$) is considered as the changes caused by the global water cycle acceleration. Those changes will be analyzed with respect to the future dynamical responses of the ocean circulation to those anthropogenic changes as well as with their impact on ocean transports and sea level.

4.3.1 Future dynamical response

Figure 4.8a shows changes in the barotropic streamfunction as they result from the RCP8.5 E–P anomaly shown in Fig. 3.4a. As can be expected from the results presented in Section 4.2, the enhanced hydrological cycle does lead to a barotropic circulation anomaly that enhances the impact of the present-day freshwater forcing. Compared to the present-day GSC (Fig. 4.1), the induced GSC in the subtropical and subpolar gyres enhances by about 20% with a stronger intensification about 50% in the Southern Ocean. This results in a further weakening of the wind-driven gyre; i.e., the gyre strength through enhanced freshwater forcing is actually decreased relative to the situation with the present hydrological cycle.

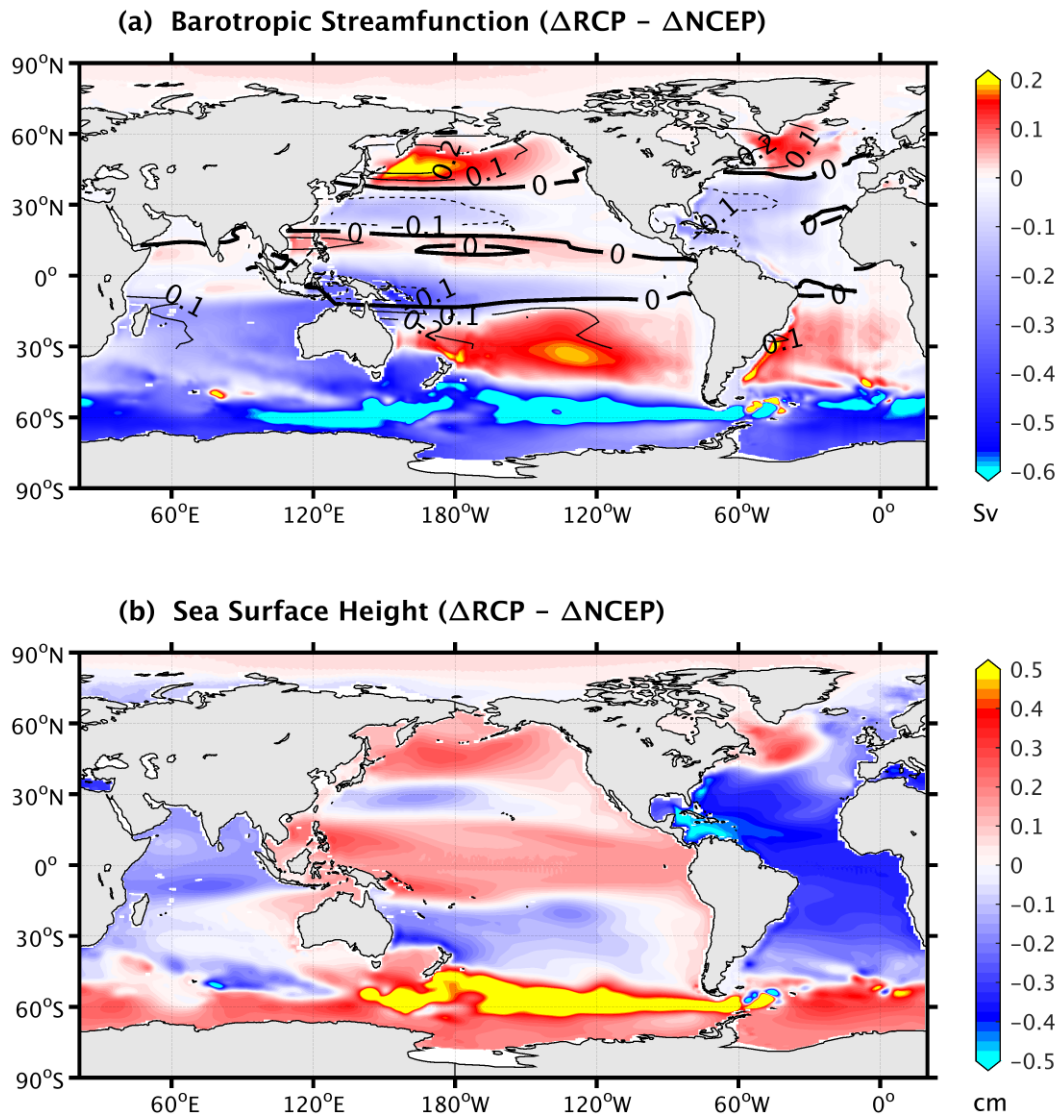


Figure 4.8 Changes in (a) barotropic streamfunction (in Sv) and (b) sea surface height (in cm) as $\Delta\text{RCP} - \Delta\text{NCEP}$. The contours in (a) are the GSC derived directly from the RCP8.5 E-P anomaly, according to the Goldsbrough-Stommel relation (equation (2.1)). The solid contours indicate positive values with the interval of 0.1 Sv.

Superimposed to Fig. 4.8a as contours are the GSC anomalies as they follow directly from the RCP8.5 E-P anomaly (Fig. 3.4a). A visual comparison shows a close relation between the barotropic circulation changes and the GSC anomalies in mid and low latitudes. However, the

largest response in the barotropic circulation is visible in the Southern Hemisphere and especially in the ACC region, where the GSC streamfunction cannot be directly calculated and the E–P anomaly forcing is small (Fig. 3.4a). Similar to the differences between the barotropic response and the GSC linear theory, the slow baroclinic adjustment of the model circulation and interaction with bottom topography may explain the discrepancy.

Changes in sea level shown in Fig. 4.8b resulting from the RCP8.5 E–P anomaly forcing are consistent with this notion and with the changes in the barotropic circulation. We note that the shown sea level changes may or may not be part of the total regional sea level changes diagnosed by *Slangen et al.* [2014] as only some but not all models use natural boundary conditions. Typical amplitude of the regional sea level changes is in the range of ± 0.5 cm, which is originated from the RCP8.5 E–P anomaly forcing. As an example, in the Southern Hemisphere, we see an increase in sea level south of the ACC by 0.5 cm. In comparison to Fig. 4.5a, the SSH changes originating from the enhanced hydrological cycle in RCP8.5 amount to roughly 50% of the impact from the present-day volume flux forcing and roughly show the same pattern. Accordingly, the decomposition in steric and barotropic (bottom pressure) anomalies is also comparable (50%). This can be considered to be a significant change through climate change processes.

As explained for the climatological response (Fig. 4.6), the sea level changes shown in Fig. 4.8b are also largely due to the temperature and salinity variations caused by the RCP8.5 E–P anomaly forcing (Figs. 4.9a and 4.9b). Changes induced by the freshwater perturbation are about half of the amplitude of the climatological response generated by the volume flux in the standard runs (Fig. 4.6). This is significant, underpinning the notion that relatively speaking changes in the hydrological cycle may have a substantial impact on the future circulation. Moreover, a visual comparison of Figs. 4.6 and 4.9 reveals differences in regional pattern, especially in the North Atlantic and the ACC region, which can result from the differences in the distribution of the freshwater perturbation relative to the volume flux used in the standard runs.

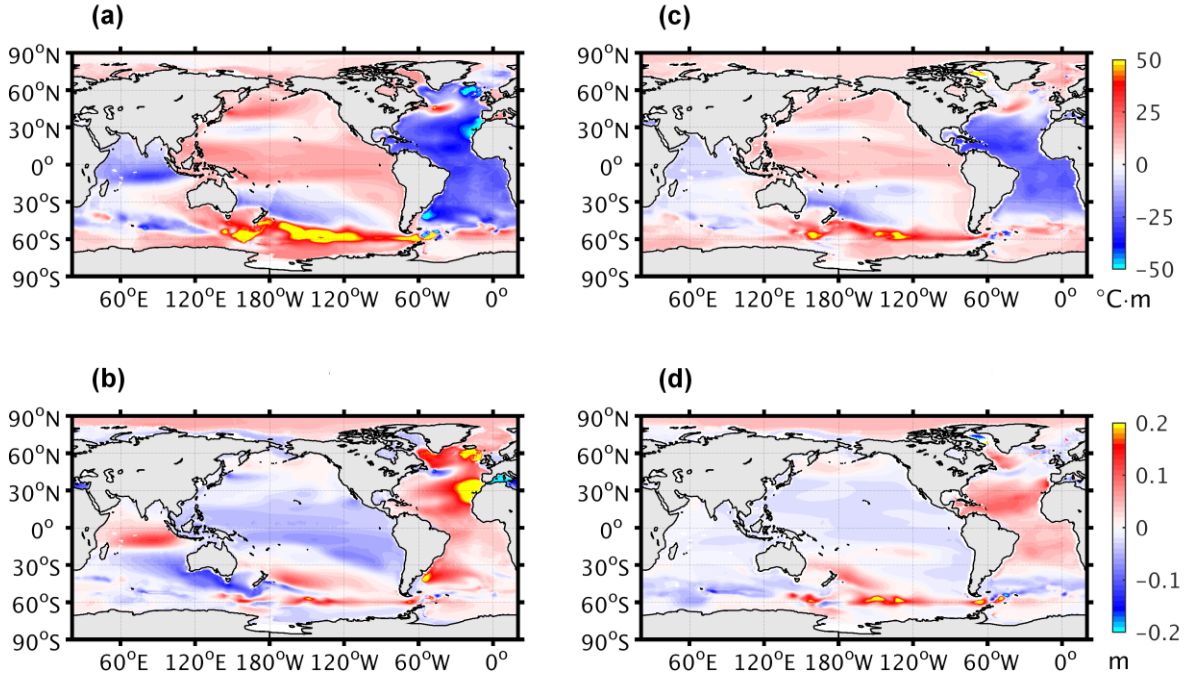


Figure 4.9 Changes in (a, c) heat content (in $^{\circ}\text{C}\cdot\text{m}$) and (b, d) freshwater content (in m) as $\Delta\text{RCP} - \Delta\text{NCEP}$, shown (left) from the freshwater perturbation forcing and (right) from the isopycnal motion caused by the perturbation (see equation (4.7) and the text for details).

One possible process that explains the future seawater temperature and salinity anomalies related to the volume flux forcing is the motion of the isopycnal surfaces [Doney *et al.*, 2007; Köhl, 2014]. Like the effect of the wind stress, the extra downward (upward) surface vertical velocity from the freshwater flux pushes down (pulls up) the isopycnals leading to the spin-up and spin-down of the GSC gyres. To verify this hypothesis, a simple diagnostic is applied to detect the temperature and salinity changes related to this motion (ΔT_{iso} and ΔS_{iso})

$$\Delta T_{\text{iso}} = \frac{\nabla T \cdot \nabla \sigma}{\|\nabla \sigma\|^2} \cdot \Delta \sigma \quad \text{and} \quad \Delta S_{\text{iso}} = \frac{\nabla S \cdot \nabla \sigma}{\|\nabla \sigma\|^2} \cdot \Delta \sigma, \quad (4.7)$$

where $\Delta \sigma$ symbolizes the density difference between each pair of runs, and the operator ∇ denotes the gradient of each variable in xyz directions. The heat content and freshwater content anomalies related to the freshwater perturbation induced isopycnal motion are shown

in Figs. 4.9c and 4.9d. Apparently, the temperature and salinity anomalies from the motion of the isopycnals contribute largely to the heat and freshwater content changes and thus also to the steric sea level changes. This is to be expected since interannual thermosteric and halosteric changes are in general dominated by isopycnal motion [Köhl, 2014]. There are regions with discrepancies, especially the subpolar North Atlantic, where deep convection and strong water mass conversion happen.

4.3.2 Transport changes

It is of interest to understand how ocean transport properties change and to detect the driving mechanism for related sea level changes. For this purpose, several decomposition analyses are used to distinguish different contributions to the heat and freshwater transport changes.

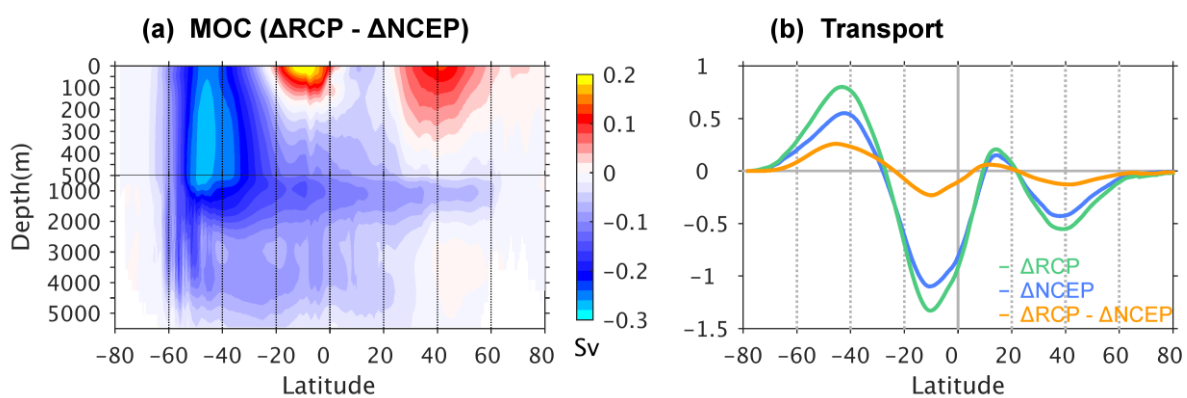


Figure 4.10 (a) Changes in global time-mean meridional overturning streamfunction (MOC, in Sv) as $\Delta RCP - \Delta NCEP$. (b) The northward volume transports from ΔRCP (green), $\Delta NCEP$ (blue), and $\Delta RCP - \Delta NCEP$ (orange).

From the above results, we can expect that the changes in the MOC diagnosed in Section 4.2 for the present-day volume flux forcing will be further enhanced through the RCP8.5 E–P anomaly forcing. This is confirmed in Fig. 4.10 showing similar anomalies as shown before in

Fig. 4.4, but now for the $\Delta\text{RCP} - \Delta\text{NCEP}$. Shown in Fig. 4.10a are the global time-mean MOC anomalies and in Fig. 4.10b the northward transports of MOC from the ΔRCP (green), the ΔNCEP (blue), and the $\Delta\text{RCP} - \Delta\text{NCEP}$ (orange). Forced by the freshwater perturbation, the volume flux driven subtropical cells are intensified by about 20%, while a stronger intensification about 50% is noticed in the Southern Ocean.

Any altered circulation will change ocean transports. To quantify the future changes in the heat and freshwater transports enforced through the projected RCP8.5 changes in the global hydrological cycle are analyzed next, divided into (i) heat and (ii) freshwater transports.

(i) Heat transport: The meridional heat transport is defined relative to a reference temperature of 0 °C and given by

$$H = \rho_o c_p \int_{-D}^0 \int_{\text{west}}^{\text{east}} v T dx dz, \quad (4.8)$$

where $\rho_o = 1029 \text{ kg m}^{-3}$ is the seawater density, $c_p = 4200 \text{ J kg}^{-1} \text{ }^\circ\text{C}^{-1}$ the specific heat capacity, v the meridional velocity of the currents, and T the potential temperature. Since there is a net transport of volume involved in the VF version but also in the individual basins of the VSF version, the associated heat and freshwater transports do not necessarily lead to changes in heat and freshwater contents of the ocean, and here the “heat transport” is more properly an enthalpy transport in the ocean. Nevertheless, as a shorthand, we use the term “heat transport” to refer to the “enthalpy transport” in this study.

Figure 4.11a shows the time-mean meridional heat transport (in PW, 1 PW = 10^{15} W) of the global ocean (blue), Atlantic (red), and Pacific-Indian oceans (green) in the VF version. A positive slope of the curve indicates a downward heat flux into the ocean (ocean heat gain). The mean transport variations along latitude generally agree with the previous results [*Ganachaud and Wunsch, 2003; Stammer et al., 2003; Köhl, 2015*], albeit with some amplitude differences.

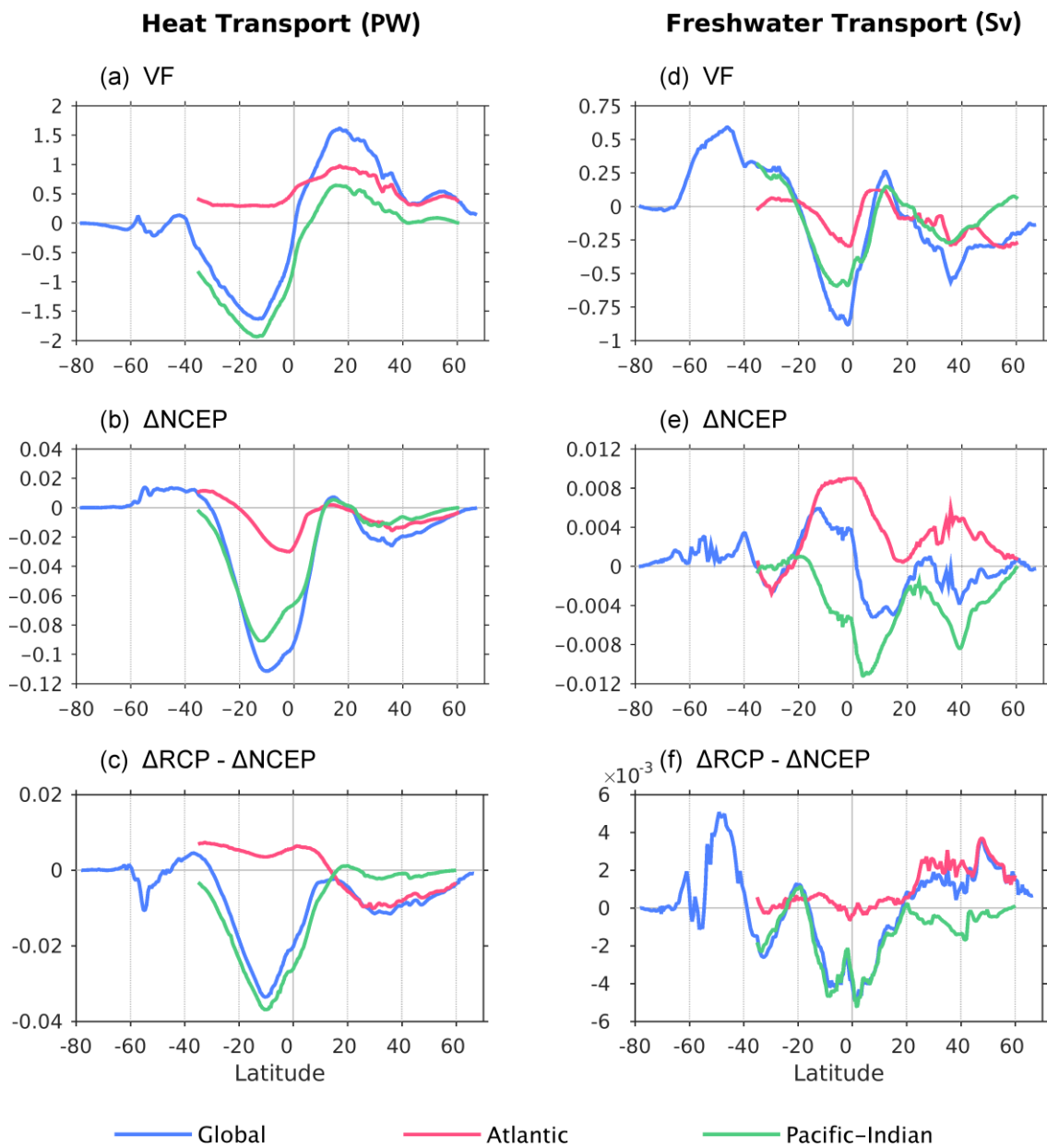


Figure 4.11 Northward meridional heat transport (left, in PW) and freshwater transport (right, in Sv) for the global ocean (blue), the Atlantic (red), and the Pacific-Indian oceans (green). The estimates are presented as (top) VF, (middle) Δ NCEP, and (bottom) Δ RCP - Δ NCEP.

It can be expected that associated with the changes in the circulation described above, changes in heat and freshwater transports will occur. Shown are the heat transports as ΔNCEP (Fig. 4.11b) and as $\Delta\text{RCP} - \Delta\text{NCEP}$ (Fig. 4.11c). As can be seen from Fig. 4.11b, the maximum of the global heat transport difference occurs in the tropical Southern Hemisphere and amounts to about 7% of the mean transport there. Across all latitudes, the heat transport differences are basically southward, except for the significant northward transport in the ACC region and south of 20°S in the Atlantic. For the northward mean heat transport, the southward difference indicates the weakening effect by volume flux forcing. As for the freshwater perturbation induced anomalies (Fig. 4.11c), the Northern Hemisphere shows further weakening and the Southern Hemisphere shows less weakening. For the Pacific-Indian oceans, however, the southward mean heat transport in the Southern Hemisphere has been enhanced by the volume flux forcing and further enhanced by the projected freshwater anomalies.

(ii) Freshwater transport: As was done for the heat transport, the global meridional freshwater transport is also split into separate contributions from the Atlantic and Pacific-Indian oceans (Fig. 4.11d), estimated as

$$FWT = \int_{-D}^0 \int_{west}^{east} v \left(1 - \frac{S}{S_0}\right) dx dz. \quad (4.9)$$

The freshwater transports as ΔNCEP are displayed in Fig. 4.11e, and as $\Delta\text{RCP} - \Delta\text{NCEP}$ are shown in Fig. 4.11f. In the Atlantic, the mean freshwater transport of the VF version is generally southward, except between about 5°N and 15°N and south of 20°S (Fig. 4.11d). We note that the sign of the freshwater transport difference in the Atlantic is anti-symmetric (northward for north of 20°S and southward for south of 20°S), resulting in a weakening effect from the volume flux forcing (Fig. 4.11e). In the Pacific-Indian oceans, as in the Atlantic, the mean net freshwater transport is mainly southward. However, opposite to the difference of the Atlantic, the freshwater transport difference is southward, revealing an enhancing effect of the volume flux forcing in the Pacific-Indian oceans. For the ACC region, the significant mean northward freshwater transport is enhanced slightly by the volume flux.

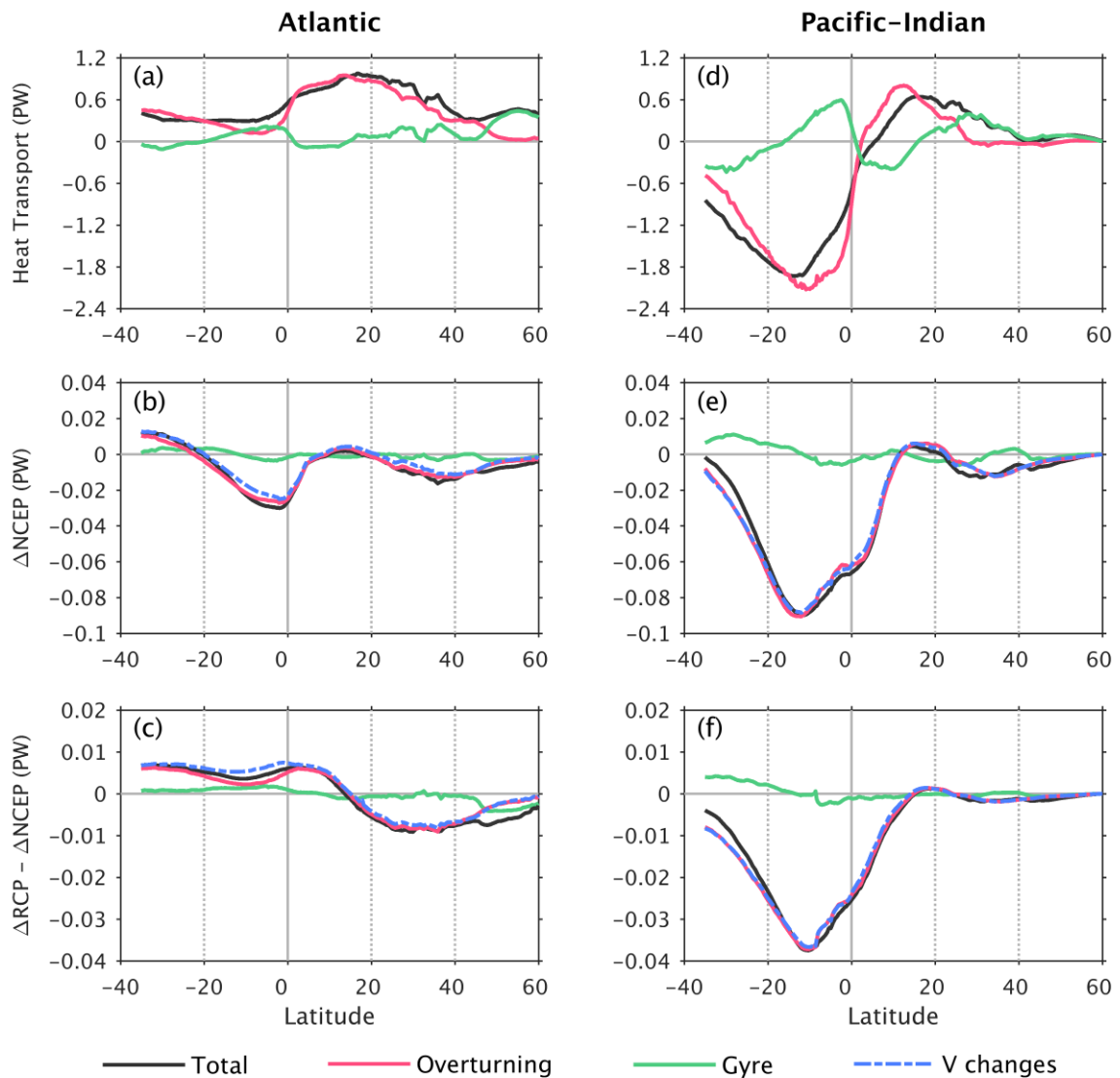


Figure 4.12 Northward meridional heat transport for (left) the Atlantic and (right) the Pacific-Indian oceans (in PW). Shown are the results for the total transport (black) as well as the overturning (red) and gyre (green) components. The dashed-blue curve exhibits the further decomposition of the overturning components as the contributions from the velocity changes. The estimations are presented as (top) VF, (middle) ΔNCEP , and (bottom) $\Delta\text{RCP} - \Delta\text{NCEP}$.

Although the impact from surface volume flux forcing to the meridional heat and freshwater transport is small, it is still important to understand the processes that govern these ocean transport changes. For this purpose, following *Böning and Bryan* [1996], the meridional heat transports have been decomposed into their overturning and gyre components (H_{ot} and H_{gy}):

$$H_{ot} = \rho_o c_p \int_{-D}^0 \int_{west}^{east} \bar{v} \bar{T} dx dz \text{ and} \quad (4.10)$$

$$H_{gy} = \rho_o c_p \int_{-D}^0 \int_{west}^{east} v' T' dx dz. \quad (4.11)$$

Here, the overbar denotes for the zonal mean of each variable, and the prime mark symbolizes the deviation from the zonal mean expressed as follows:

$$v = \bar{v} + v' \text{ and } T = \bar{T} + T' \quad (4.12)$$

The original concept of a decomposition into gyre/overturning automatically accommodates any kind of vertical distribution of the flow once acknowledged that the overturning contours do not necessarily need to close. It is therefore not necessary to assume a barotropic flow to compensate for the mass flux differences [*Treguier et al.*, 2014] and to separate the transports into the parts carried by this barotropic velocity and its deviation.

Because the GSC represents the ocean gyre circulation generated by the surface volume flux, we would expect that the gyre components of the difference might play a role in explaining the heat transport difference. In contrast, the gyre components of ΔNCEP and $\Delta\text{RCP} - \Delta\text{NCEP}$ are negligible (green lines in the middle and bottom panels of Fig. 4.12); instead, the overturning components dominate the change of the total heat transport as ΔNCEP and as $\Delta\text{RCP} - \Delta\text{NCEP}$ nearly over all latitudes. A further decomposition of the overturning components suggests the dominant contribution from the velocity changes (dashed-blue curves in Fig. 4.12), supporting the previous MOC-related analysis.

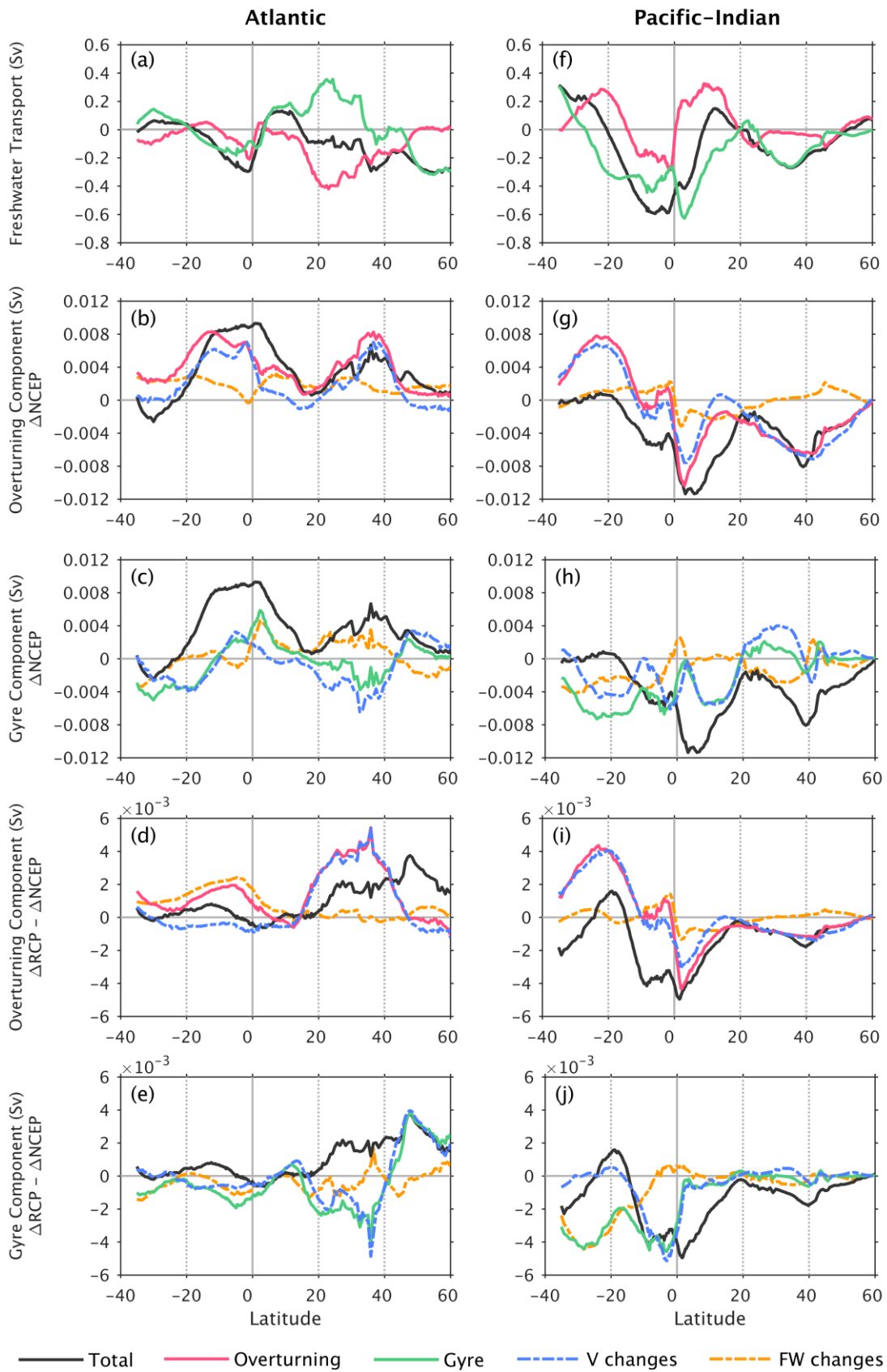


Figure 4.13 Northward meridional freshwater transport for (left) the Atlantic and (right) the Pacific-Indian oceans (in Sv). The solid curves represent the total transport (black) as well as the overturning (red) and gyre (green) components, while the dashed lines show the further decomposition of overturning and gyre components as the contributions from velocity changes (blue) and freshwater changes (orange). The estimations are presented as (1st row) VF, (2nd and 3rd row) Δ NCEP, (4th and 5th row) Δ RCP – Δ NCEP.

The same decompositions have been applied to the freshwater transports (Fig. 4.13). Decomposing the transports into overturning and gyre components, they apparently oppose each other at most latitudes. The further decomposition of overturning and gyre components of the Δ NCEP (2nd and 3rd row of Fig. 4.13) and the Δ RCP – Δ NCEP (4th and 5th row of Fig. 4.13) quantifies the contributions from velocity changes (blue) and freshwater changes (orange). The overturning components are dominated by velocity changes and explain the majority of the meridional variations of the total differences, except for the southern Pacific-Indian oceans. The gyre components have the tendency to oppose the overturning components, contributing to balance the northward overturning components with southward gyre transports. Since contributions from the velocity changes and freshwater changes anti-correlate with each other at most latitudes and since amplitudes are larger for the former, it is suggested that the transports associated with circulation changes drive freshwater content changes, which evoke the transports associated with freshwater changes as a negative feedback. Overall, the velocity changes dominate the overturning components, which in turn dominate the total heat and freshwater transport changes caused by the surface volume flux forcing, except for the freshwater transport difference in the southern Pacific-Indian oceans.

4.4 Concluding remarks

The ultimate goal of this chapter is to understand the dynamical adjustment of the ocean circulation to the projected future changes in the global hydrological cycle. From the

ensemble-mean MPI-ESM LR RCP8.5 surface freshwater flux anomalies, we note an intensification of about 13.2% (on global average) in response to a 3.6 °C warming by the end of the century relative to its beginning. In response to the enhanced surface freshwater flux, the induced GSC and the associated MOC increase by around 20% in mid and low latitudes, while a stronger intensification about 50% is noticed in the Southern Ocean, comparing to the present-day response.

The changes in the circulation also lead to a response in sea level, which is similar in pattern to the barotropic circulation but shows longer adjustment time scales. A significant contribution to the regional sea level changes is found in form of steric change, which is related to the changes in seawater temperature and salinity induced largely by the motion of the isopycnals. The typical amplitude of sea level changes in response to the present-day volume flux forcing is of the order of 1 cm, and the amplitude increases when adding the extra projected E–P anomaly perturbation.

To understand the possible mechanisms responsible for the changes of the oceanic transport properties in response to future surface freshwater flux anomalies, heat and freshwater transport differences were decomposed into overturning and gyre components, and then further partitioned into the contributions from velocity and freshwater changes. The decomposition of these transport differences reveals that the velocity changes determine the overturning components and largely explain the total changes, especially for the heat transport. For the gyre components of the freshwater transport, the anti-correlation between the contributions from velocity and freshwater changes suggests a negative feedback of freshwater anomalies caused by the changed barotropic circulation.

The volume flux mostly weakens the mean MOC in the upper 500 m, while slightly enhances the deep meridional overturning. The overturning components of the transport differences are associated with meridional overturning changes that are the continuation of net surface volume flux into the interior. Furthermore, differences between the pathways of volume and fresh water were illustrated by calculating a freshwater function analogous to the heat function of *Boccaletti et al.* [2005]. The freshwater spreading concentrates mainly in the

shallow cells and follows the volume distribution near the surface but diverges substantially with depth. In other words, the continuation of the atmospheric freshwater cycle into the ocean interior takes somewhat different pathways for volume and the associated salinity signal.

Note that the glacier melting, which is one of the key elements of the climate research and also one of the sources of the surface volume flux, is not included in this study. The rapid and slower ocean adjustments in response to the Greenland and Antarctic ice sheet melting were analyzed with a focus on the sea level rising in previous studies [*Stammer, 2008; Lorbacher et al., 2012; Agarwal et al., 2014*].

CHAPTER 5

Freshwater budget in the Atlantic

5.1 Introduction

Associated with changes in the global water cycle, the variations of freshwater content in the ocean, particularly in the Atlantic Ocean, are of great importance for understanding the ocean dynamics as well as the climate. Many studies have investigated the freshwater content changes in the Arctic as well as the variations of the freshwater export from the Arctic into the North Atlantic [*Häkkinen and Proshutinsky, 2004; Köberle and Gerdes, 2007; Jahn et al., 2010; Köhl and Serra, 2014*]. The large freshwater export from the Arctic through the passages of the Canadian Arctic Archipelago enters the North Atlantic, changes the seawater density and thereby plays a role in the large-scale thermohaline circulation [*Dickson et al., 2002*]. *Rahmstorf [1996]* demonstrated that an important contributor to the Atlantic meridional overturning circulation (AMOC) stability is the salinity balance among the surface freshwater flux, the freshwater transport by the overturning circulation and the freshwater import by the gyre circulation in the South Atlantic. Besides, the long-term salinity variations are reported as an important contributor to the regional sea level changes in the Atlantic, where the halosteric changes strongly compensate the thermosteric changes [*Antonov et al., 2002; Levitus et al., 2005; Durack et al., 2014*].

The ocean salinity field has long been considered as a reflection of a long-term balance between surface freshwater flux and ocean processes. The temporal and spatial variations of surface salinity and/or near-surface salinity have caught a lot of attention. Recent studies have demonstrated the link between the distributions of SSS and surface freshwater flux is region-dependent as well as timescale-dependent, highlighting the importance of the role of upper ocean dynamics [Qu *et al.*, 2011; Yu, 2011; Vinogradova and Ponte, 2013]. The ocean surface is indeed of great interest, especially with the accessible salinity data sets via the novel remote sensing missions Aquarius [Lagerloef, 2012] and Soil Moisture and Ocean Salinity (SMOS) [Font *et al.*, 2013], whereas the subsurface salinity variations at mid and low latitudes in the Atlantic and the related mechanisms are less known and need to be understood as well.

Large-scale and coherent long-term salinity changes in the Atlantic have been documented, revealing a deep freshening in the subpolar regions whereas a shallower and stronger increase in salinity at lower latitudes [Curry *et al.*, 2003; Boyer *et al.*, 2005; Durack and Wijffels, 2010; Skliris *et al.*, 2014]. This feature was also reported by Boyer *et al.* [2007] with an analysis of the freshwater content changes in the upper 2000 m, revealing a decrease over the period 1955–2006 in the North Atlantic as a whole (0° – 80° N) with a freshening from the late 1960s to early 1990s in the subpolar North Atlantic and Nordic Seas (to the north of 50° N). Boyer *et al.* [2007] found that surface freshwater flux is an important contributor to the freshwater content changes especially in the subpolar North Atlantic but not in other regions, implying the importance of ocean processes.

Besides the surface freshwater flux, the oceanic freshwater transport is obviously one of the major factors influencing the freshwater content changes. The estimates of the Atlantic freshwater transport have been provided based on observations as well as model simulations [Wijffels, 2001; Talley, 2008; Valdivieso *et al.*, 2014; Köhl, 2015; McDonagh *et al.*, 2015]. Studies have demonstrated that the freshwater loss in the subtropical South Atlantic is balanced by the freshwater import through the wind-driven subtropical gyre and the fresh water in the high-latitude North Atlantic is transported southward via the flow of North Atlantic Deep Water [Rahmstorf, 1996; Talley, 2008]. Additionally, the freshwater transport

by the overturning circulation has been underscored and suggested as an indicator of the AMOC bistability [Rahmstorf, 1996; de Vries and Weber, 2005; Hawkins *et al.*, 2011; Mecking *et al.*, 2017]. However, the temporal variation of freshwater transport over the past 50 years and more importantly its role in changing the freshwater content at mid and low latitudes in the Atlantic are not crystal clear yet, which will be the focuses of this chapter.

In this chapter, an analysis of the freshwater content and freshwater transport in the Atlantic is carried out using the GECCO2 ocean synthesis. The primary objective is to address the main mechanisms causing the interannual to decadal variations of the freshwater content changes in three regions over the past 50 years.

The structure of this chapter is as follows. The model data and the study area will be introduced in Section 5.2. The results are divided into two parts: Section 5.3 presents the variations of freshwater transport by decomposing it into the overturning and gyre components; in Section 5.4, the regional freshwater budgets are analyzed regarding the variations of surface freshwater flux and freshwater transport with a focus on detecting the main driving force for the freshwater content changes. A summary can be found in Section 5.5.

5.2 Data and study area

The data set used in this chapter is the most up-to-date version of the GECCO2 ocean synthesis covering the period 1948–2014. The first decade has been taken out in this analysis because of the spin up adjustment of the model. The model configuration, the assimilation approach (adjoint method), and the evaluation of the results from iteration 23 are described in detail in Köhl [2015]. Note that there is a possible artificial 4-year cycle in the data set because of the assimilation window length and the associated dependence of the adjustments within each window. Though using the window shifting method the artificial 4-year cycle is partly reduced in this new version, the results associated with this time scale still need to be

interpreted with caution, especially in the regions with strong adjustments (see more information in the data quality description at <http://icdc.cen.uni-hamburg.de/1/daten/reanalysis-ocean/gecco2.html>).

The freshwater content (FWC) is calculated as follows,

$$FWC(x, y, t) = \int_{-D}^0 1 - \frac{S}{S_0} dz, \quad (5.1)$$

where S is the seawater salinity, S_0 is the reference salinity (35 psu), and D is the depth of the ocean. The time-mean freshwater content and zonal-mean salinity in the Atlantic over the period 1961–2014 are shown in Fig. 5.1 with the dark green lines indicating the boundary positions of each box for the freshwater budget calculation in Section 5.4. As shown, the Atlantic Ocean is divided into three boxes as the subtropical and subpolar North Atlantic ($23.5^\circ\text{N} - 60^\circ\text{N}$), the tropical North Atlantic ($0^\circ - 23.5^\circ\text{N}$), and the tropical South Atlantic ($23.5^\circ\text{S} - 0^\circ$).

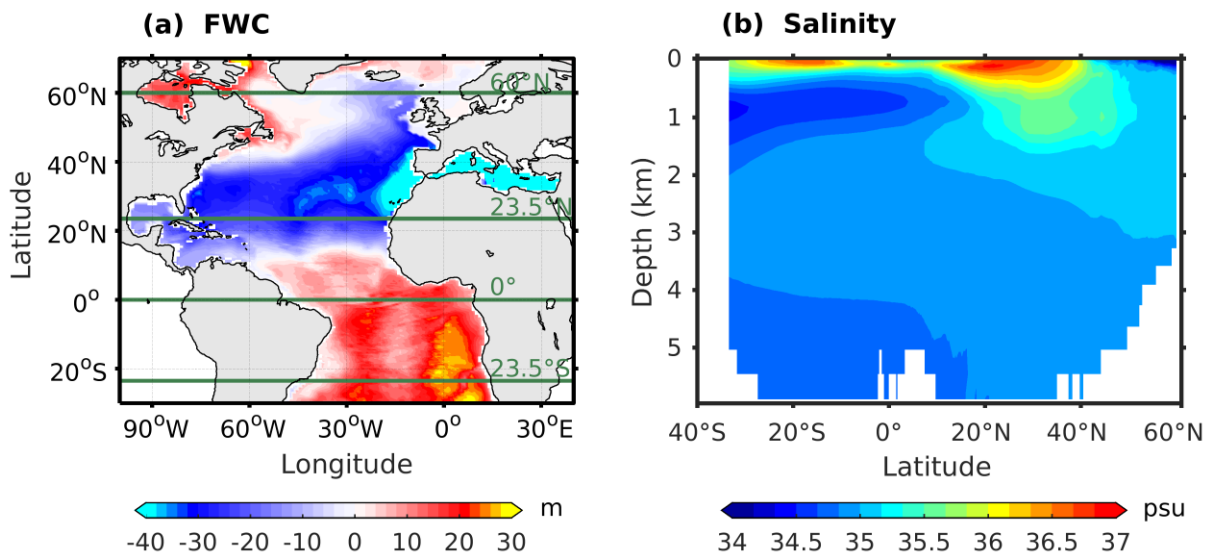


Figure 5.1 (a) Time-mean freshwater content in the Atlantic (m). The dark green lines define the boundaries of each box used for calculating the freshwater budget. (b) Zonal-mean salinity in the Atlantic (psu) shown in the latitude-depth plane. The Mediterranean Sea has been excluded while calculating (b).

The freshwater content in the subtropical and subpolar North Atlantic has lower value and higher variability (see the standard deviation in Fig. 5.2a). For the region to the south of 10°N, the freshwater content is higher but with lower variability. As for the time scales of the variability, the interannual and decadal variability is the main contribution, while the seasonal variability is very small (in the range of 0–1 m) so it is not a focus of this study. The trend is also part of the variability since the decreasing freshwater content is observed throughout most of the basin, which is due to the small imbalance of the net surface freshwater flux in the Atlantic ($E > P + R$). Different from the previous results [e.g. *Curry et al.*, 2003; *Curry and Mauritzen*, 2005; *Boyer et al.*, 2007; *Holliday et al.*, 2008], the freshening trend of freshwater content in the northern North Atlantic (to the north of 50°N) from the late 1960s to early 1990s is not captured in this data set.

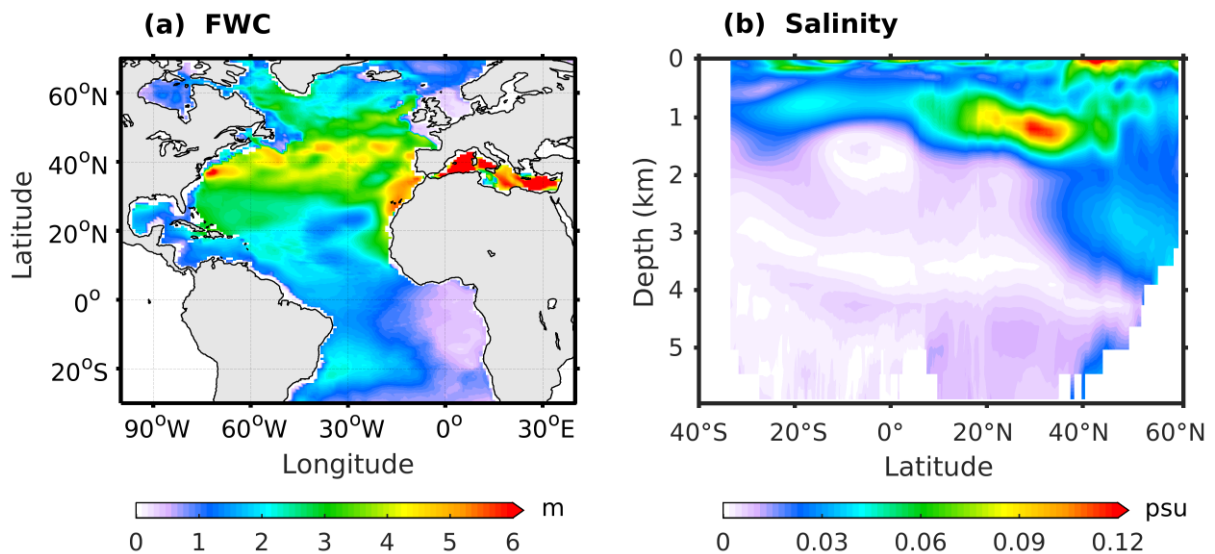


Figure 5.2 Standard deviations of the annual (a) freshwater content (m) and (b) zonal-mean salinity (psu).

Shown by the time mean and the standard deviation of the zonal-mean salinity (Figs. 5.1b and 5.2b), the high variability concentrates at the surface to the north of 40°N. To the south of

40°N, the high variability centralizes around the depth of 1000 m, of which the strongest signal is located at the subtropical latitudes and gets weaker in the tropical region. Moreover, in the tropical region, the amount of salinity variability at the surface is comparable to that at 1000 m depth, which indicates that the surface processes are as important as the deep circulation processes and could be influenced by the surface freshwater flux and/or the transports by the shallow overturning cells. Therefore, the following study will try to understand the processes that are responsible for changing the freshwater content in three regions in the Atlantic with a focus on the interannual and decadal time scales.

5.3 Freshwater transport variability

To better understand the oceanic freshwater transport (FWT), it is useful to distinguish the transport associated with the overturning circulation (FWT_{ot}) from the transport associated with the gyre circulation (FWT_{gy}). A well-established decomposition method regarding the zonal mean and the deviations from the zonal mean [Böning and Bryan, 1996] is applied here (see also equations (4.10)–(4.12) in Chapter 4),

$$FWT = FWT_{ot} + FWT_{gy} \quad (5.2)$$

$$= \int_{-D}^0 \int_{west}^{east} (\bar{v}\bar{F}_a + v'F'_a) dx dz, \quad (5.3)$$

where the overbar represents the zonal mean and the prime symbolizes the deviation from the zonal mean. F_a is the freshwater anomaly defined as follows,

$$F_a = 1 - \frac{S}{S_0}. \quad (5.4)$$

The combination of the overturning component ($\bar{v}\bar{F}_a$) and gyre component ($v'F'_a$) is able to represent the total freshwater transport. The variations of freshwater transport in terms of the total, the overturning component and the gyre component are shown in Figs. 5.3a–5.3c,

respectively. The decadal variability is in general the dominant signal in all the transports, superimposed with interannual variability. The overturning component south of 40°N accounts for most of the variations of the total transport there. The most obvious exception to this is the strongly enhanced gyre component between 30°N and 40°N during the 1990s. To the north of 40°N , the gyre component shows strong coherence with the total transport. These features are reflected in the green and red curves in Fig. 5.3d, which show the correlations between the total transport and the two components at each latitude. In addition to the correlations with the total transport, the overturning component also anti-correlates with the gyre component at 34°S as well as between 20°N and 40°N (black curve in Fig. 5.3d). Considering the autocorrelation effect of the data, the significance of correlations is assessed by a nonparametric resampling method proposed by *Ebisuzaki* [1997], which is specially designed for the serially correlated data.

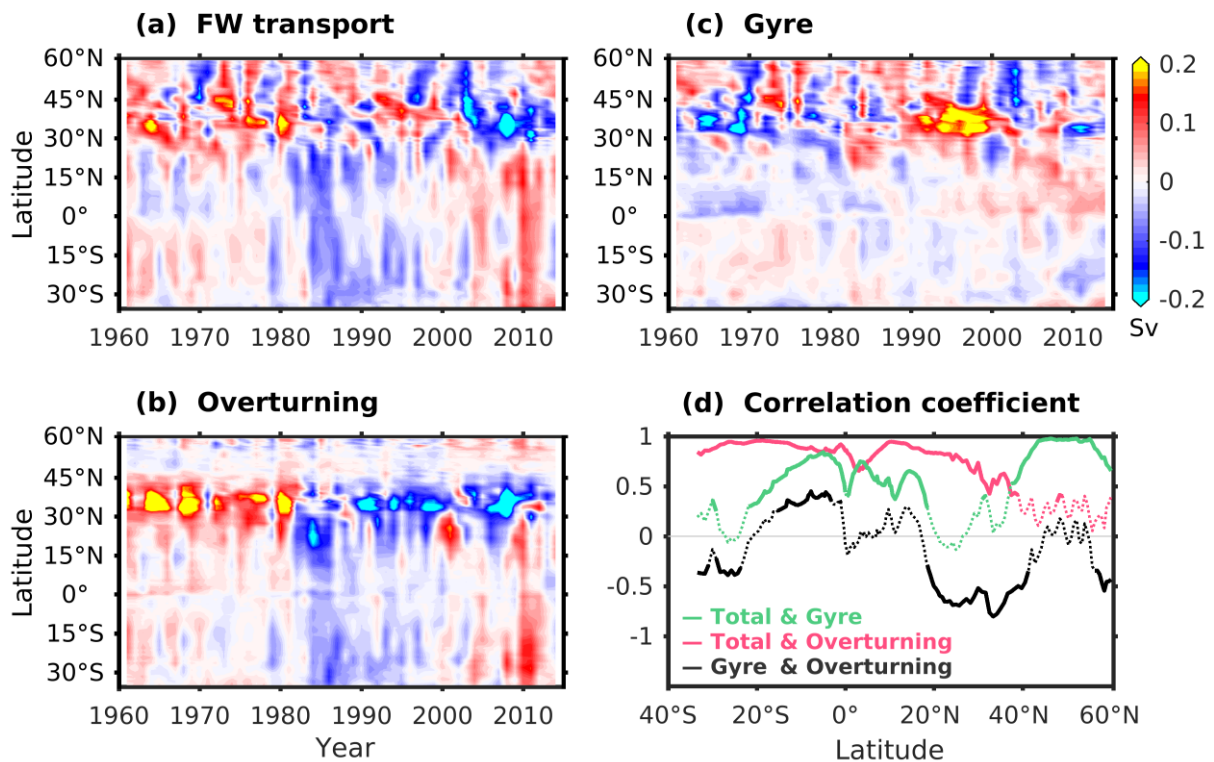


Figure 5.3 Hovmöller diagrams of the annual northward freshwater transport anomalies shown as (a) total, (b) overturning component and (c) gyre component. (d) Correlation

coefficients between total and gyre component (green), total and overturning component (red), as well as gyre and overturning components (black). The correlation coefficients are calculated after detrending and shown in bold where significant at 95% confidence level estimated by the method of *Ebisuzaki* [1997].

5.4 Freshwater content variability

This section will analyze the freshwater budget of the three prescribed regions in the Atlantic, aiming to address the main mechanisms causing the interannual to decadal variations of the freshwater content change in each region over the past 50 years. Three components are considered to contribute to the freshwater content change (ΔFWC) in each box, including the surface flux into the ocean (SF), the freshwater transports across the northern boundary (Tn) and the southern boundary (Ts). Southward is denoted as the positive direction for the two transport components. The freshwater content change (ΔFWC) is defined as the anomaly of the monthly time step (t) relative to the former time step ($t-1$) shown as follows,

$$\Delta FWC(t) = \left(\int_S^N \int_E^W FWC(x, y, t) dx dy - \int_S^N \int_E^W FWC(x, y, t-1) dx dy \right) / \Delta t. \quad (5.5)$$

Thus, a positive (negative) value of ΔFWC means that the seawater gets fresher (saltier) relative to the former time step. The freshwater budget is expressed as follows,

$$\Delta FWC = SF + Tn - Ts + res, \quad (5.6)$$

where *res* denotes the residual. Note that fluxes entering the box should increase the freshwater content in the box. Thus, a minus sign is added to Ts because a positive transport at the southern boundary is directed out of the box and reduces the freshwater content in the box. The convergence and divergence of the transports across the boundaries are defined as the net oceanic transport (T_{net}),

$$T_{net} = Tn - Ts. \quad (5.7)$$

For the freshwater budget analysis, a 4-year running mean is applied to all time series. Because according to the data description there is a possible artificial 4-year cycle introduced by the assimilation method, notably in the regions of strong adjustments (e.g. the regions of the strong western boundary currents).

5.4.1 Subtropical and subpolar North Atlantic

The freshwater budget analysis for the subtropical and subpolar North Atlantic box (23.5°N – 60°N) is shown in Fig. 5.4. The negative values of ΔFWC are detected before the late 1990s, confirming the basin-scale decrease of freshwater content. It is noticeable that there is a positive trend in ΔFWC , which correlates very well with the increasing input from the surface flux. Even after detrending, the correlation of surface flux with ΔFWC is 0.71, suggesting that the surface flux is influential in changing ΔFWC . The net freshwater transport contributes to the variations of ΔFWC as well ($r = 0.7$), especially when the variations of surface flux are small (e.g. the period 1980–1990).

The transports across the northern and southern boundaries are both important to the net transport ($r = 0.66$ and 0.77 , respectively). Before 1990, the variations of T_{net} are largely governed by T_{n} . After 1990 when the variations of T_{n} become smaller, T_{s} is in charge of the T_{net} variations. The residuals, which can be noted as the offset between ΔFWC and SUM , are relatively small. A residual is not avoidable because of the eddy fluxes, the lateral mixing processes and the possible estimation errors. However, generally small and nearly constant residuals indicate that it is possible to close the regional freshwater budget with the current fluxes since the major contributions are captured.

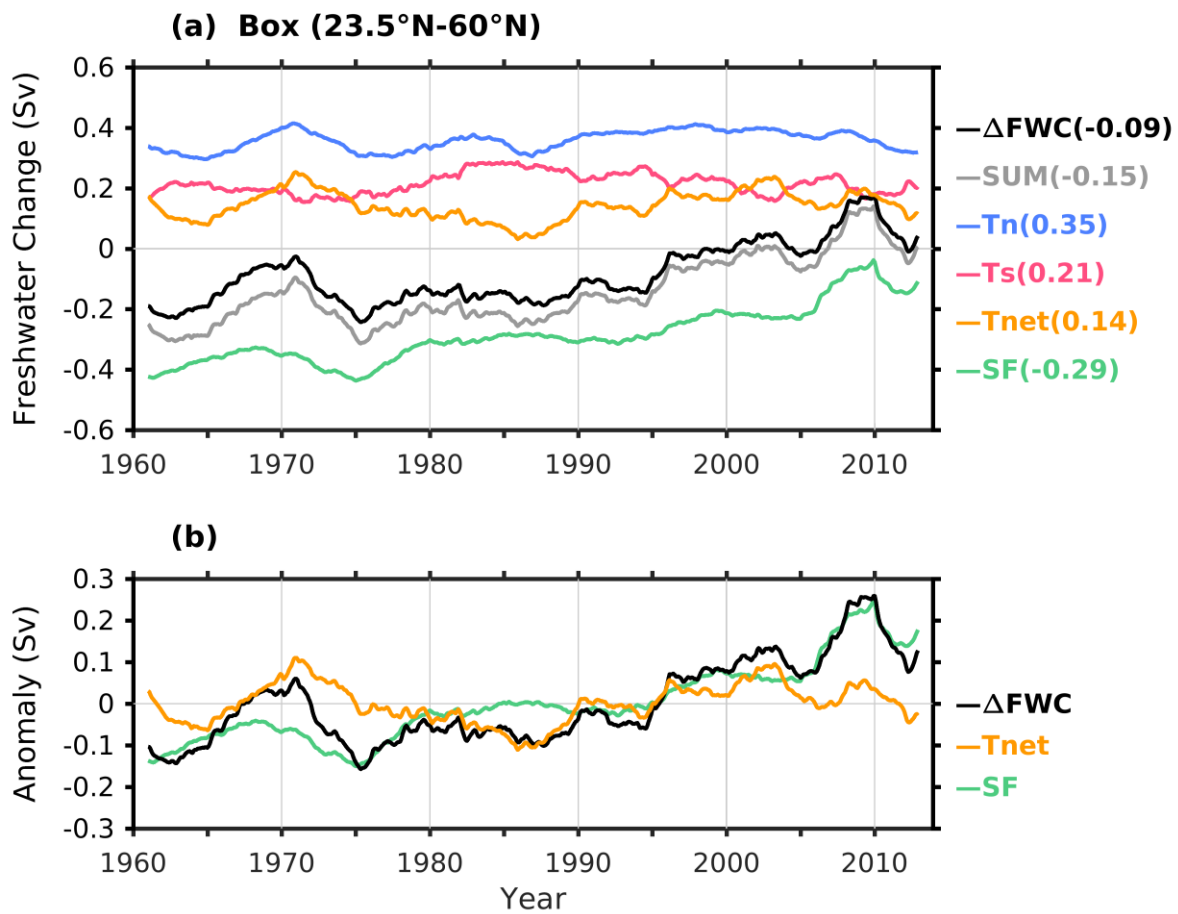


Figure 5.4 Freshwater budget analysis for the subtropical and subpolar North Atlantic box (23.5°N – 60°N). (a) Time series of the freshwater content changes (ΔFWC , black), the contributions of the freshwater transports across the northern boundary (T_n , blue) and the southern boundary (T_s , red), the convergence of T_n and T_s (T_{net} , orange), the surface freshwater flux (SF , green) and the sum of T_{net} and SF (SUM , grey). The mean value of each component is given in brackets. The fluxes into the box are denoted as positive, while southward is positive for T_n and T_s . (b) The anomalies of ΔFWC , T_{net} and SF . The time series are all smoothed with a 4-year running mean.

There is a large freshwater input from the surface since the mid-1990s that controls the variations of ΔFWC , which makes identifying the regions of the large input interesting. The

annual variations of the zonal-mean surface freshwater input anomalies are shown in Fig. 5.5. The strong positive trend of surface freshwater flux is mainly found to the north of 37°N in the subpolar region. The increased freshwater input in the subpolar region has been reported by the E–P trends in previous research [e.g. *Josey and Marsh, 2005; Skliris et al., 2014*]. The amplitude from GECCO2 is obviously too large to be natural. The surface freshwater flux from GECCO2 is calculated by the model using bulk formulae and adjusted using the adjoint method. The large freshwater input in the subpolar region could be attributed to the adjustment because the modeled salinity is larger in comparison to the salinity profiles used for assimilation, which became densely available with the Argo program in the early 2000s.

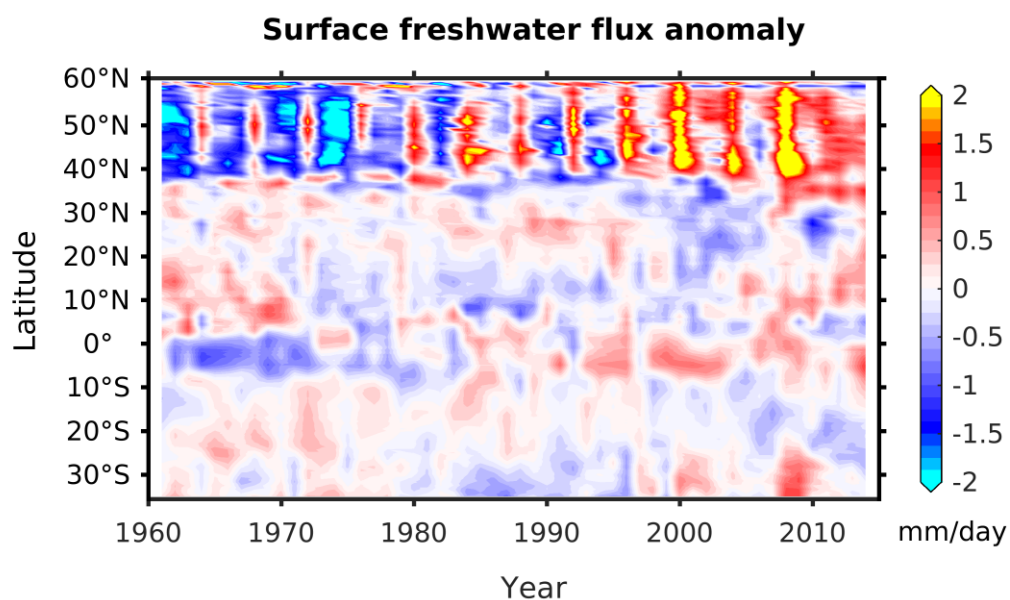


Figure 5.5 Hovmöller diagram of the anomalies of zonal-mean surface freshwater flux into the ocean (mm/day).

To the south of 37°N in the subtropical region, the variations of surface flux are relatively small and no significant trend can be noticed. This feature is also shown by the freshwater budget analysis of the sub-region ($23.5^{\circ}\text{N} - 37^{\circ}\text{N}$) (green curve in Fig. 5.6a). Since the variability of the surface flux in this sub-region is very small, it can barely contribute to the

variations of ΔFWC . Obviously, in this sub-region, the freshwater content change is dominated by the variations of the net transport ($r = 0.95$), which is well controlled by the transport across the northern boundary (blue curve in Fig. 5.6a). Moreover, the increased southward freshwater transport across 37°N since the mid-1990s coincides with the large surface freshwater input at the higher latitudes, suggesting that the large input at the higher latitudes could be a driving force of the freshwater content changes of the adjacent area in the south. This agrees with the known concept that the ocean transports the excess fresh water in the high latitudes to the lower latitudes to balance the freshwater loss there [Talley, 2008].

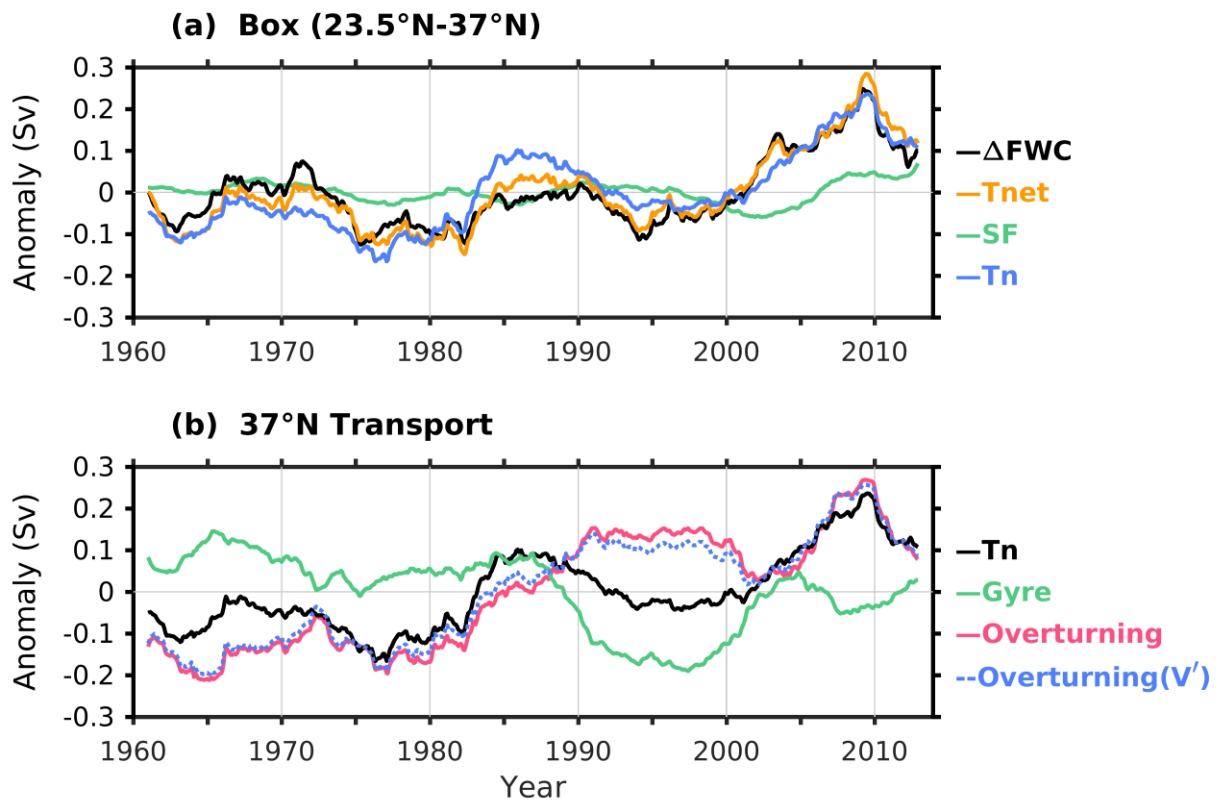


Figure 5.6 (a) The anomalies of ΔFWC (black), T_{net} (orange), SF (green) and T_n (blue) for the sub-region in the northern North Atlantic box ($23.5^\circ\text{N} - 37^\circ\text{N}$). (b) The anomalies of the transport at 37°N (T_n , black), the decomposition into the gyre component (green) and overturning component (red), as well as the contribution from the velocity changes to the overturning component (dashed-blue).

Since the transport at 37°N is important to the net transport in this sub-region, it is decomposed into the gyre and overturning components (Fig. 5.6b). The transport at 37°N is mainly influenced by the overturning component. However, there are exceptions (e.g. during the 1960s and more obviously the 1990s) when the strength of the gyre component increases to a competitive level as the strength of the overturning component and then its impact on the total transport surpasses the impact from overturning component. This connects to the anti-correlation between the overturning and gyre components shown by the black curve in Fig. 5.3d. In addition, the further decomposition of the overturning component indicates that the primary contribution to its variation is from the velocity changes, which is denoted as Overturning (V') shown by the dashed-blue curve in Fig. 5.6b.

5.4.2 Tropical North Atlantic

Shown in Fig. 5.7 is the freshwater budget analysis for the tropical North Atlantic box ($0^{\circ} - 23.5^{\circ}\text{N}$). The values of ΔFWC are found being negative or close to zero during the entire study period, in agreement with the basin-scale negative trend of freshwater content. Comparing with ΔFWC in the northern North Atlantic box (Fig. 5.4), the variation amplitude is smaller and the trend is much weaker in the tropical area. The correlation between ΔFWC and the net transport ($r = 0.7$) is slightly smaller than its correlation with the surface flux ($r = 0.77$).

As for T_n and T_s , they correlate well in general, while T_s reveals less interannual variability. Separately, neither of them shows significant correlation with ΔFWC ($r = 0.3$ and 0.2 , respectively). However, the convergence and divergence of them show considerable impact on the ΔFWC variations.

In addition, the net transport is mainly dominated by the northern boundary transport ($r = 0.8$) with no statistically significant correlation found with the southern boundary transport. As known from the transport analysis in Section 5.3, the transport at 23.5°N is governed by the

overturning component, which is controlled by the velocity changes and compensated by the gyre component with less variability (Fig. 5.7c).

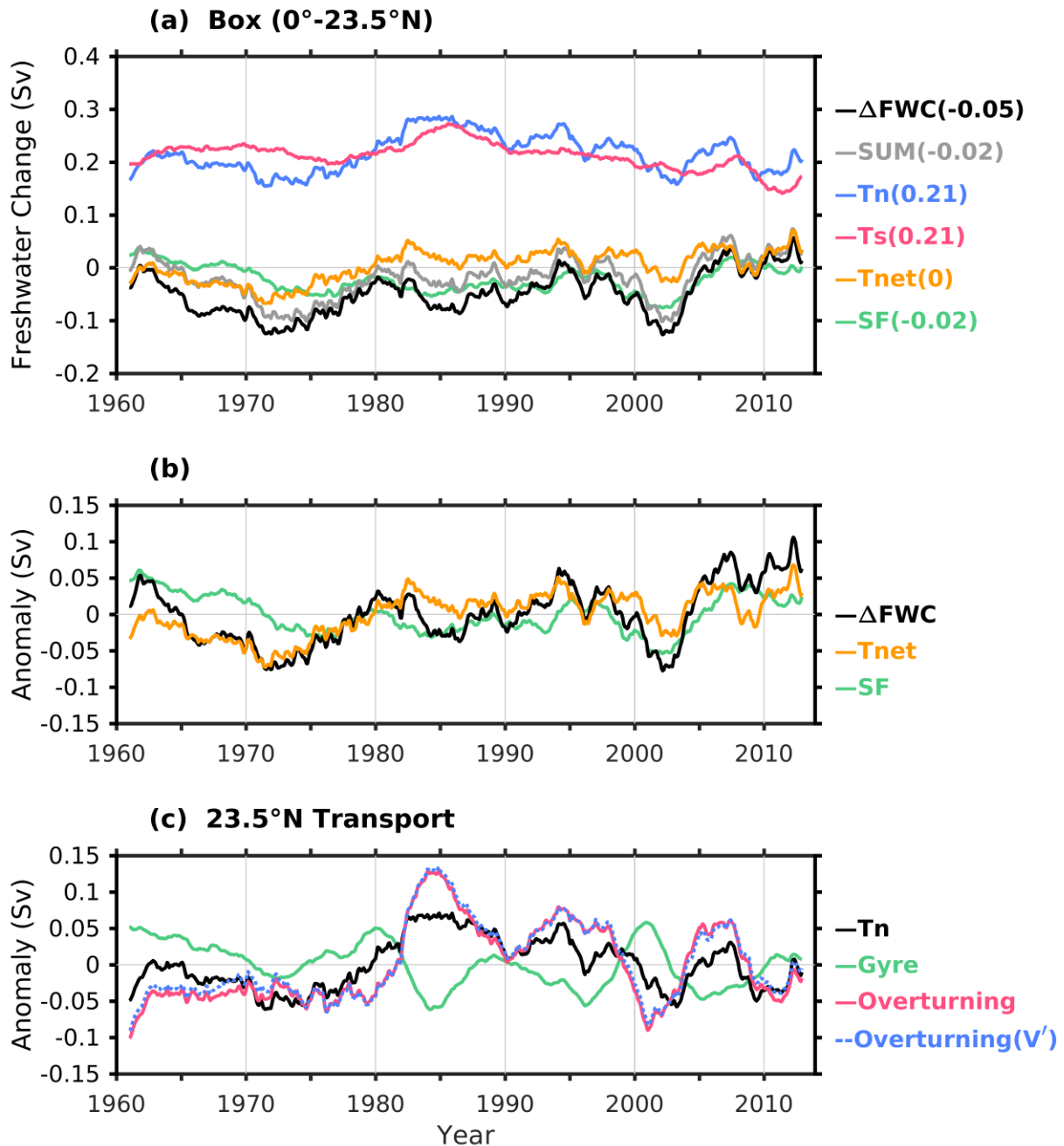


Figure 5.7 (a and b) Freshwater budget analysis same as Fig. 5.4 but for the tropical North Atlantic box (0° – 23.5°N). (c) The anomalies of the transport at 23.5°N (Tn , black), the

decomposition into the gyre component (green) and overturning component (red), as well as the contribution from the velocity changes to the overturning component (dashed-blue).

5.4.3 Tropical South Atlantic

Shown in Fig. 5.8 is the freshwater budget analysis for the tropical South Atlantic box ($23.5^{\circ}\text{S} - 0^{\circ}$). Similar to ΔFWC in the tropical North Atlantic box, the values of ΔFWC are almost always negative over the study period. The surface flux reveals relatively small variability and no statistically significant correlation with ΔFWC . The net transport, on the other hand, plays an important role in changing ΔFWC ($r = 0.8$). Like the transports across the boundaries in the tropical North Atlantic box, neither T_n nor T_s presents significant correlation with ΔFWC ($r = 0.2$ and 0.4 , respectively).

Especially, this region is where the transports across both boundaries actually converge over the entire study period, meaning southward transport across the northern boundary and northward transport across the southern boundary. The fresh water obtained from the transports balances partly the freshwater loss through the surface.

The variations of T_{net} are mostly controlled by the southern boundary transport ($r = 0.74$) with no significant correlation with the northern boundary transport. Based on the transport analysis in Section 5.3, freshwater transport at 23.5°S is predominantly governed by the overturning component typically by the contribution from the velocity changes. Different from the decomposition of the freshwater transport at 23.5°N , the variability of the gyre component at 23.5°S is generally too small to play a role except for the last few years (Fig. 5.8c).

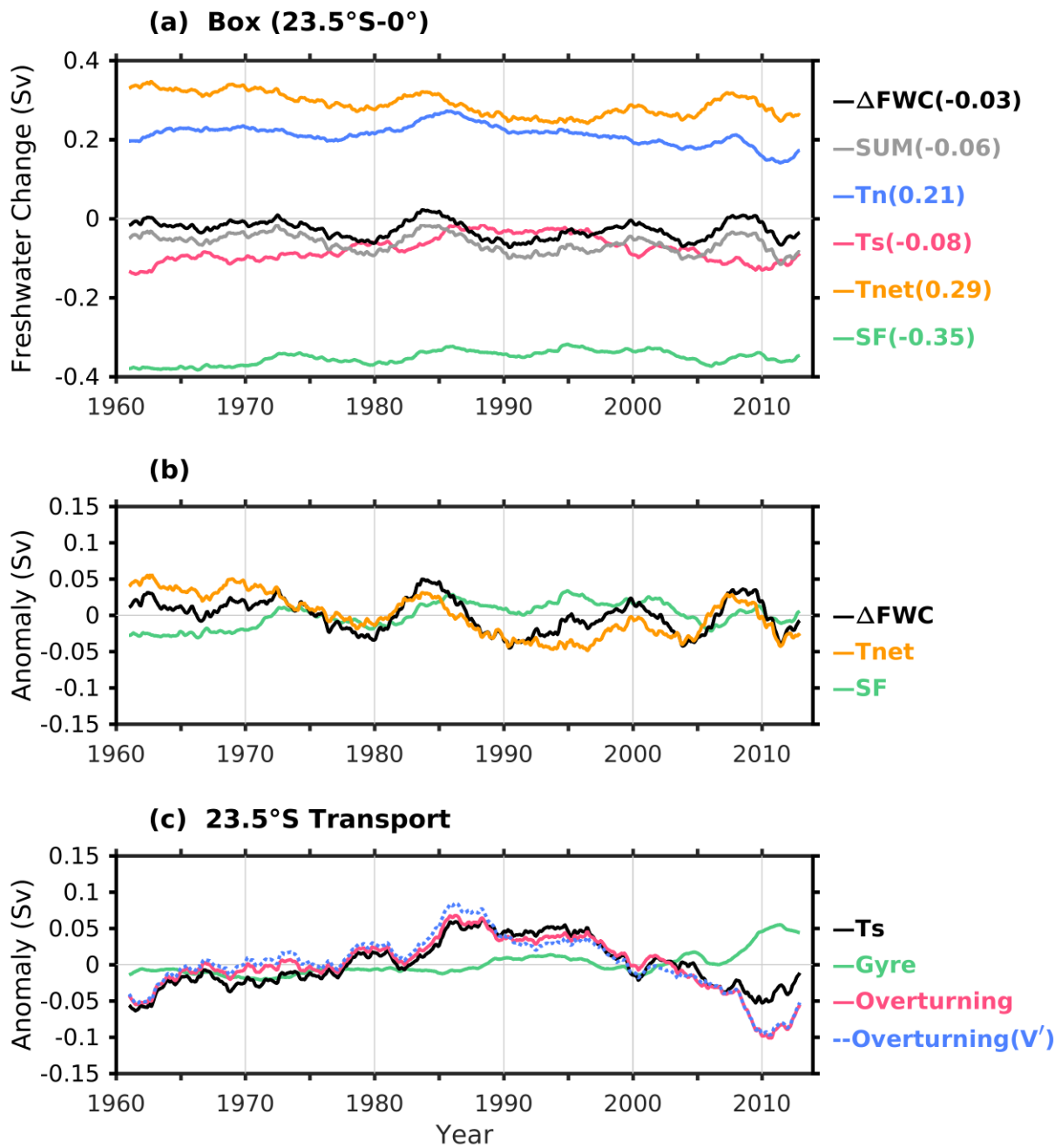


Figure 5.8 (a and b) Freshwater budget analysis same as Fig. 5.4 but for the tropical South Atlantic box (23.5°S – 0°). (c) The anomalies of the transport at 23.5°S (T_s , black), the decomposition into the gyre component (green) and overturning component (red), as well as the contribution from the velocity changes to the overturning component (dashed-blue).

5.4.4 Importance of the shallow overturning cells

The shallow overturning cells, also known as subtropical cells (STCs), are mainly wind-driven circulations and considered important in the tropical oceans [McCreary and Lu, 1994; Lu *et al.*, 1998]. The STCs have impact on the heat and water exchanges between the tropical and subtropical oceans. The presence of the STCs in the tropical Atlantic makes it intriguing to determine the relative contributions of the shallow overturning circulation and the deep overturning circulation to the temporal variations of freshwater transport.

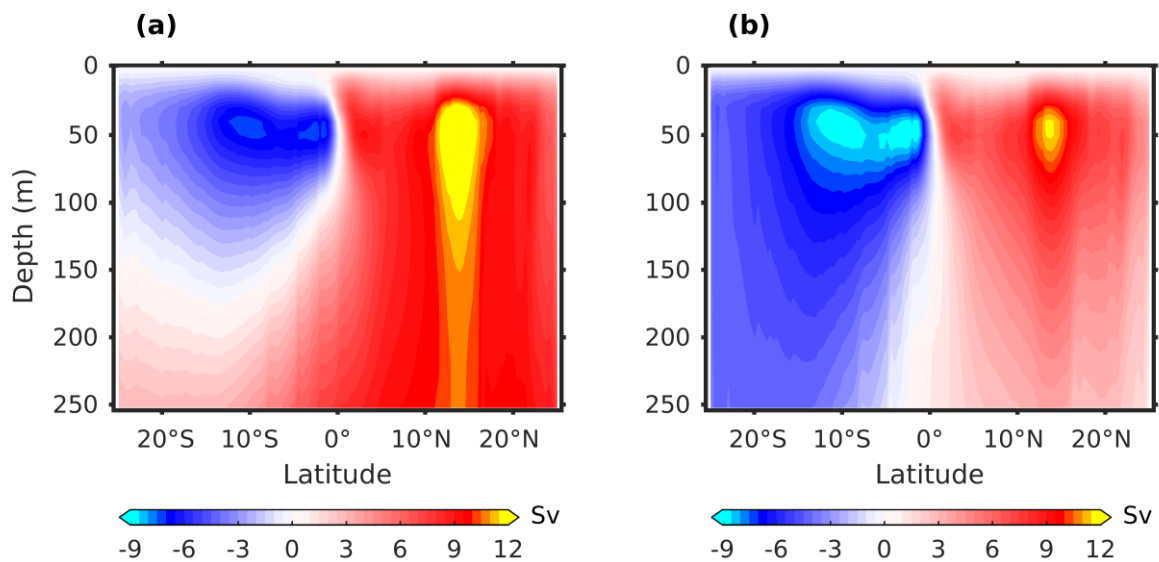


Figure 5.9 The time-mean meridional overturning streamfunction over the upper 250 m of the tropical Atlantic Ocean, shown as (a) the original structure and (b) the structure of the shallow overturning cells after decomposition (see equation (5.8) and text for details).

Figure 5.9 shows the meridional overturning streamfunction for the upper tropical Atlantic Ocean. An important feature is that only one closed shallow overturning cell can be detected and it is located south of the equator. The northern cell is more complicated because of the superimposed cross-equatorial meridional mean flow, which relates to the deep overturning circulation (hereinafter also referred to as the contribution from the deep overturning

circulation). To separate the superimposed meridional mean flow from the shallow overturning circulation, a decomposition analysis is applied and defined as follows,

$$\psi = \int_{-D}^0 \int_{west}^{east} (\bar{v} + v') dx dz. \quad (5.8)$$

Here, the overbar (\bar{v}) represents the meridional average between 25°S and 25°N, and the prime (v') denotes the deviation from the meridional average. The idea of this decomposition is to partition the deep overturning circulation related transport from the transport by the shallow overturning cells and to isolate the structure of the shallow overturning cells. As shown in Fig. 5.9b, the centers of the shallow overturning cells lie around the depth of 50 m at 14°N for the northern cell and at 10°S for the southern cell.

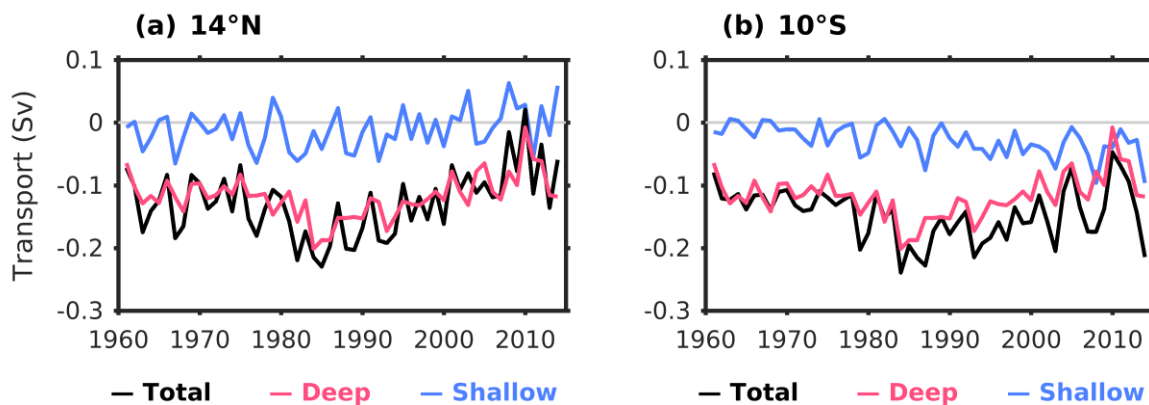


Figure 5.10 Annual time series of the northward freshwater transport as total (black) and the contributions from the deep overturning circulation (red) and the shallow overturning cells (blue), shown as the transports (a) at 14°N for the northern cell and (b) at 10°S for the southern cell.

Using the same method as shown by equation (5.8), the freshwater transports at 14°N and 10°S can be decomposed into the contributions from the deep overturning circulation and the shallow overturning circulation (Fig. 5.10). For both cells, the long-term variations of the freshwater transport are largely explained by the deep overturning contribution, while the short-term variations are more related to the shallow cell contribution, especially when the

contribution is relatively large (e.g. 1979, 1989, 1995, 2003, and 2008). For the northern cell at 14°N, the contributions from the deep overturning and the shallow cell are almost equally important to the variations of the freshwater transport ($r = 0.8$ and 0.75 , respectively). For the southern cell at 10°S, the total freshwater transport correlates better with the deep overturning contribution ($r = 0.87$) than with the shallow cell contribution ($r = 0.58$). The correlation between the shallow cell contribution and the total transport increases to 0.77 for the period 1986–2014, when the variability of the shallow cell contribution becomes larger since the mid-1980s.

As suggested by Fig. 5.3, the meridional freshwater transport in the tropical Atlantic is highly related to its overturning component ($r = 0.88$ and 0.92 for 14°N and 10°S, respectively), which traditionally represents the freshwater transport associated with the AMOC. This analysis helps to clarify the influence of different parts of the AMOC and highlights the importance of the shallow overturning cells in the tropical region especially for case studies. Due to its potential to indicate the freshwater transport by the shallow overturning cells, further investigation regarding the role of shallow cell strength would be worthwhile.

5.5 Discussion and summary

In this chapter, the outputs of the GECCO2 ocean synthesis over the period 1961–2014 are used to analyze the variabilities of the Atlantic freshwater transport and surface freshwater flux, especially their roles in changing the freshwater content on interannual and decadal time scales. For this purpose, three study areas have been evaluated separately with a focus to determine the dominant driving force of the regional freshwater content changes in the Atlantic Ocean.

To advance the understanding of the Atlantic freshwater transport variability, decomposition analysis is used to distinguish different contributions from the overturning and gyre circulation. In general, the overturning component that is governed by the velocity changes

predominates the total freshwater transport variations to the south of 40°N , while the gyre component plays a role in the tropical region and to the north of 40°N . The gyre and overturning components reveal anti-correlation with each other at 34°S as well as the latitudes between 20°N and 40°N .

The freshwater budget analysis for the North Atlantic box ($23.5^{\circ}\text{N} - 60^{\circ}\text{N}$) suggests that the net freshwater transport and the surface flux are both important to the ΔFWC variations. An increased surface freshwater input is observed over the last two decades in the subpolar region to the north of 37°N , which tends to increase the freshwater content in the box. In the sub-region to the south of 37°N where the variations of surface flux are very small, the ΔFWC variations are fully under the control of the net transport, which is largely influenced by the transport at 37°N . Interestingly, the positive trend in the southward freshwater transport at 37°N since the mid-1990s coincides with the increasing freshwater input at the higher latitudes. It suggests that the large surface freshwater input at the higher latitudes could be a driving force of the freshwater content changes of the adjacent area in the south, via affecting the transport variations by the overturning circulation.

For the northern tropical box, both the net transport and the surface flux contribute to the freshwater content changes. Moreover, the net transport is mainly related to the transport at 23.5°N , which is controlled by the overturning component and reduced by the gyre component with less variability. Different from the northern tropical box, the variations of ΔFWC in the southern tropical box are mainly due to the variations of the transport convergence across the boundaries. The variations of the transport convergence are governed by the transport at 23.5°S , where the variability of the gyre component is very small so the overturning component prevails. The surface flux with relatively small variability does not play a role here.

Given the importance of the overturning component to the total freshwater transport variations in the tropical and subtropical Atlantic and the existence of the shallow overturning cells, a study is carried out to partition the contributions from the deep overturning circulation and the shallow cells. The result suggests that the shallow cell contribution is influential to the

interannual variations of the freshwater transport, whereas the deep overturning contribution dominates the decadal variations.

CHAPTER 6

Conclusions and outlook

6.1 Thesis overview

This thesis focuses on two aspects. The first is to understand the dynamical adjustment of ocean circulation to the projected future changes in the global hydrological cycle. The second is to investigate the freshwater content changes in the Atlantic with respect to the roles of the oceanic freshwater transport and the surface freshwater flux. The main results and conclusions are summarized in Section 6.1 and followed by the recommendations for further work in Section 6.2.

6.1.1 The impacts of surface volume flux on ocean circulation

The impacts of surface volume flux on ocean circulation were studied using the GECCO2 configuration with a focus to understand the GSC response to the projected future changes in the global hydrological cycle. Four simulations were carried out using two salinity boundary conditions (virtual salt flux formulation and volume flux forcing formulation) forced by the present-day NCEP freshwater flux first and then by the additional projected E–P anomalies.

From the ensemble-mean MPI-ESM LR RCP8.5 surface freshwater flux anomalies, we note an intensification of about 13.2% (on global average) in response to a 3.6 °C warming by the end of the century relative to its beginning. In response to the enhanced surface freshwater flux, the induced GSC and the associated MOC increase by around 20% in mid and low latitudes, while a stronger intensification about 50% is noticed in the Southern Ocean, comparing to the present-day response.

Associated with the circulation component is a response in temperature and salinity, based on which a significant contribution to the regional sea level changes is found in form of steric change. These changes can be largely attributed to the displacement of the isopycnals. The typical amplitude of sea level changes induced by the projected freshwater flux anomalies is of the order of 0.5 cm.

In most parts of the ocean, total changes of the transport properties relate to the overturning components, which are dominated by the velocity changes, especially for the heat transport. For the gyre components of the freshwater transport, the anti-correlation between the contributions from velocity and freshwater changes suggests a negative feedback of freshwater anomalies caused by the changed barotropic circulation.

The volume flux mostly weakens the mean MOC in the upper 500 m, while slightly enhances the deep meridional overturning. The MOC changes that naturally connect regions of net surface volume flux divergence with those of net convergence in the interior, indicating that the overturning components of the heat and freshwater transport changes are carried by the volume transports mainly through the shallow cells in the ocean, without changing the heat and freshwater contents. The decomposition into the barotropic and baroclinic components confirms the coexistence of the short-term barotropic and long-term baroclinic adjustments in response to the volume flux forcing. In addition, the freshwater function analysis suggests that the continuation of the atmospheric freshwater cycle into the interior of the ocean is different from the assumed simple barotropic transport and takes somewhat different pathways for volume and the associated salinity signal.

Our study confirms that the volume signal associated with changes in the net freshwater forcing anticipated to occur in the future as a result of an accelerated global hydrological cycle will induce the ocean circulation changes that to a large extent can be rationalized in terms of a barotropic response to the surface freshwater volume flux as described by the GSC theory. Changes also occur in the MOC, and jointly the circulation changes will result in changes of transport pattern leading to a redistribution of heat and freshwater and impacting the regional sea level patterns.

Although changes related to the RCP scenarios in sea level and barotropic gyre circulation are small in comparison to the total changes, understanding the related changes contributes to understand ocean's response to global warming, in particular also to explain differences between models that facilitate volume flux forcing or virtual salt flux forcing.

6.1.2 The roles of surface freshwater flux and freshwater transport in the Atlantic freshwater content variations

The processes and mechanisms related to the Atlantic freshwater content changes over the period 1961–2014 were analyzed using the GECCO2 ocean synthesis, particularly focusing on the characteristics of the freshwater transport variations. This was done by the freshwater budget analyses in three regions: the subtropical and subpolar North Atlantic ($23.5^{\circ}\text{N} - 60^{\circ}\text{N}$), the tropical North Atlantic ($0^{\circ} - 23.5^{\circ}\text{N}$), and the tropical South Atlantic ($23.5^{\circ}\text{S} - 0^{\circ}$).

The freshwater content changes in the subtropical and subpolar North Atlantic ($23.5^{\circ}\text{N} - 60^{\circ}\text{N}$) can be attributed to the combined impacts of the surface freshwater flux and the net freshwater transport across the boundaries. The latitude 37°N needs to be emphasized in this study area, because large variability is observed around this latitude almost for every variable in the study, e.g. freshwater content, seawater salinity at 1000 m depth, freshwater transport and its decomposed components. Caution should be exercised here since the large variability could be partly due to the 4-year cycle associated with the dependence of the adjustments

within each assimilation window. A strongly increased surface freshwater input is also found to the north of 37°N over the last two decades, which can be partly explained by the natural variability of the global water cycle intensification and partly by the model adjustment because of the assimilation. More importantly, the increased freshwater input enhances the southward transport at 37°N through the overturning circulation, by which it plays a role in changing the freshwater content of the sub-region to the south of 37°N .

For the two tropical boxes, the surface flux plays a role in changing the freshwater content in the northern box but shows no significant impact in the southern box because of the relatively weak interannual variations. The net transports, on the other hand, are of importance to the freshwater content changes in both tropical boxes. The freshwater transport variability to the south of 40°N is largely determined by its overturning component, which conventionally represents the freshwater transport associated with AMOC. The analysis used to separate the contributions of the deep overturning circulation and the shallow overturning cells clarifies that the deep overturning contribution is far-reaching for the decadal variations, while the shallow cell contribution is more influential to the interannual variations, especially when the contribution is relatively large.

6.2 Future work

The findings of the thesis have also evoked new questions as well as interests in need of further investigation. Some suggestions for future efforts are highlighted in this section. The answers to these questions will also improve the understanding of the fundamental physical processes in the ocean and their interactions with climate change.

- 1) It would be interesting to use a climate model to evaluate the impacts of surface volume flux under different RCP scenarios regarding the possible interactions with the warming effect. This study has discussed the expected GSC intensification using the projected E–P anomalies, aiming to provide dynamical explanations about the impacts of the accelerated water cycle on

the ocean circulation as a starting point. Continued efforts on this topic are needed by using climate models for future work.

2) As for the study about the Atlantic freshwater content variability, the presented results could be model-dependent. Therefore, one could take the opportunity to use the newly available observations (e.g. the time-varying ocean salinity field from the Argo float system and the AMOC transport at 26.5°N since April 2004 from the RAPID array) and compare/combine with the model simulations to get a fresh view on the ocean dynamics.

3) Furthermore, as a vital element of the Atlantic climate system, the stability of the AMOC in response to global warming is always one of the key topics. The overturning component of the freshwater transport at 34°S has been suggested as an AMOC stability indicator in previous studies [*Rahmstorf, 1996; de Vries and Weber, 2005; Hawkins et al., 2011; Mecking et al., 2017*]. Several studies have proposed to use the divergence of the overturning component of the freshwater transport across the Atlantic as a better indicator [*Huisman et al., 2010; Liu et al., 2017*]. The variability of freshwater transport at 34°S is not a focus in this study. The overturning component, however, anti-correlates with the gyre component at 34°S as shown in Fig. 5.3d. Investigating how they interact with each other around this latitude may provide a better understanding of this stability indicator of AMOC.

References

- Agarwal, N., A. Köhl, C. R. Mechoso, and D. Stammer (2014), On the early response of the climate system to a meltwater input from Greenland, *J. Climate*, 27(21), 8276–8296, doi: 10.1175/jcli-d-13-00762.1.
- Allan, R. P., C. Liu, M. Zahn, D. A. Lavers, E. Koukouvagias, and A. Bodas-Salcedo (2014), Physically consistent responses of the global atmospheric hydrological cycle in models and observations, *Surveys in Geophysics*, 35(3), 533–552, doi: 10.1007/s10712-012-9213-z.
- Allen, M. R., and W. J. Ingram (2002), Constraints on future changes in climate and the hydrologic cycle, *Nature*, 419(6903), 224–232, doi: 10.1038/nature01092.
- Andersson, A., K. Fennig, C. Klepp, S. Bakan, H. Graßl, and J. Schulz (2010), The Hamburg Ocean Atmosphere Parameters and Fluxes from Satellite Data – HOAPS-3, *Earth Syst. Sci. Data*, 2(2), 215–234, doi: 10.5194/essd-2-215-2010.
- Antonov, J. I., S. Levitus, and T. P. Boyer (2002), Steric sea level variations during 1957–1994: Importance of salinity, *J. Geophys. Res.*, 107(C12), 8013, doi: 10.1029/2001jc000964.
- Antonov, J. I., R. A. Locarnini, T. P. Boyer, A. V. Mishonov, and H. E. Garcia (2006), World Ocean Atlas 2005, Volume 2: Salinity, *NOAA Atlas NESDIS*, vol. 62, edited by S. Levitus, 182 pp., U.S. Government Printing Office, Washington, D.C.

- Arakawa, A., and V. R. Lamb (1977), Computational design of the basic dynamical processes of the UCLA general circulation model, in *General Circulation Models of the Atmosphere, Methods Comput. Phys.*, edited by J. Chang, Vol. 17, pp. 173–265, Academic Press, San Diego, Calif.
- Boccaletti, G., R. Ferrari, A. Adcroft, D. Ferreira, and J. Marshall (2005), The vertical structure of ocean heat transport, *Geophys. Res. Lett.*, 32(10), L10603, doi: 10.1029/2005gl022474.
- Böning, C. W., and F.O. Bryan (1996), Large-scale transport processes in high-resolution circulation models, *The Warmwatersphere of the North Atlantic Ocean*, edited by W. Krauss, pp. 91–128, Gebr. Bornträger, Berlin, Stuttgart.
- Boyer, T. P., S. Levitus, J. I. Antonov, R. A. Locarnini, and H. E. Garcia (2005), Linear trends in salinity for the World Ocean, 1955–1998, *Geophys. Res. Lett.*, 32(1), L01604, doi: 10.1029/2004gl021791.
- Boyer, T., S. Levitus, J. Antonov, R. Locarnini, A. Mishonov, H. Garcia, and S. A. Josey (2007), Changes in freshwater content in the North Atlantic Ocean 1955–2006, *Geophys. Res. Lett.*, 34(16), L16603, doi: 10.1029/2007gl030126.
- Bryan, F. (1986), High-latitude salinity effects and interhemispheric thermohaline circulations, *Nature*, 323(6086), 301–304, doi: 10.1038/323301a0.
- Chou, C., and J. D. Neelin (2004), Mechanisms of Global Warming Impacts on Regional Tropical Precipitation, *J. Climate*, 17(13), 2688–2701, doi: 10.1175/1520-0442(2004)017<2688:mogwio>2.0.co;2.
- Chou, C., J. C. H. Chiang, C.-W. Lan, C.-H. Chung, Y.-C. Liao, and C.-J. Lee (2013), Increase in the range between wet and dry season precipitation, *Nature Geosci*, 6(4), 263–267, doi: 10.1038/NGEO1744.
- Collins, M., R. Knutti, J. Arblaster, J.-L. Dufresne, T. Fichefet, P. Friedlingstein, X. Gao, W.J. Gutowski, T. Johns, G. Krinner, M. Shongwe, C. Tebaldi, A.J. Weaver and M. Wehner (2013), Long-term Climate Change: Projections, Commitments and

- Irreversibility, in: *Climate Change 2013: The Physical Science Basis. Contribution of Working Group I to the Fifth Assessment Report of the Intergovernmental Panel on Climate Change*, edited by T. F. Stocker, Cambridge University Press, Cambridge, United Kingdom and New York, NY, USA.
- Cunningham, S. A., et al. (2007), Temporal variability of the Atlantic meridional overturning circulation at 26.5°N, *Science*, 317(5840), 935–938, doi: 10.1126/science.1141304.
- Curry, R., B. Dickson, and I. Yashayaev (2003), A change in the freshwater balance of the Atlantic Ocean over the past four decades, *Nature*, 426(6968), 826–829, doi: 10.1038/nature02206.
- Curry, R., and C. Mauritzen (2005), Dilution of the northern North Atlantic Ocean in recent decades, *Science*, 308(5729), 1772–1774, doi: 10.1126/science.1109477.
- de Vries, P., and S. L. Weber (2005), The Atlantic freshwater budget as a diagnostic for the existence of a stable shut down of the meridional overturning circulation, *Geophys. Res. Lett.*, 32, L09606, doi: 10.1029/2004gl021450.
- Deshayes, J., R. Curry, and R. Msadek (2014), CMIP5 model intercomparison of freshwater budget and circulation in the North Atlantic, *J. Climate*, 27(9), 3298–3317, doi: 10.1175/jcli-d-12-00700.1.
- Dickson, B., I. Yashayaev, J. Meincke, B. Turrell, S. Dye, and J. Holfort (2002), Rapid freshening of the deep North Atlantic Ocean over the past four decades, *Nature*, 416(6883), 832–837, doi: 10.1038/416832a.
- Doney, S. C., S. Yeager, G. Danabasoglu, W. G. Large, and J. C. McWilliams (2007), Mechanisms governing interannual variability of upper-ocean temperature in a global ocean hindcast simulation, *J. Phys. Oceanogr.*, 37(7), 1918–1938, doi: 10.1175/JPO3089.1.
- Durack, P. J., T. Lee, N. T. Vinogradova, and D. Stammer (2016), Keeping the lights on for global ocean salinity observation, *Nature Clim. Change*, 6(3), 228–231, doi: 10.1038/nclimate2946.

- Durack, P. J., and S. E. Wijffels (2010), Fifty-year trends in global ocean salinities and their relationship to broad-scale warming, *J. Climate*, 23(16), 4342–4362, doi: 10.1175/2010JCLI3377.1.
- Durack, P. J., S. E. Wijffels, and R. J. Matear (2012), Ocean salinities reveal strong global water cycle intensification during 1950 to 2000, *Science*, 336(6080), 455–458, doi: 10.1126/science.1212222.
- Durack, P. J., S. E. Wijffels, and P. J. Gleckler (2014), Long-term sea-level change revisited: the role of salinity, *Environ. Res. Lett.*, 9(11), 114017, doi: 10.1088/1748-9326/9/11/114017.
- Ebisuzaki, W. (1997), A method to estimate the statistical significance of a correlation when the data are serially correlated, *J. Climate*, 10(9), 2147–2153, doi: 10.1175/1520-0442(1997)010<2147:amtets>2.0.co;2.
- Fekete, B. M., C. J. Vorosmarty, and W. Grabs (1999), An improved global spatially-distributed runoff data set based on observed river discharge and simulated water balance, 35 pp., report, *Complex Syst. Res. Cent., Univ. of New Hampshire, Durham*.
- Fennig, K., A. Andersson, S. Bakan, C. Klepp, and M. Schroeder (2012), Hamburg Ocean Atmosphere Parameters and Fluxes from Satellite Data - HOAPS 3.2 - Monthly Means / 6-Hourly Composites. Satellite Application Facility on Climate Monitoring. doi:10.5676/EUM_SAF_CM/HOAPS/V001.
- Font, J., et al. (2013), SMOS first data analysis for sea surface salinity determination, *Int. J. Remote Sens.*, 34(9–10), 3654–3670, doi: 10.1080/01431161.2012.716541.
- Ganachaud, A., and C. Wunsch (2003), Large-scale ocean heat and freshwater transports during the World Ocean Circulation Experiment, *J. Climate*, 16(4), 696–705, doi: 10.1175/1520-0442(2003)016<0696:LSOHAF>2.0.CO;2.
- Gent, P. R., and J. C. McWilliams (1990), Isopycnal mixing in ocean circulation models, *J. Phys. Oceanogr.*, 20(1), 150–155, doi: 10.1175/1520-0485(1990)020<0150:imiocm>2.0.co;2.

- Giorgetta, M., et al. (2012a), *CMIP5 Simulations of the Max Planck Institute for Meteorology (MPI-M) Based on the MPI-ESM-LR Model: The historical experiment, served by ESGF*, WDCC, DKRZ, doi: 10.1594/WDCC/CMIP5.MXELhi.
- Giorgetta, M., et al. (2012b), *CMIP5 Simulations of the Max Planck Institute for Meteorology (MPI-M) Based on the MPI-ESM-LR Model: The rcp45 experiment, served by ESGF*, WDCC, DKRZ, doi: 10.1594/WDCC/CMIP5.MXELr4.
- Giorgetta, M., et al. (2012c), *CMIP5 Simulations of the Max Planck Institute for Meteorology (MPI-M) Based on the MPI-ESM-LR Model: The rcp85 experiment, served by ESGF*, WDCC, DKRZ, doi: 10.1594/WDCC/CMIP5.MXELr8.
- Giorgetta, M. A., et al. (2013), Climate and carbon cycle changes from 1850 to 2100 in MPI-ESM simulations for the Coupled Model Intercomparison Project phase 5, *J. Adv. Model Earth Systems*, 5(3), 572–597, doi: 10.1002/jame.20038.
- Goldsbrough, G. R. (1933), Ocean currents produced by evaporation and precipitation, *Proc. R. Soc. London Ser. A*, 141(844), 512–517, doi: 10.1098/rspa.1933.0135.
- Griffies, S. M., et al. (2014), An assessment of global and regional sea level for years 1993–2007 in a suite of interannual CORE-II simulations, *Ocean Modelling*, 78, 35–89, doi: 10.1016/j.ocemod.2014.03.004.
- Häkkinen, S., and A. Proshutinsky (2004), Freshwater content variability in the Arctic Ocean, *J. Geophys. Res.*, 109(C3), C03051, doi: 10.1029/2003jc001940.
- Hawkins, E., R. S. Smith, L. C. Allison, J. M. Gregory, T. J. Woollings, H. Pohlmann, and B. de Cuevas (2011), Bistability of the Atlantic overturning circulation in a global climate model and links to ocean freshwater transport, *Geophys. Res. Lett.*, 38(10), L10605, doi: 10.1029/2011gl047208.
- Held, I. M., and B. J. Soden (2006), Robust responses of the hydrological cycle to global warming, *J. Climate*, 19(21), 5686–5699, doi: 10.1175/jcli3990.1.

- Helm, K. P., N. L. Bindoff, and J. A. Church (2010), Changes in the global hydrological-cycle inferred from ocean salinity, *Geophys. Res. Lett.*, 37, L18701, doi: 10.1029/2010gl044222.
- Holliday, N. P., et al. (2008), Reversal of the 1960s to 1990s freshening trend in the northeast North Atlantic and Nordic Seas, *Geophys. Res. Lett.*, 35(3), L03614, doi: 10.1029/2007gl032675.
- Hosoda, S., T. Suga, N. Shikama, and K. Mizuno (2009), Global surface layer salinity change detected by Argo and its implication for hydrological cycle intensification, *J. Oceanography*, 65(4), 579–586, doi: 10.1007/s10872-009-0049-1.
- Hough, S. S. (1897), On the application of harmonic analysis to the dynamical theory of the tides. Part I. On Laplace's "Oscillations of the First Species," and on the dynamics of ocean currents, *Philosophical Transactions of the Royal Society of London A: Mathematical, Physical and Engineering Sciences*, 189, 201–257, doi: 10.1098/rsta.1897.0009.
- Huang, R. X. (1993), Real freshwater flux as a natural boundary condition for the salinity balance and thermohaline circulation forced by evaporation and precipitation, *J. Phys. Oceanogr.*, 23(11), 2428–2446, doi: 10.1175/1520-0485(1993)023<2428:RFFAAN>2.0.CO;2.
- Huang, R.X. (2010), *Ocean Circulation: Wind-driven and Thermohaline Processes*, 791 pp., Cambridge University Press, Cambridge.
- Huang, R. X., and R. W. Schmitt (1993), The Goldsbrough-Stommel circulation of the world oceans, *J. Phys. Oceanogr.*, 23(6), 1277–1284, doi: 10.1175/1520-0485(1993)023<1277:Tgcotw>2.0.Co;2.
- Huisman, S. E., M. d. Toom, H. A. Dijkstra, and S. Drijfhout (2010), An indicator of the multiple equilibria regime of the Atlantic meridional overturning circulation, *J. Phys. Oceanogr.*, 40(3), 551–567, doi: 10.1175/2009jpo4215.1.

- IPCC (2014), Climate Change 2014: Synthesis Report, *Contribution of Working Groups I, II and III to the Fifth Assessment Report of the Intergovernmental Panel on Climate Change*, Core Writing Team, edited by R.K. Pachauri and L.A. Meyer, 151 pp., IPCC, Geneva, Switzerland.
- Jahn, A., B. Tremblay, L. A. Mysak, and R. Newton (2010), Effect of the large-scale atmospheric circulation on the variability of the Arctic Ocean freshwater export, *Clim. Dynam.*, *34*(2), 201–222, doi: 10.1007/s00382-009-0558-z.
- Josey, S. A., and R. Marsh (2005), Surface freshwater flux variability and recent freshening of the North Atlantic in the eastern subpolar gyre, *J. Geophys. Res.*, *110*, C05008, doi: 10.1029/2004jc002521.
- Kalnay, E., et al. (1996), The NCEP/NCAR 40-year reanalysis project, *Bull. Am. Meteorol. Soc.*, *77*(3), 437–471, doi: 10.1175/1520-0477(1996)077<0437:Tnyrp>2.0.Co;2.
- Köberle, C., and R. Gerdes (2007), Simulated variability of the Arctic Ocean freshwater balance 1948–2001, *J. Phys. Oceanogr.*, *37*(6), 1628–1644, doi: 10.1175/jpo3063.1.
- Köhl, A. (2014), Detecting processes contributing to interannual halosteric and thermosteric sea level variability, *J. Climate*, *27*(6), 2417–2426, doi: 10.1175/JCLI-D-13-00412.1.
- Köhl, A. (2015), Evaluation of the GECCO2 ocean synthesis: transports of volume, heat and freshwater in the Atlantic, *Q. J. Roy. Meteor. Soc.*, *141*(686), 166–181, doi: 10.1002/qj.2347.
- Köhl, A., and N. Serra (2014), Causes of decadal changes of the freshwater content in the Arctic Ocean, *J. Climate*, *27*(9), 3461–3475, doi: 10.1175/jcli-d-13-00389.1.
- Köhl, A., F. Siegmund, and D. Stammer (2012), Impact of assimilating bottom pressure anomalies from GRACE on ocean circulation estimates, *J. Geophys. Res.*, *117*, C04032, doi: 10.1029/2011jc007623.
- Lagerloef, G., R. Schmitt, J. Schanze, and H. Y. Kao (2010), The ocean and the global water cycle. *Oceanography*, *23*(4), 82–93, doi: 10.5670/oceanog.2010.07.

- Lagerloef, G. (2012), Satellite mission monitors ocean surface salinity. *Eos Trans. AGU*, 93(25), 233–234, doi: 10.1029/2012eo250001.
- Lago, V., Wijffels, S. E., Durack, P. J., Church, J. A., Bindoff, N. L., and Marsland, S. J. (2016). Simulating the role of surface forcing on observed multidecadal upper-ocean salinity changes, *J. Climate*, 29(15), 5575–5588, doi: 10.1175/jcli-d-15-0519.1.
- Large, W. G., J. C. McWilliams, and S. C. Doney (1994), Oceanic vertical mixing: A review and a model with a nonlocal boundary layer parameterization, *Rev. Geophys.*, 32(4), 363–403, doi: 10.1029/94rg01872.
- Levang, S. J., and R. W. Schmitt (2015), Centennial changes of the global water cycle in CMIP5 models, *J. Climate*, 28(16), 6489–6502, doi: 10.1175/jcli-d-15-0143.1.
- Levitus, S., J. I. Antonov, T. P. Boyer, H. E. Garcia, and R. A. Locarnini (2005), Linear trends of zonally averaged thermosteric, halosteric, and total steric sea level for individual ocean basins and the world ocean, (1955–1959)–(1994–1998), *Geophys. Res. Lett.*, 32(16), L16601, doi: 10.1029/2005gl023761.
- Liu, C. L., and R. P. Allan (2013), Observed and simulated precipitation responses in wet and dry regions 1850–2100, *Environ. Res. Lett.*, 8(3), 034002, doi: 10.1088/1748-9326/8/3/034002.
- Liu, W., S.-P. Xie, Z. Liu, and J. Zhu (2017), Overlooked possibility of a collapsed Atlantic Meridional Overturning Circulation in warming climate, *Science Advances*, 3(1), e1601666, doi: 10.1126/sciadv.1601666.
- Lorbacher, K., S. J. Marsland, J. A. Church, S. M. Griffies, and D. Stammer (2012), Rapid barotropic sea level rise from ice sheet melting, *J. Geophys. Res.*, 117, C06003, doi: 10.1029/2011jc007733.
- Lu, P., J. P. McCreary, and B. A. Klinger (1998), Meridional circulation cells and the source waters of the Pacific equatorial undercurrent, *J. Phys. Oceanogr.*, 28(1), 62–84, doi: 10.1175/1520-0485(1998)028<0062:mccats>2.0.co;2.

- Maltrud, M. E., and J. L. McClean (2005), An eddy resolving global $1/10^\circ$ ocean simulation, *Ocean Modelling*, 8(1–2), 31–54, doi: 10.1016/j.ocemod.2003.12.001.
- Marshall, J., C. Hill, L. Perelman, and A. Adcroft (1997), Hydrostatic, quasi-hydrostatic, and nonhydrostatic ocean modeling, *J. Geophys. Res.*, 102(C3), 5733–5752, doi: 10.1029/96jc02776.
- McCreary, J. P., and P. Lu (1994), Interaction between the subtropical and equatorial ocean circulations: The subtropical cell, *J. Phys. Oceanogr.*, 24(2), 466–497, doi: 10.1175/1520-0485(1994)024<0466:ibtsae>2.0.co;2.
- McDonagh, E. L., B. A. King, H. L. Bryden, P. Courtois, Z. Szuts, M. Baringer, S. A. Cunningham, C. Atkinson, and G. McCarthy (2015), Continuous estimate of Atlantic oceanic freshwater flux at 26.5°N , *J. Climate*, 28(22), 8888–8906, doi: 10.1175/jcli-d-14-00519.1.
- Mecking, J. V., S. S. Drijfhout, L. C. Jackson, and M. B. Andrews (2017), The effect of model bias on Atlantic freshwater transport and implications for AMOC bi-stability, *Tellus A*, 69(1), 1299910, doi: 10.1080/16000870.2017.1299910.
- Oki, T., and S. Kanae (2006), Global hydrological cycles and world water resources, *Science*, 313(5790), 1068–1072, doi: 10.1126/science.1128845.
- Qu, T., S. Gao, and I. Fukumori (2011), What governs the North Atlantic salinity maximum in a global GCM?, *Geophys. Res. Lett.*, 38(7), L07602, doi: 10.1029/2011gl046757.
- Rahmstorf, S. (1996), On the freshwater forcing and transport of the Atlantic thermohaline circulation, *Clim. Dynam.*, 12(12), 799–811, doi: 10.1007/s003820050144.
- Romanova, V., A. Köhl, D. Stammer, C. Klepp, A. Andersson, and S. Bakan (2010), Sea surface freshwater flux estimates from GECCO, HOAPS and NCEP, *Tellus A*, 62(4), 435–452, doi: 10.1111/j.1600-0870.2010.00447.x.
- Rodell, M., et al. (2015), The observed state of the water cycle in the early twenty-first century, *J. Climate*, 28(21), 8289–8318, doi: 10.1175/jcli-d-14-00555.1.

- Roulet, G., and G. Madec (2000), Salt conservation, free surface, and varying levels: a new formulation for ocean general circulation models, *J. Geophys. Res.*, *105*(C10), 23927–23942, doi: 10.1029/2000jc900089.
- Santer, B. D., et al. (2007), Identification of human-induced changes in atmospheric moisture content, *P. Natl. Acad. Sci. USA*, *104*(39), 15248–15253, doi: 10.1073/pnas.0702872104.
- Schanze, J. J., R. W. Schmitt, and L. L. Yu (2010), The global oceanic freshwater cycle: A state-of-the-art quantification, *J. Mar. Res.*, *68*(3–4), 569–595, doi: 10.1357/002224010794657164.
- Schmitt, R. W. (1995), The ocean component of the global water cycle, *Rev. Geophys.*, *33*(S2), 1395–1409, doi: 10.1029/95rg00184.
- Schmitt, R. W. (2008), Salinity and the global water cycle, *Oceanography*, *21*(1), 12–19, doi: 10.5670/oceanog.2008.63.
- Skliris, N., R. Marsh, S. A. Josey, S. A. Good, C. Liu, and R. P. Allan (2014), Salinity changes in the World Ocean since 1950 in relation to changing surface freshwater fluxes, *Clim. Dynam.*, *43*(3), 709–736, doi: 10.1007/s00382-014-2131-7.
- Skliris, N., J. D. Zika, G. Nurser, S. A. Josey, and R. Marsh (2016), Global water cycle amplifying at less than the Clausius-Clapeyron rate, *Scientific Reports*, *6*, 38752, doi: 10.1038/srep38752.
- Slangen, A. B. A., M. Carson, C. A. Katsman, R. S. W. van de Wal, A. Köhl, L. L. A. Vermeersen, and D. Stammer (2014), Projecting twenty-first century regional sea-level changes, *Clim. Change*, *124*(1), 317–332, doi: 10.1007/s10584-014-1080-9.
- Stammer, D. (2008), Response of the global ocean to Greenland and Antarctic ice melting, *J. Geophys. Res.*, *113*, C06022, doi: 10.1029/2006jc004079.
- Stammer, D., C. Wunsch, R. Giering, C. Eckert, P. Heimbach, J. Marotzke, A. Adcroft, C. N. Hill, and J. Marshall (2003), Volume, heat, and freshwater transports of the global

- ocean circulation 1993–2000, estimated from a general circulation model constrained by World Ocean Circulation Experiment (WOCE) data, *J. Geophys. Res.*, *108*(C1), 3007, doi: 10.1029/2001jc001115.
- Stommel, H. (1957), A survey of ocean current theory, *Deep Sea Res.*, *4*(3), 149–184, doi: 10.1016/0146-6313(56)90048-X.
- Stommel, H. (1984), The delicate interplay between wind-stress and buoyancy input in ocean circulation: the Goldsbrough variations, *Tellus Ser. A*, *36*(2), 111–119, doi: 10.3402/tellusa.v36i2.11474.
- Stommel, H., and A. B. Arons (1959), On the abyssal circulation of the world ocean—I. Stationary planetary flow patterns on a sphere, *Deep Sea Res.*, *6*, 140–154, doi: 10.1016/0146-6313(59)90065-6.
- Talley, L. D. (2002), Salinity Patterns in the Ocean, in *Encyclopedia of Global Environmental Change* (vol. 1), *The Earth System: Physical and Chemical Dimensions of Global Environmental Change*, edited by M. C. MacCracken and J. S. Perry., pp. 629–640.
- Talley, L. D. (2008), Freshwater transport estimates and the global overturning circulation: Shallow, deep and throughflow components, *Prog. Oceanogr.*, *78*(4), 257–303, doi: 10.1016/j.pocean.2008.05.001.
- Tartinville, B., J. M. Campin, T. Fichefet, and H. Goosse (2001), Realistic representation of the surface freshwater flux in an ice-ocean general circulation model, *Ocean Modelling*, *3*(1–2), 95–108, doi: 10.1016/S1463-5003(01)00003-8.
- Treguier, A. M., J. Deshayes, J. Le Sommer, C. Lique, G. Madec, T. Penduff, J.-M. Molines, B. Barnier, R. Bourdallé-Badie, and C. Talandier (2014), Meridional transport of salt in the global ocean from an eddy-resolving model, *Ocean Science*, *10*(2), 243–255, doi: 10.5194/os-10-243-2014.
- Trenberth, K. E. (2011), Changes in precipitation with climate change, *Clim. Res.*, *47*(1–2), 123–138, doi: 10.3354/cr00953.

- Valdivieso, M., K. Haines, H. Zuo, and D. Lea (2014), Freshwater and heat transports from global ocean synthesis, *J. Geophys. Res.*, *119*(1), 394–409, doi: 10.1002/2013jc009357.
- Vinogradova, N. T., and R. M. Ponte (2013), Clarifying the link between surface salinity and freshwater fluxes on monthly to interannual time scales, *J. Geophys. Res.*, *118*(6), 3190–3201, doi: 10.1002/jgrc.20200.
- Wadley, M. R., G. R. Bigg, D. P. Stevens, and J. A. Johnson (1996), Sensitivity of the North Atlantic to surface forcing in an ocean general circulation model, *J. Phys. Oceanogr.*, *26*(7), 1129–1141, doi: 10.1175/1520-0485(1996)026<1129:SOTNAT>2.0.CO;2.
- Wentz, F. J., L. Ricciardulli, K. Hilburn, and C. Mears (2007), How much more rain will global warming bring?, *Science*, *317*(5835), 233–235, doi: 10.1126/science.1140746.
- Wijffels, S. (2001), Ocean transport of fresh water, *Ocean Circulation and Climate*, edited by G. Siedler, J. Church, and J. Gould, pp. 475–488, Academic Press.
- Willebrand, J., S. G. H. Philander, and R. C. Pacanowski (1980), The oceanic response to large-scale atmospheric disturbances, *J. Phys. Oceanogr.*, *10*(3), 411–429, doi: 10.1175/1520-0485(1980)010<0411:Tortls>2.0.Co;2.
- Wunsch, C. (2011), The decadal mean ocean circulation and Sverdrup balance, *J. Mar. Res.*, *69*(2–3), 417–434, doi: 10.1357/002224011798765303.
- Yin, J. J., R. J. Stouffer, M. J. Spelman, and S. M. Griffies (2010), Evaluating the uncertainty induced by the virtual salt flux assumption in climate simulations and future projections, *J. Climate*, *23*(1), 80–96, doi: 10.1175/2009JCLI3084.1.
- Yu, L. (2011), A global relationship between the ocean water cycle and near-surface salinity, *J. Geophys. Res.*, *116*, C10025, doi: 10.1029/2010jc006937.
- Zhang, J. L., and D. Rothrock (2000), Modeling Arctic sea ice with an efficient plastic solution, *J. Geophys. Res.*, *105*(C2), 3325–3338, doi: 10.1029/1999jc900320.

List of figures

- Figure 1.1 The global water cycle — the oceanic perspective. Reservoirs are represented by grey boxes with units 10^3 km^3 . Fluxes are represented by arrows and the red and blue boxes with units of Sv (Sverdrups; $10^6 \text{ m}^3 \text{ s}^{-1}$). [*Figure 1* from *Durack et al.*, 2016]..... 2
- Figure 1.2 Schematic diagram of projected changes in major components of the water cycle. The blue arrows indicate major types of water movement changes through the Earth’s climate system: poleward water transport by extratropical winds, evaporation from the surface and runoff from the land to the oceans. The shaded regions denote areas more likely to become drier or wetter. Yellow arrows indicate an important atmospheric circulation change by the Hadley Circulation, whose upward motion promotes tropical rainfall, while suppressing subtropical rainfall. Model projections indicate that the Hadley Circulation will shift its downward branch poleward in both the Northern and Southern Hemispheres, with associated drying. Wetter conditions are projected at high latitudes, because a warmer atmosphere will allow greater precipitation, with greater movement of water into these regions. [*FAQ 12.2, Figure 1* from *Collins et al.*, 2013] 3
- Figure 2.1 (a) The Goldsbrough gyre driven by evaporation and precipitation, and presented by him in 1933 as a model of the North Atlantic. (b) *Stommel’s* [1957; 1984] idea of using the western boundary currents to

	close a circulation forced by a more realistic distribution of evaporation and precipitation. [Figure 5.102 from Huang, 2010].....	11
Figure 2.2	The Goldsbrough-Stommel circulation of the world oceans, neglecting the inter-basin transports. Each arrow indicates the horizontal mass flux integrated over a $5^\circ \times 5^\circ$ box, in Sv; along the western boundary of each basin, there is a curve indicating the northward mass flux within the western boundary, which is required to close the circulation. [Figure 2 from Huang and Schmitt, 1993].....	13
Figure 2.3	Time series of global annual change in mean surface temperature for the 2006–2100 period (relative to 1986–2005) from CMIP5 concentration-driven experiments. Projections are shown for the multi-model mean (solid lines) and the 5 to 95% range across the distribution of individual models (shading). The number of CMIP5 models used to calculate the multi-model mean is indicated above each line. [Figure 2.1b from the IPCC, 2014].....	15
Figure 3.1	Global annual river discharge into the oceans from Fekete et al. [1999], which is imposed onto the E–P surface flux from NCEP and HOAPS data sets.	20
Figure 3.2	(a) Climatological mean field and (b) zonal mean of E–P–R (mm/day) from NCEP for the period 1988–2011.....	21
Figure 3.3	(a) Climatological mean field and (b) zonal mean of E–P–R (mm/day) from HOAPS for the period 1988–2011. The superimposed black curve in (b) is the zonal mean from NCEP as a reference for comparison.	22
Figure 3.4	(a) E–P anomalies for the RCP8.5 scenario over the period 2081–2100 relative to 1986–2005 from the ensemble-mean of the MPI-ESM LR data set. (b) Zonal means of the E–P anomalies for RCP4.5 (orange) and RCP8.5 scenarios (red); superimposed are the zonal mean E–P	

over the reference period from the historical experiment (green) and the zonal mean from NCEP (black) as references for comparison. 24

Figure 3.5 Annual time series of the E–P changes (in Sv) over the (a) E dominating and (b) P dominating regions for historical (green, 1850–2005), RCP4.5 (orange, 2006–2100), and RCP8.5 scenarios (red, 2006–2100). The E (P) dominating regions are defined by the positive (negative) grids based on the time-mean E–P from the historical simulation over the reference period 1986–2005, which is marked between the two vertical grey lines. 25

Figure 3.6 Test of the relaxation. The first 10 years time-mean barotropic streamfunction difference (BSFd) between VF and VSF (a) with relaxation and (b) without relaxation. 31

Figure 4.1 Time-mean barotropic streamfunction from VF is shown in contours (in Sv; the contour interval is 20 Sv). Color shading shows the difference between VF and VSF. The solid contours indicate positive values, which in the Northern Hemisphere represent an anticyclonic circulation. The four colored lines in the Northern Hemisphere indicate the locations of the sections from which time series of meridional averages are calculated (Fig. 4.7). 35

Figure 4.2 Time-mean Goldsbrough-Stommel circulation (in Sv) calculated directly from the surface volume flux from (a) NCEP and (b) HOAPS, averaged over the period 1988–2011. 36

Figure 4.3 Time-mean meridional overturning streamfunction (in Sv), shown for (a and b) the Atlantic and (c and d) the Pacific-Indian oceans. The estimations are displayed as (a and c) VF, and (b and d) the difference between VF and VSF. 39

Figure 4.4 Global time-mean meridional overturning streamfunction from (a) the difference between VF and VSF, and (b) the freshwater function (see

- equation (4.2) and text for details). (c) Barotropic and (d) baroclinic components from the decomposition of the field shown in (a)..... 41
- Figure 4.5 Time-mean difference between VF and VSF of (a) sea surface height (in cm), (b) steric height (in cm), and (c) bottom pressure expressed in form of equivalent water height (in mm; note the nonlinear color scale). The global mean offsets have been removed. 44
- Figure 4.6 Time-mean difference between VF and VSF of (a) heat content (in $^{\circ}\text{C}\cdot\text{m}$) and (b) freshwater content (in m). 46
- Figure 4.7 Time series of the annual-mean barotropic streamfunction difference (BSFd, in Sv, red), the sea surface height difference (SSHd, in cm, green) along the meridional sections marked in Fig. 4.1 with colored lines, and the mean volume flux into the ocean averaged from the eastern boundary of each basin to the sections considered (VFin, in mm/day, blue), shown for (a and b) the North Atlantic and (c and d) the North Pacific. The results are presented in (a and c) for the subtropical gyres and (b and d) for the subpolar areas. Note the mean volume flux can be interpreted as the GSC using the Goldsbrough relation. Depending on the L^*f/β , the factors are (from a to d) 0.22, 0.25, 0.34 and 0.4 Sv/(mm/day), respectively. 48
- Figure 4.8 Changes in (a) barotropic streamfunction (in Sv) and (b) sea surface height (in cm) as $\Delta\text{RCP} - \Delta\text{NCEP}$. The contours in (a) are the GSC derived directly from the RCP8.5 E-P anomaly, according to the Goldsbrough-Stommel relation (equation (2.1)). The solid contours indicate positive values with the interval of 0.1 Sv..... 50
- Figure 4.9 Changes in (a, c) heat content (in $^{\circ}\text{C}\cdot\text{m}$) and (b, d) freshwater content (in m) as $\Delta\text{RCP} - \Delta\text{NCEP}$, shown (left) from the freshwater perturbation forcing and (right) from the isopycnal motion caused by the perturbation (see equation (4.7) and the text for details). 52

Figure 4.10 (a) Changes in global time-mean meridional overturning streamfunction (MOC, in Sv) as $\Delta\text{RCP} - \Delta\text{NCEP}$. (b) The northward volume transports from ΔRCP (green), ΔNCEP (blue), and $\Delta\text{RCP} - \Delta\text{NCEP}$ (orange)..... 53

Figure 4.11 Northward meridional heat transport (left, in PW) and freshwater transport (right, in Sv) for the global ocean (blue), the Atlantic (red), and the Pacific-Indian oceans (green). The estimates are presented as (top) VF, (middle) ΔNCEP , and (bottom) $\Delta\text{RCP} - \Delta\text{NCEP}$ 55

Figure 4.12 Northward meridional heat transport for (left) the Atlantic and (right) the Pacific-Indian oceans (in PW). Shown are the results for the total transport (black) as well as the overturning (red) and gyre (green) components. The dashed-blue curve exhibits the further decomposition of the overturning components as the contributions from the velocity changes. The estimations are presented as (top) VF, (middle) ΔNCEP , and (bottom) $\Delta\text{RCP} - \Delta\text{NCEP}$ 57

Figure 4.13 Northward meridional freshwater transport for (left) the Atlantic and (right) the Pacific-Indian oceans (in Sv). The solid curves represent the total transport (black) as well as the overturning (red) and gyre (green) components, while the dashed lines show the further decomposition of overturning and gyre components as the contributions from velocity changes (blue) and freshwater changes (orange). The estimations are presented as (1st row) VF, (2nd and 3rd row) ΔNCEP , (4th and 5th row) $\Delta\text{RCP} - \Delta\text{NCEP}$ 60

Figure 5.1 (a) Time-mean freshwater content in the Atlantic (m). The dark green lines define the boundaries of each box used for calculating the freshwater budget. (b) Zonal-mean salinity in the Atlantic (psu) shown in the latitude-depth plane. The Mediterranean Sea has been excluded while calculating (b)..... 66

- Figure 5.2 Standard deviations of the annual (a) freshwater content (m) and (b) zonal-mean salinity (psu).67
- Figure 5.3 Hovmöller diagrams of the annual northward freshwater transport anomalies shown as (a) total, (b) overturning component and (c) gyre component. (d) Correlation coefficients between total and gyre component (green), total and overturning component (red), as well as gyre and overturning components (black). The correlation coefficients are calculated after detrending and shown in bold where significant at 95% confidence level estimated by the method of *Ebisuzaki* [1997].69
- Figure 5.4 Freshwater budget analysis for the subtropical and subpolar North Atlantic box (23.5°N – 60°N). (a) Time series of the freshwater content changes (ΔFWC , black), the contributions of the freshwater transports across the northern boundary (T_n , blue) and the southern boundary (T_s , red), the convergence of T_n and T_s (T_{net} , orange), the surface freshwater flux (SF , green) and the sum of T_{net} and SF (SUM , grey). The mean value of each component is given in brackets. The fluxes into the box are denoted as positive, while southward is positive for T_n and T_s . (b) The anomalies of ΔFWC , T_{net} and SF . The time series are all smoothed with a 4-year running mean.72
- Figure 5.5 Hovmöller diagram of the anomalies of zonal-mean surface freshwater flux into the ocean (mm/day).73
- Figure 5.6 (a) The anomalies of ΔFWC (black), T_{net} (orange), SF (green) and T_n (blue) for the sub-region in the northern North Atlantic box (23.5°N – 37°N). (b) The anomalies of the transport at 37°N (T_n , black), the decomposition into the gyre component (green) and overturning component (red), as well as the contribution from the velocity changes to the overturning component (dashed-blue).74

- Figure 5.7 (a and b) Freshwater budget analysis same as Fig. 5.4 but for the tropical North Atlantic box ($0^{\circ} - 23.5^{\circ}\text{N}$). (c) The anomalies of the transport at 23.5°N (T_n , black), the decomposition into the gyre component (green) and overturning component (red), as well as the contribution from the velocity changes to the overturning component (dashed-blue). 76
- Figure 5.8 (a and b) Freshwater budget analysis same as Fig. 5.4 but for the tropical South Atlantic box ($23.5^{\circ}\text{S} - 0^{\circ}$). (c) The anomalies of the transport at 23.5°S (T_s , black), the decomposition into the gyre component (green) and overturning component (red), as well as the contribution from the velocity changes to the overturning component (dashed-blue). 78
- Figure 5.9 The time-mean meridional overturning streamfunction over the upper 250 m of the tropical Atlantic Ocean, shown as (a) the original structure and (b) the structure of the shallow overturning cells after decomposition (see equation (5.8) and text for details). 79
- Figure 5.10 Annual time series of the northward freshwater transport as total (black) and the contributions from the deep overturning circulation (red) and the shallow overturning cells (blue), shown as the transports (a) at 14°N for the northern cell and (b) at 10°S for the southern cell. 80

List of symbols

c_p	Specific heat capacity of seawater ($c_p = 4200 \text{ J kg}^{-1} \text{ }^\circ\text{C}^{-1}$)
D	Depth of the ocean
E	Evaporation
f	Coriolis parameter
F	Sea ice freezing
F_a	Freshwater anomaly
F_{vf}	Salt flux in the volume flux run
F_{vsf}	Equivalent virtual salt flux
FWC	Freshwater content
FWT	Freshwater transport
FWT_{gy}	Gyre component of the freshwater transport
FWT_{ot}	Overturning component of the freshwater transport
H	Heat transport
H_{gy}	Gyre component of the heat transport
H_{ot}	Overturning component of the heat transport
HC	Heat content
M	Sea ice melting
M_y	Northward mass transport
P	Precipitation
r	Correlation coefficient
res	Residual in the freshwater budget analysis
R	River runoff

S	Salinity
S_0	Reference salinity ($S_0 = 35$ psu)
SF	Surface freshwater flux into the ocean for the budget analysis
$Snow$	Snowfall on the sea ice
T	Temperature
Tn	Freshwater transport across the northern boundary for the budget analysis
$Tnet$	Net freshwater transport across the northern and southern boundaries
Ts	Freshwater transport across the southern boundary for the budget analysis
v	Meridional velocity
vf	Surface volume flux
w_{vf}	Surface vertical velocity for the volume flux run
w_{vsf}	Surface vertical velocity for the virtual salt flux run
β	Meridional gradient of the Coriolis parameter
ρ_o	Seawater density ($\rho_o = 1029$ kg m ⁻³)
τ	Wind stress
Sv	Sverdrups (1 Sv = 10 ⁶ m ³ s ⁻¹)
PW	Petawatt (1 PW = 10 ¹⁵ W)

Abbreviations

ACC	Antarctic Circumpolar Current
AMOC	Atlantic meridional overturning circulation
BSF	Barotropic streamfunction
CC	Clausius-Clapeyron
CMIP5	Coupled Model Intercomparison Project Phase 5
ENSO	El Niño-Southern Oscillation
E	Evaporation
E–P	Evaporation minus precipitation
E–P–R	Evaporation minus precipitation minus runoff
GECCO	German contribution to the Estimating the Circulation and Climate of the Ocean
GSC	Goldsbrough-Stommel circulation
HOAPS	Hamburg Ocean Atmosphere Parameters and Fluxes from Satellite Data
IPCC AR5	Intergovernmental Panel on Climate Change the Fifth Assessment Report
ITCZ	Intertropical convergence zone
KPP	K-Profile Parameterization
MOC	Meridional overturning circulation
MPI-ESM LR	Max-Planck-Institute Earth System Model low resolution version
NADW	North Atlantic Deep Water
NCAR	National Center for Atmospheric Research
NCEP	National Centers for Environmental Prediction
OGCM	Ocean general circulation model

P	Precipitation
R	River runoff
RCP	Representative Concentration Pathway
SMOS	Soil Moisture and Ocean Salinity
SSH	Sea surface height
SSS	Sea surface salinity
STCs	Subtropical cells
VF	Volume flux run
VF_{N+RCP}	Volume flux run with perturbation
VSF	Virtual salt flux run
VSF_{N+RCP}	Virtual salt flux run with perturbation
$\Delta NCEP$	Difference between VF and VSF
ΔRCP	Difference between VF_{N+RCP} and VSF_{N+RCP}
$\Delta RCP - \Delta NCEP$	Difference between ΔRCP and $\Delta NCEP$

Acknowledgements

I would like to express my deepest gratitude to my supervisor Prof. Detlef Stammer for his guidance during my PhD and for his patience, enthusiasm as well as insightful comments. My sincere appreciation also goes to my co-advisor Dr. Armin Köhl for always being present during the past four years, for every suggestion he gave me, and for the kind compassion he showed when I lost the senses of my tongue. My knowledge in this topic has learned from them, and I could not have finished this dissertation without their help.

I am truly grateful that I can be a member of the Remote Sensing and Assimilation Group from the Institute of Oceanography. Thanks to all my fantastic colleagues, who are super friendly and willing to help every time when I knocked their doors. I would like to thank Guokun especially for the enlightening discussions. A big thank you to Julia and Meike for their kind help with the “Zusammenfassung”. Many thanks to Mark for his patience to my silly English grammar questions. To my dear friend Xueyuan, for the happy and sad moments we shared and for the cheering words when I was down. To my wonderful friends Marjan and Yulia, as well as our new friend Sayantani, for making my life so colorful and enjoyable.

I would like to thank the Deutsche Forschungsgemeinschaft (DFG) funded Forschergruppe 1740 for supporting this work. All model simulations were performed at the German high-performance computing center (Deutsches Klimarechenzentrum, DKRZ). Thanks to our IT group for their technical support.

Many thanks to my former advisors Prof. Yiquan Qi, Dr. Jing Wang, Dr. Xuhua Cheng and Prof. Yan Du from the South China Sea Institute of Oceanography. They have guided me to

the great door of science and encouraged me to continue. I also want to thank Dr. Weiqiang Wang. Because of him, I got the opportunity to meet Prof. Stammer and start my study here in Hamburg.

I will be forever thankful to Prof. Ruixin Huang and Prof. Bo Qiu for their kindness, inspiration, and willingness to help during my application. The best thing I have learned from them is the caring attitude towards the younger generation.

Special thanks to my families for their unwavering love and support. To all of my friends, near and far, thanks for being in my life. And finally, to my husband Xing, who fills my life with love and laughter.

Declaration

I hereby declare, on oath, that I have written the present dissertation on my own and have not used other than the acknowledged resources and aids.

Hamburg, 2017

Xin Liu

